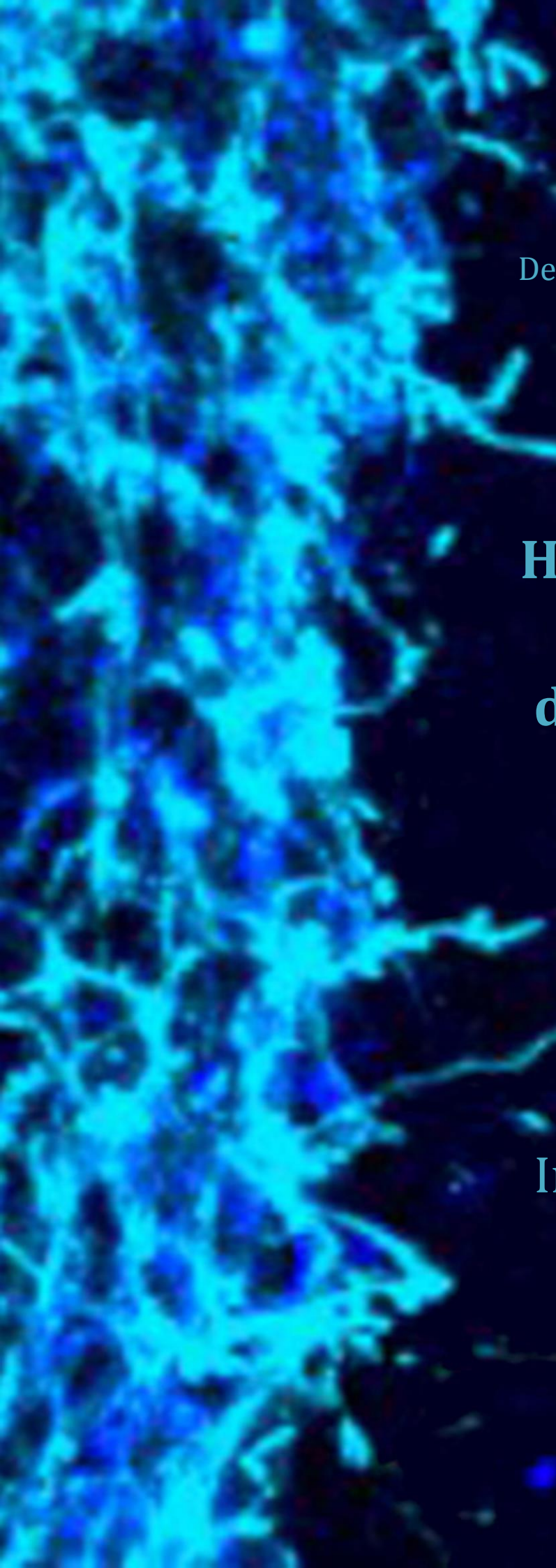

Universidad Autónoma de Madrid

Facultad de Ciencias

Departamento de Biología Molecular

Dynamics of Hedgehog signaling filopodia during *Drosophila melanogaster* epithelia morphogenesis

Irene Seijo Barandiarán

Madrid, 2017

Departamento de Biología Molecular
Facultad de Ciencias
Universidad Autónoma de Madrid

Dynamics of Hedgehog signaling filopodia during *Drosophila melanogaster* epithelia morphogenesis

Thesis submitted by
Irene Seijo Barandiarán
Licenciada en Biología
To accomplish the requirements of the Doctorate Degree in Molecular Biology

Thesis director
Isabel Guerrero Vega
Work tutored by
Esteban Montejo de Garcini

Centro de Biología Molecular Severo Ochoa (UAM-CSIC)
Madrid, 2017

Dr. Isabel Guerrero Vega certifies that the research work presented in this memory by Irene Seijo Barandiarán was carried out under her supervision in Centro de Biología Molecular Severo Ochoa (CSIC-UAM). This thesis was supported by the *Formación del Personal Investigador (FPI)* fellowship associated to the project *Mecanismos de señalización de Hedgehog* (BFU2011-25987) fully funded by Ministerio de Economía y Competitividad

Acknowledgements

En primer lugar, agradecer a mi directora de tesis, Isabel Guerrero, por haberme dado la oportunidad de entrar en el laboratorio y aprender todo lo que he aprendido durante estos años. Por ayudarme en todo lo que ha estado en sus manos y su dedicación a la corrección de este manuscrito.

Gracias a toda la gente que habéis ido formando parte del laboratorio. En especial, gracias a Carmen Ibañez, por tantos buenos momentos y por enseñarme en mis primeros pasos como científica. A Carmen Rodriguez, gracias por enseñarme tanto de molecular y por esas frases hechas tan tuyas. A Citlali, por enseñarme en mis primeros años, por la alegría que traes al laboratorio y por tu ayuda con correcciones de este manuscrito. A David, por ser tan buen compañero, tanto en el principio como ahora. A Adri, mi "compi P3", gracias por ser como un hermano y compartir tantas charlas, risas y buenos recuerdos. A Laura, mi "compi" de las mañanas, gracias por todo el apoyo, el cariño y los buenos momentos tanto en el laboratorio como fuera. A Gus, gracias por ser como eres, por ese punto de locura que nos hace reir en todo momento. A Jorge (GG) y a Julia (la peque) porque no sólo habéis aprendido vosotros, sino que yo he aprendido mucho trabajando a vuestro lado y estoy muy orgullosa del trabajo realizado como científicos y de lo que sois como personas y compañeros. A Pedro, por ser tan especial, tan risueño, detallista, por tu humor y por acogernos con tanto cariño. A Esteban, gracias por tu ayuda y tus primeros consejos como tutor, pero además por hacernos reír cada vez que venías a visitarnos. A Nicole, gracias por todos tus consejos. A Jaime, gracias por todas las risas que nos has ido sacando y por tus consejos para editar la tesis. A Julia, por ser tan especial, por todo lo que hemos pasado juntas y por toda la ayuda que me has dado a lo largo de estos años. A Carol, porque eres una más del laboratorio y por tu ayuda y consejos estos últimos meses. A Pau, gracias por todos los momentos vividos en Madrid, pero sobre todo en St Andrews.

Marcus Bischoff, thank you for the opportunity to visit St Andrews and learn about the wonderful pupal world. Also, thank you for all your help this last year, for your dedication to read the manuscript and for being so nice as allways. I really appreciate it.

Denise Montell, thank you for the opportunity to spend 4 months in your laboratory in Santa Barbara. It was a pleasure learning from you as a scientist. Also thanks to all the lab people. Specially Joe, for being great as a scientist and as a person and for your dedication to read this manuscript; Jim and Wei for your help and dedication in Santa Barbara; and Abhinava, Sreesankar and Yewubdar for the good time spent together.

Gracias a todo el personal del SMOC del CBM por su ayuda durante todos estos años, en especial a Vero por haberme enseñado tanto en mis principios y a Carmen, Ángeles y Carlos por todos los consejos, vuestra ayuda y disposición siempre que lo he necesitado.

Gracias a David Abia del servicio de Bioinformática del CBM por los consejos para realizar la mutagénesis y por el estudio *in silico*.

ACKNOWLEDGEMENTS

A Marta e Inés, por conoceros en el máster y disfrutar aprendiendo junto con vosotras, sobre todo de "mi pequeña caracol" y sus protocolos de mutagénesis.

A las mejores compañeras de carrera, Bea, Roci y Laura. Todo empezó en esos años en los que nos formábamos como biólogas. Siempre me habéis apoyado, aunque no pudiésemos vernos todo lo que queríamos. Parece que el tiempo no pasa cuando nos volvemos a ver y estoy muy agradecida de poder teneros a mi lado.

A todos los que habéis formado parte del gran grupo de danza contemporánea de la UAM y a la mejor profesora Sara Manzanos. Gracias. Porque no sólo me habéis hecho amar aún más la danza, sino que habéis hecho que todos estos años, tanto los momentos buenos como los malos, me olvidase de todo y disfrutase junto a todos y cada uno de vosotros de una de las cosas que más me gusta en la vida, bailar. Nunca dejemos de bailar y disfrutar.

A mi gente de Manzanares, especialmente a Ixi, Leti, Sele, Lauri, Ania, Eva y Marta. Porque sois muy importantes en mi vida y sin vosotras esto no habría sido lo mismo. Orgullosa de tener amigas como vosotras a mi lado.

A toda la gente de Colmenar que últimamente ha hecho que me sienta como en casa, me han animado en momentos difíciles y me han hecho pasar mejor aún los momentos buenos.

A mi familia. Mi abuela, mis tías, y mis primos de España, así como los de Cuba. Porque todos me dais un cariño inmenso y habéis sido un gran apoyo para seguir con mis metas.

A mi otra familia colmenareña, gracias a todos por hacerme sentir una más, en especial a Sergio (cuñi!), Araceli y Juan Pablo. Siempre recordaré buenos momentos juntos.

A mis padres, por todo lo que me habéis dado en la vida, por enseñarme a disfrutar. Gracias por apoyarme en todo momento y porque habéis formado parte de este trabajo, ayudándome tanto cuando lo necesitaba, por la gran ayuda de mi padre para llevar a cabo el modelo y de mi madre para seguir adelante cuando no podía con ello. Estoy orgullosa de lo que sois, como padres y personas. Nunca tendría palabras suficientes de agradecimiento.

A Raúl, una de las personas más especiales en mi vida y mi gran apoyo en todos estos años. Porque hemos superado todo juntos y por todo lo bonito que hemos ido viviendo y construyendo durante este tiempo. Gracias. Gracias por dejarme compartir contigo mi felicidad.

Finalmente, a todas las personas que no he nombrado, pero de alguna manera han formado parte de mi vida y han sido un apoyo durante estos años. Gracias.

Summary

Hedgehog (Hh) signaling is a well-conserved pathway essential for many developmental processes. Hh is a morphogen that spreads from posterior (P) compartment producing cells to anterior (A) compartment receiving cells in a graded manner, activating different target genes depending on the signal concentration. Hh is a dually lipid-modified molecule, being therefore hydrophobic and tightly attached to membranes. To further research the mechanisms of Hh transport and signaling, we have used two paradigms in *Drosophila melanogaster*: fixed larval wing imaginal disc epithelium and *in vivo* pupal abdominal histoblasts epithelium. In this work, we show that Hh signaling is regulated by both actin dynamics and intracellular vesicular traffick machineries. We describe that the Hh ligand and its receptor Patched (Ptc) are transported in vesicles along dynamic filopodia-like structures (cytonemes) at the basolateral surface of the epithelium. These cytonemes comprise a dynamic network that is independent of the presence of Hh or Ptc. They are easily visualized by overexpression of the Hh co-receptor Interference hedgehog (Ihog) due to its role in regulating cytoneme dynamics. We have seen that this stabilization is independent of its homologous protein Brother of Ihog (Boi). Besides we have identified the fibronectin type III domains of Ihog as responsible for the regulation of cytoneme dynamics. Ihog also plays a role in Hh retention and both of these two functions control the formation of the Hh morphogenetic gradient. Finally, we have seen that FNIII domains of Ihog also regulate integrins levels at the A/P compartment border between Hh-sending and Hh-receiving cells. We propose that Ihog interactions with integrins and components of the extracellular matrix could be responsible for Ihog functions as regulator of cytoneme dynamics, Hh retention and signaling gradient formation.

Index

Index of figures

Figures - Introduction

Figures – Materials and Methods

Figures – Results

Figures – Discussion

Figures – Annex I: Supplementary figures

Index of tables

Tables – Materials and Methods

Tables – Results

Index of movies

Movies can be displayed by clicking at their name either in the text or in Annex I, where there is a detailed description of each movie.

Movie – Materials and Methods

Movies – Results

Abbreviations

Genes are specified in the text in lowercase and italics, while for proteins the first letter is a capital letter.

βPS	β chain of integrins
A	Anterior
ADH	Anterior dorsal histoblast nest
AnxB11	Annexin B11
AP	Antero-posterior
Ap	Apterous
Arrβ2	β-arrestin-2
Bnl	Branchless
BOC	Brother Of CDO
Boi	Brother of Ihog
BSA	Bovine serum albumin
Btl	Breathless
cDNA	Complementary DNA
CDO	Cell adhesion molecule down-regulated by oncogenes
CG31729	Drosophila homologous for the P4-ATPase
Ci	Cubitus interruptus
Ct	Carboxi terminus
D	Dorsal
Dally	Division abnormally delayed
Dhh	Desert hedgehog
Disp	Dispatched
Dlp	Dally-like protein
DP	Disc proper
Dpp	Decapentaplegic
DV	Dorso-ventral
Dvl2	Dishevelled2
ECM	Extracellular matrix
EGF	Epidermal growth factor
EGFR	Epidermal Growth Factor Receptor
En	Engrailed
ESCRT	Endosomal sorting complexes required for transport
Evi	Evenness interrupted
EVs	Exovesicles
F-actin	Filamentous actin
FGF	Fibroblast growth factor
Flo2	Flotillin 2
FLP	Flippase
Fn1	First FNIII domain
Fn2	Second FNIII domain
Fn3	Third FNIII domain
FNIII	Fibronectin type III
FRT	Flippase Recombination Target
GFP	Green Fluorescence Protein
GMA	Actin-binding domain of moesin
h APF	Hours After Puparium Formation
Hh-N	Hh signaling N-terminus
Hh	Hedgehog
Hrs	Hepatocyte growth factor–associated tyrosine kinase
Ig	Immunoglobulin
Ihh	Indian hedgehog
Ihog	Interference hedgehog
L3	Third longitudinal vein
L4	Fourth longitudinal vein

ABBREVIATIONS

LECs	Larval epidermal cells
Lgr	Leucin-rich G-protein-coupled receptors
Lifeact	Actin-binding peptide
Lrp6	Low-density lipoprotein receptor-related protein 6
M3	Insect specific media
MVBs	Multivesicular bodies
P	Posterior
PBS	Phosphate Buffered Saline
PBT	Phosphate Buffered Saline+ Triton X-100 0,1%
PC	Pupal case
PCR	Polymerase chain reaction
PDS	Posterior dorsal histoblast nest
PFA	Paraformaldehyde
PM	Peripodial membrane
PSC	Posterior signaling center
Ptc	Patched
Qhh	Qiqihar hedgehog
RFP	Red Fluorescence Protein
RNAi	RNA interference
RT	Room temperature
Shf	Shifted
Shh	Sonic hedgehog
Sm	Smoothened
SOPs	Sensory organ precursors
Spi	Spitz
Tkv	Thickveins
Tub	Tubulin
Twhh	Tiggywinkle hedgehog Ehh: Echidna hedgehog
UAS	Upstream Activation Sequence
Ubi	Ubiquous
V	Ventral
Vps	Vacuolar protein sorting-associated protein
WD	Wing imaginal disc
Wg	Wingless
Wnt	Wingless-related integration site
WP	Wing pouch
YFP	Yellow Fluorescence

Introduction

1. Hedgehog signaling during morphogenesis

1. 1. Morphogenesis in development

Development of complex multicellular organisms from a single cell requires coordinated cell proliferation, cell death, cell determination and cell differentiation processes. Regulation of these processes will let proliferating cells to form different tissues that will result in different organs with certain sizes, patterns and shapes. The biological processes that give rise to those different tissues and organs comprise **morphogenesis**. For this purpose, cells need to produce, transmit and receive molecular signals and mechanical forces in order to communicate with each other and achieve a coordinated cell behavior that will result in changes in tissue size, pattern and shape.

Most of the signals transmitted from different populations of cells during morphogenesis are known as **morphogens**. These signaling molecules are secreted from producing cells and disperse towards receiving cells in a graded manner, forming concentration gradients that would induce different cell responses, activating different gene targets depending on the signal concentration. Morphogenetic gradients need to be tightly regulated; as deregulation of these gradients could lead to disorders such as cancers (Rogers & Schier, 2011; Turing, 1990; Wolpert, 1969).

In cell-cell signaling, it is important to consider not only the ligand-receptor interaction, but also the intracellular and intercellular processes that are taking place within the whole developmental scenario: the interactions of intracellular pathway components and the cell-cell and cell-extracellular matrix adhesions.

1. 2. Hedgehog signaling in metazoan development

Hedgehog (Hh) proteins are morphogens essential for tissue development in vertebrates and invertebrates, being highly **conserved** in evolution (Ingham et al., 2011). There are up to six Hh family members in vertebrates divided in three subgroups: Desert hedgehog (**Dhh**), Indian hedgehog (**Ihh**) and Sonic hedgehog (**Shh**). Birds and mammals have one Hh gene of each group, while zebrafish have three extra, due to duplication and rearrangements in the genome: Tiggywinkle hedgehog (**Twhh**) of the Shh subgroup, and Echidna hedgehog (Ehh) and Qiqihar hedgehog (**Qhh**) of the Ihh subgroup. Shh and Ihh are more closely related to each other, whereas Dhh is more related to the *Drosophila* Hh (reviewed in Varjosalo & Taipale 2008).

Hh proteins are synthesized as precursors that suffer **two** post-translational **lipid modifications**. Hh precursor undergoes an autocatalytic process resulting in a signaling N-terminus (Hh-N) fraction (Lee et al., 1994) and a C-terminus fraction, required for the precursor protein processing. Next, the C-terminus fraction is degraded and replaced by a **cholesterol** moiety, added covalently to the C-terminus end of Hh-N (Porter et al., 1996). Subsequently, a **palmitic acid** is covalently added to the N-terminus of Hh-N (Pepinsky et al., 1998). These lipid modifications are necessary for Hh signaling in both *Drosophila melanogaster* (Callejo et al., 2006; Chamoun et al., 2001; Gallet et al., 2006) and vertebrates (Pepinsky et al. 1998; Lewis et al. 2001; Taylor et al. 2001; Chen et al. 2004; Ohlig et al. 2011); and confer Hh proteins a tight association to the membranes (Peters et al., 2004), making difficult to consider Hh transport by free diffusion (reviewed in Guerrero & Chiang 2007; Gradilla & Guerrero 2013b; Guerrero & Kornberg, 2014).

The **Hh signaling pathway** is conserved in evolution. The dually lipid-modified Hh protein is released to form a gradient at the basolateral part of polarized epithelia in *Drosophila* (Callejo et al., 2011) and Shh is also released basolaterally in polarized mammalian tissue cultured cells (Etheridge et al., 2010) and in vertebrates neuroepithelia (Cardozo et al., 2014). The Hh ligand is received by the receptor Patched (**Ptc**) (Goodrich et al., 1996; Marigo et al., 1996) that relieves the Smoothened (**Smo**) repression by Ptc and elicits the intracellular signal cascade triggering the activation of the Hh target genes by its transcription factor Cubitus interruptus (**Ci**), Gli proteins in vertebrates (reviewed in Ingham et al., 2001).

Hh signaling pathway is fundamental for **embryonic pattern formation** and for **adult homeostatic** processes, such as tissue maintenance and regeneration; as Hh is a key factor for the maintainance of the stem cell population. Aberrant Hh signaling can lead to embryonic pattern disruptions: segmentation and tissue pattern defects in *Drosophila melanogaster*, altered Shh-derived holoprosencephaly and other birth defects in mammals; post-embryonic dysfunction can result in proliferative disorders such as the growth of malignant tumors or tissue degeneration (reviewed in Briscoe & Therond 2013).

1. 3. Drosophila melanogaster: a model to study Hh signaling

Drosophila melanogaster, also known as the fruit fly, is a holometabolic insect with a short life cycle which comprises four stages: embryo, larva, pupa and imago or adult (Figure I-1A). At temperatures of 25ºC, a fertilized egg gives rise to an embryo one day after egg laying, 24h later gives rise to the first instar larva, which eats and grows until reaching the third instar larva, then it stops feeding and its cuticle would harden to form the puparium.

Then, adult tissues will replace larval tissues in a period known as metamorphosis, which occurs within the next four days, until the adult ecloses.

Drosophila melanogaster is a good model organism to study genetics, molecular biology, cellular biology and developmental biology because of its short life cycle, easy maintenance, elevated progeny and its well-known genetics.

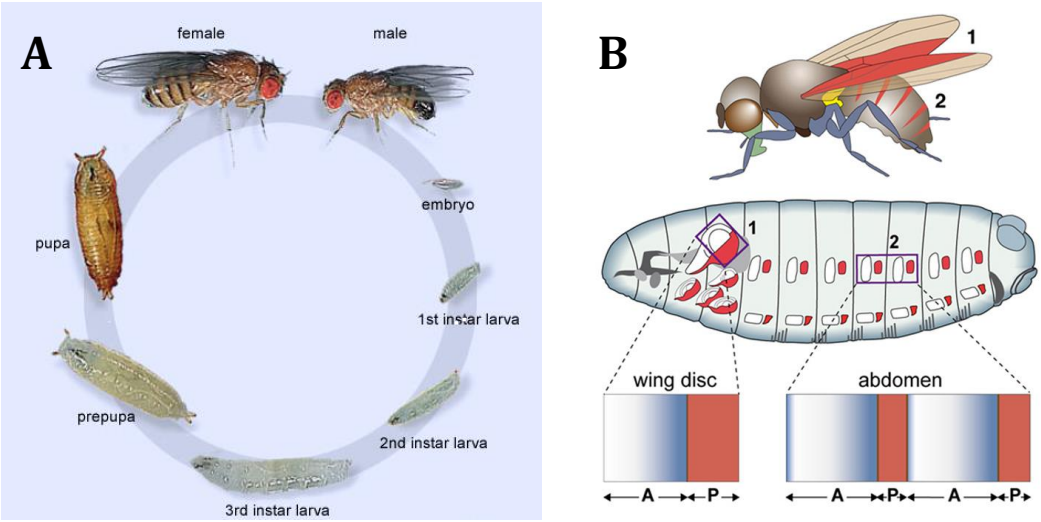

Figure I-1. Drosophila melanogaster: a model to study Hh signaling.
A: The life cycle of *Drosophila melanogaster*. Image modified from *FlyMove*. **B: Hh signaling in wing discs and abdominal histoblasts.** Drawing depicting Hh produced in posterior (P) compartment Hh-expressing cells (red) and distributed towards anterior (A) compartment Hh-responding cells (blue), in a gradient manner, in both larval wing discs (1) and abdominal histoblasts (2) to develop adult wings (1) and abdominal epithelia (2). Image taken from Guerrero & Kornberg 2014.

The *hedgehog* (*hh*) gene was identified in a screen of genes that specify the formation of embryonic pattern segmentation in *Drosophila melanogaster* and its name derived from the hedgehog-like abnormal pattern of bristles of the *hh* mutant larvae (Nüsslein-Volhard & Wieschaus, 1980).

Hh signaling is essential for the development of different imaginal discs: wing imaginal discs (Basler & Struhl, 1994; Mullor et al., 1997), leg discs (Diaz-Benjumea et al., 1994), eye discs (Domínguez, 1999) and genital discs (Gorfinkiel et al., 2003). Additionally, Hh is involved in morphogenesis of the gut (Pankratz & Hoch, 1995), the abdomen (Struhl et al., 1997), the tracheal system (Glazer & Shilo, 2001), the embryonic germ cells migration (Deshpande et al., 2001), the hematopoietic lymph gland development (Mandal et al., 2007), the homeostasis of ovary stem cells (Rojas-Ríos et al., 2012) among others.

In this work, we study Hh signaling function in the larval wing imaginal discs and pupal abdominal histoblasts epithelia, which are going to develop into the adult wings and abdominal epithelia, respectively (Figure I-1B).

1. 4. Drosophila melanogaster wing imaginal disc as a model to study Hh signaling

Larval imaginal discs are pseudoephitelia derived from a specific group of cells that segregate from the embryo epidermis. The imaginal discs will give rise to all the cuticle structures in adults (head, thorax, wings, halters, legs and genitalia-analia), except for the abdominal cuticle, which has a different origin: the histoblasts that develop during metamorphosis (Figure I-1B).

The **wing imaginal disc** consists of a columnar pseudostratified epithelium (disc proper, DP) and a squamous epithelium (peripodial membrane, PM), which are separated in their apical surfaces by a lumen. Adult wings are formed from the wing pouch (WP) region of the disc proper cells (Figure I-2A). The wing disc, as the other larval imaginal discs, is divided in compartments composed of different

cellular populations with distinct adhesion affinities, which maintain lineage restriction boundaries between them (Garcia-Bellido et al., 1973). There are four compartments in the wing imaginal disc and two boundaries between them: anterior (A), posterior (P), dorsal (D) and ventral (V) compartments; and antero-posterior (AP) and dorso-ventral (DV) boundaries. The homeotic selector genes *engrailed (en)* and *apterous (ap)* maintain the P and D compartment identities, respectively.

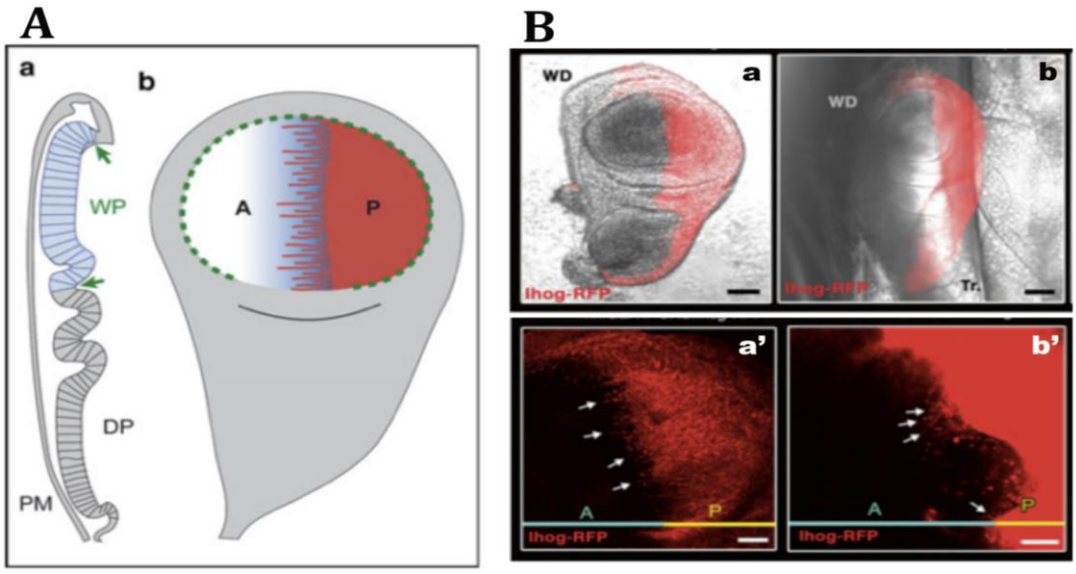

Figure I-2. Drosophila melanogaster wing disc: a model to study Hh signaling. **A: Scheme depicting *Drosophila melanogaster* wing disc and filopodia-mediated Hh signaling. (a)** Transversal section of the wing imaginal disc showing the two juxtaposed epithelia: squamous peripodial membrane (PM) and pseudostratified columnar disc proper (DP). **(b)** Longitudinal section of the wing imaginal disc showing the posterior compartment (P) Hh signaling filopodia (red), which invade the anterior compartment (A) to form the Hh morphogenetic gradient, shown by the graded *ptc* expression. The wing pouch (WP) is delimited by green arrows in **(a)** and by green dotted line in **(b)**. **B: *Ex vivo* and *in vivo* wing imaginal disc Hh signaling filopodia.** *Ex vivo* in M3 media **(a, a')** and *in vivo* in a living third instar larva **(b, b')** wing imaginal discs (WD) expressing Ihog-RFP in Hh-producing cells (red) and using transmitted light **(a, b)** to visualize structures as the second thoracic lateral tracheal branch (Tr.) which is next to the wing disc of the larva. Hh-producing cells filopodia (arrows) are easily visualized in basal views of the disc proper of WD **(a', b')**. Images modified from Seijo-Barandiarán et al. 2015.

Hh signaling is responsible for patterning the central part of the wing, which comprises the region between L3 and L4 veins (Mullor et al., 1997). During wing development, Hh is produced and secreted by P compartment cells of the imaginal disc; it is transported across the AP compartment border towards the receiving A compartment cells, decreasing in concentration as it spreads away from the AP border. Hh triggers the expression of different target genes on the receiving cells depending on the Hh ligand concentration they receive. (Figure I-1B; FigureI-2A).

As mentioned before, Hh is a dually lipid-modified molecule and therefore highly hydrophobic, and tightly attached to membranes. This attachment to membranes impedes Hh free diffusion in an aqueous extracellular medium. The mode Hh is being transported to form its morphogenetic gradient has been under debate during the last decade, leading to different models: associated to lipoproteins, which are produced in the fat body, secreted to the hemolymph and distributed to tissues (Callejo et al., 2006; Panáková et al., 2005); assembled in multimers that can be soluble in aqueous media (Gallet et al., 2006); in exosomes in the wing disc and abdominal histoblasts (Gradilla et al., 2014) or as budding fragments of plasma membranes in the wing disc (Matusek et al., 2014); and by signaling filopodia also known as cytonemes in wing disc and abdominal histoblasts epithelia (Bilioni et al., 2013; Bischoff, Gradilla, Seijo, Andrés, Rodríguez-navas, et al., 2013; Callejo et al., 2011).

It has been shown that different components of the Hh signaling pathway localize to cytonemes situated at the basolateral part of the wing primordium epithelium (Bilioni et al., 2013; Bischoff et al., 2013; Callejo et al., 2011). Among these components are: the Hh receptor complex proteins, formed by the co-receptors Interference

hedgehog (**Ihog**), Brother of Ihog (**Boi**) and the glypican Dally-like (**Dlp**), involved in both Hh reception (Desbordes & Sanson, 2003; Lum et al., 2003; Williams et al., 2010) and Hh vesicular trafficking in Hh-secreting cells (Callejo et al., 2011); the other *Drosophila* glypican Division abnormally delayed (**Dally**) is required for Hh release (Eugster et al., 2007); Dispatched (**Disp**), also essential in Hh release (Burke et al., 1999); and Shifted (**Shf),** necessary for the extracellular Hh stability and dispersion (Gorfinkiel et al., 2005).

During this work, we have focused our attention in the role of Hh-signaling filopodia (cytonemes), which can be visualized in fixed tissues, but also in *ex vivo* wing discs and *in vivo* in living larvae (Figure I-2B; Seijo-Barandiarán et al. 2015).

1. 5. Drosophila melanogaster abdominal histoblasts: a model to study Hh signaling in vivo

Drosophila melanogaster adult abdominal epidermis is developed from **abdominal histoblasts**, the epidermal adult precursors that replace the larval epidermal cells (LECs) during metamorphosis. These abdominal histoblasts cells are quiescent during larval stages and are arranged in groups known as histoblasts nests. There are **dorsal anterior** and **posterior nests**, anlage and ventral nests for each abdominal segment, separated from each other by LECs until metamorphosis (Figure I-3A). At the beginning of metamorphosis, **0-8h APF** (hours After Puparium Formation), these clusters of cells begin to **proliferate** in a **synchronous** way (Figure I-3A c). Subsequently, the division cycles are slower and histoblasts begin to expand replacing the dying LECs. The anterior dorsal nest is **fused** with the posterior dorsal nest around **20h APF** (Figure I-3B compare b with a and d’ with d) and together **migrate** towards the dorsal midline (Figure I-3B d’) substituting the LECs, which die and extrude

basally (Figure I-3B c, c') being removed by haemocytes (macrophages). Finally, histoblasts begin to **differentiate** at around **36h APF** (Madhavan & Madhavan, 1980).

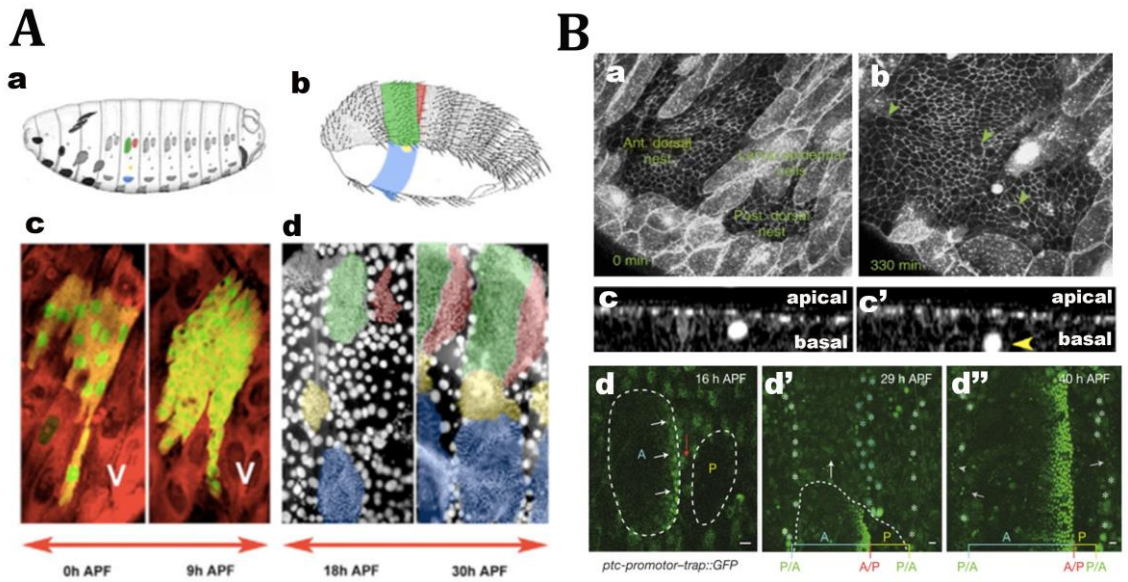

Figure I-3. Abdominal epidermis development during metamorphosis.
A) Proliferation and migration of the histoblast nests. Drawings depicting larval histoblast nest **(a)** and adult epidermis **(b)**. Images showing synchronous histoblast divisions in early pupal stages (0-9h APF) **(c)** and stochastic histoblast divisions in late pupal stages (18-30h APF) **(d)**. Histoblast nests and their respective adult epidermis are coloured: green=anterior dorsal, red=posterior dorsal, yellow=spiracular and blue=ventral. **B) Hh signaling in dorsal histoblasts.** Images showing anterior dorsal (ADH) and posterior dorsal (PDH) nests separated by a row of LECs (a) and just after hisotoblast nest fusion (b). Transversal section of the histoblast nest. Yellow arrow shows a death LEC extruding basally **(c, c')**. Hh signaling reporter (*ptc*) expression in A cells **(d-d'')** in early stage, where ADH and PDH nests are separated **(d)**; later stage **(d')** when ADH and PDH are fused and migrate towards midline (arrow indicates movement); and latest stage **(d'')** where *ptc* is also expressed in A cells of segments of the following posterior segment after the segmental fusion of the histoblast (arrow). A/P and P/A indicate anteroposterior compartment (in a segment) and segment (between two consecutive segments) borders, respectively. Images modified from Ninov et al. 2007, Ninov & Martín-Blanco 2007 and Bischoff et al. 2013.

Hh signaling is involved in **morphogenesis** of the abdomen during metamorphosis (Struhl et al., 1997). It is expressed in **P** compartments of **LECs** and **histoblasts** (Figure I-1B; Figure I-4A; Struhl et al. 1997; Kopp et al. 1997), and signals towards the A

compartment cells both anteriorly (in each abdominal segment) and posteriorly (between segments, in the next posterior segment) of the Hh source (Figure I-4A; Struhl et al. 1997). At the beginning of morphogenesis of dorsal histoblasts, ***ptc***, as a **readout** of Hh signaling, is expressed in the anterior dorsal histoblast (**ADH**) nest (Madhavan & Madhavan, 1980), before it fuses with the posterior dorsal histoblast (**PDH**) nest (Figure I-3B d; Struhl et al. 1997). Afterwards, when ADH and PDH nests meet at the **AP compartment border** and move towards the midline, *ptc* expresses in a **graded manner** in the A compartment cells (Figure I-3B d). Finally, when two consecutive segments meet at the **PA segment border**, they fuse and *ptc* expression can be visualized in a **narrow stripe** in the most anterior part of the immediately P segment (Figure I-3B d''; Figure I-4A; Kopp et al. 1997). This *ptc* expression pattern is only established during morphogenesis of the adult epidermis (Gradilla & Guerrero, 2013b; Kopp & Duncan, 2002; Kopp et al., 1997; Struhl et al., 1997).

Throughout this work, we have attempted to further elucidate the function of specialized Hh-signaling filopodia (cytonemes) in Hh gradient formation in the wing imaginal discs. We have performed *in vivo* analyses using live imaging of pupal abdominal histoblasts (Figure I-4B; Seijo-Barandiarán et al. 2015), as tracking cytonemes in time-lapse recording in the wing primordial tissue is difficult due to internal movements of living larvae. This model system has been demonstrated to be excellent for live imaging studies during morphogenesis as the process does not interfere with the development of living tissues (Ninov & Martín-Blanco, 2007). Using this technique, we have analyzed the formation of the Hh morphogenetic gradient and showed that Hh is transported on

exosomes along cytonemes from Hh-producing cells to Hh-receiving cells (Bischoff et al., 2013; Gradilla et al., 2014).

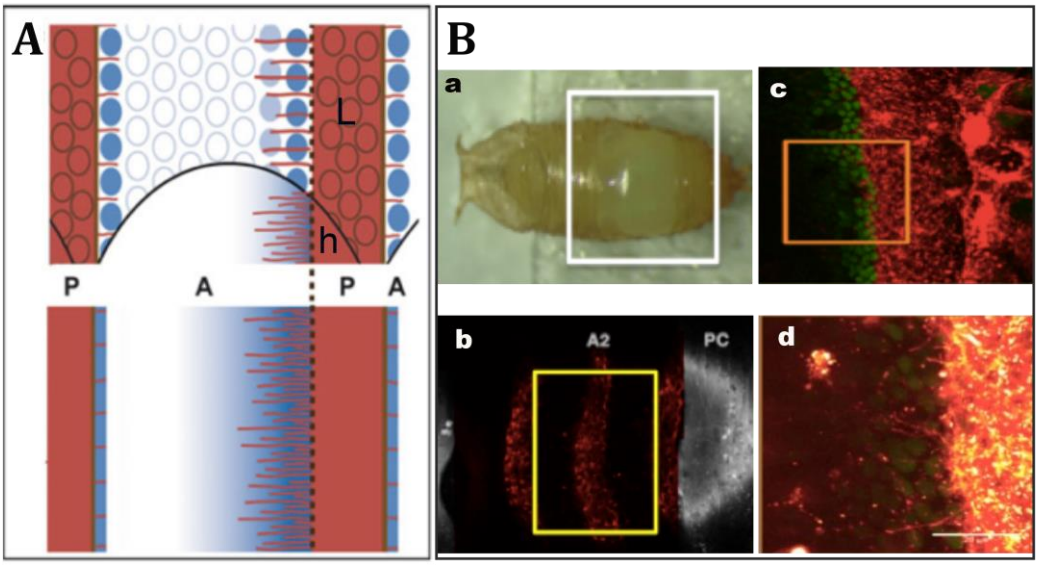

Figure I-4. Drosophila melanogaster abdominal histoblasts as a model to study Hh signaling. **A: Scheme depicting Hh signaling filopodia in one abdominal segment.** Posterior compartment (P) Hh signaling filopodia (red) and anterior compartment (A) *ptc* expression (blue) in histoblasts (h) and LECs (L) are shown. During histoblast spreading, both histoblasts and LECs extend Hh signaling filopodia and *ptc* gradient is being formed in both histoblasts and LECs as well as in a row of LECs at the segment boundaries (top panel). Histoblasts replace LECs to form the adult tissue. Hh-producing cells filopodia (red) and *ptc* (blue) expressed in an anterior gradient in one segment and in a narrow stripe at the segment boundaries of the next posterior segment are shown (bottom panel). **B: *In vivo* Hh signaling in abdominal histoblasts.** Dorsal views of a pupa with a window made to take off the pupal case only in the abdominal region (a, b). Image taken with a dissecting scope **(a)** and with a confocal microscope **(b)**. The pupal case (PC) and the P compartments (red) of abdominal segments A1, A2, and A3 are shown. Overview **(c)** and enlarge view **(d)** of Hh-producing histoblasts emiting Ihog-stabilized filopodia (red) and *ptc* expression (green) in Hh-responding histoblasts of abdominal epithelium of around 30h APF (hours After Puparium Formation). Images modified from Seijo-Barandiarán et al. 2015.

2. Signaling filopodia during metazoan development

Filopodia, spike-like actin-rich cellular protrusions, are usually produced at the leading edge of migrating cells, and function as sensors of the extracellular environment. Hence, filopodia had mainly been described in several works regarding cell movement (reviewed in Ridley 2011; Gomez & Letourneau 2014; Pocha & Montell 2014).

Long thin **actin-rich filopodia** were first observed during **sea urchin** embryogenesis (Wolpert & Gustafson, 1961) and were suggested to be involved in **distant cell-cell communication** associated with **ligand-receptor** interactions in patterning, due to their characteristics and dynamics that do not correlate to cell motility filopodia (Miller et al., 1995).

Later, in the work of Ramirez-Weber and Kornberg (1999) a new function came into view for **specialized signaling filopodia.** They were called "**cytonemes**" and involved in transmitting signaling proteins between cells. In this publication, *Drosophila melanogaster* third instar larval wing imaginal discs are shown to emit cytonemes that project towards a **signaling center** for the transforming growth factor-β (TGFβ) member **Decapentaplegic (Dpp)** morphogen (Ramírez-Weber & Kornberg, 1999). Since then, different **ligands** and **receptors** have been visualized on these kind of specialized filopodia in **different model systems** (reviewed in Gradilla & Guerrero 2013a; Roy & Kornberg 2015; Pröls et al. 2016).

2. 1. Signaling filopodia in vertebrate development

In **mice** preimplantation **embryonic** blastocysts, the **fibroblast growth factor (FGF)** receptor **FGFR2** is present in vesicle-like structures through actin-based short and long filopodia of the FGF4-

receiving cells (the trophectoderm cells). These filopodia connect with the FGF4-producing cells (the inner cell mass cells) through the blastocoelic fluid (Salas-Vidal & Lomelí, 2004). Another FGF receptor (**FGFR1c**) was localized in Rab5-coated punctae moving in a net retrograde flow towards the cell body through actin-based filopodia of **mouse mesenchymal cultured cells** C3H/10T1/2 transfected with Cdc42 or RhoD. These cellular protrusions extent toward fibroblast growth factor 2/4/8 (**FGF 2/4/8**)-coated beads (Koizumi et al., 2012).

The **epidermal growth factor (EGF)** receptor **ErbB3** was localized on vesicles across trophoectoderm in long but not short filopodia of **mouse** preimplantation **embryos** blastocysts (Salas-Vidal & Lomelí, 2004). Similarly, the EGF receptor **ErbB1** was found associated to actin-based filopodia of **human epidermal** (A431) **cell line** in real-time imaging. The ligand-receptor complex is transported along the filopodium in a retrograde flow, until it reaches the lamellipodial base of the filopodium, where this complex is endocytosed (Lidke et al., 2005).

Wingless-related integration site (Wnt) signaling components have also been localized at filopodia in different species. Secretion of active **Wnt2b** is regulated by its transport along microtubules on live Wnt-producing ***Xenopus laevis*** fibroblasts. In addition, Wnt2b transfected XTC cells accumulate the ligand on **tips of filopodia** or moving in cytoplasmic spots along microtubules. Wnt2b spots also move in retracting membrane-protrusions of non-transfected Wnt-receiving XTC cells and rapidly internalize (Holzer et al., 2012). During neural plate patterning in living **zebrafish** embryos, **Wnt8a** ligand is localized at punctate structures on producing cells filopodia of the **blastoderm** margin. These punctate structures can be

released from sending filopodia and co-localized with **Frizzled** receptor clusters in signal-receiving cells of the prospective neural plate, but not in filopodial structures (Luz et al., 2014). In live imaging **zebrafish** embryonic **epiblast** cells, **Wnt8a** localizes on **tips** of Cdc42/N-Wasp nucleation complex containing actin-based filopodia that orient towards the animal pole. Equally, in **zebrafish** fibroblasts PAC2 **cultured cells**, Wnt8a is localized on filopodial tips making contacts with Dishevelled2 (**Dvl2**) containing neighbouring cells. In addition, in gastrulating zebrafish embryos, Wnt8a punctae at filopodial tips co-localize with Evenness interrupted (**Evi**), necessary fot Wnt8a secretion, with the co-receptor Low-density lipoprotein receptor-related protein 6 (**Lrp6**) and with the signal transducers **Dvl2** and **Axin1** at the plasma membranes of the receiving cells (Stanganello et al., 2015). During somite development of **chick embryos,** epithelial cells produce two populations of actin and tubulin rich filopodia-like protrusions. There are partially stable cellular extensions formed at the basal part of the **Wnt**-receiving epithelial dermomyotome, that transport the receptor **Frizzled-7** in a retrograde flow and connect to the Wnt-producing ectoderm crossing the subectodermal space; as well as also dynamic cellular protrusions that extend to all directions but do not seem to transport the Wnt receptor along them (Sagar et al., 2015).

A study using *in vivo* imaging of **chick** limb bud **mesenchymal cells** revealed the localization in long specialized actin-based filopodia of both the vertebrate Hh signaling ligand, Sonic Hedgehog (**Shh**), from Hh-sending cells and the co-receptors Cell adhesion molecule down-regulated by oncogenes (**CDO**) and Brother of CDO (**BOC**) from Hh-responding cells. These filopodia extend several cell diameters and generate stable interactions between them (Sanders et al., 2013).

Live imaging in **zebrafish** during pigment stripe patterning showed long membrane projections extending from melanophores, which express the Delta/Notch signaling receptor **Notch1a**, towards the xanthopores, which express the ligand **DeltaC**, to make direct contact. However, Delta/Notch signal transduction at filopodial contact sites remains to be confirmed (Hamada et al., 2014).

Real-time imaging of **human** HEK **cell line** transfected with the stem cells specific proteins **leucin-rich G-protein-coupled receptors Lgr4** or **Lgr5** revealed dynamic long actin-rich membrane protrusions directed towards the basolateral surface. The actin motor protein myosin X and the signaling effector β-arrestin-2 (**Arrβ2**) were also shown in those filopodia (Snyder et al., 2015).

2. 2. Signaling filopodia in Drosophila melanogaster

During the last decade, several studies have shown specialized signaling filopodia for different signaling pathways in diverse *Drosophila melanogaster* tissues (reviewed in Kornberg & Roy 2014).

Tom Kornberg's group has been investigating the specificity of cytonemes for different signaling proteins. For example, during the **tracheal system** development, the *Drosophila* **FGF receptor Breathless (Btl**) is present at small punctate structures through actin-based filopodia emited by *btl*-expressing air sac primordium (ASP) tracheoblast cells in late third instar larvae. These membrane protrusions were oriented towards the *Drosophila* FGF **ligand *branchless* (*bnl*)** expressing columnar epithelium **wing imaginal disc** cells (Sato & Kornberg, 2002). In third instar larval **wing imaginal discs** where the **Dpp** receptor Thickveins (Tkv) is overexpressed, **Tkv** is localized in punctae that move along apical

cytonemes, in anterograde and retrograde flows, oriented towards the AP border, where the ligand Dpp is produced (Hsiung et al., 2005). There are also apical cytonemes oriented towards the Wingless (**Wg)** expressing cells in the wing primordium (Roy et al., 2011), while basal cytonemes are formed for **Hh** dispersion (Bilioni et al., 2013; Bischoff, Gradilla, Seijo, Andrés, Rodríguez-navas, et al., 2013; Callejo et al., 2011; Roy et al., 2011). **Eye discs** form apical cytonemes oriented to equator and morphogenetic furrow in **EGF** reception (Roy et al., 2011). **Frizzled** (Fz)-punctae containing myoblasts (flight muscle progenitors) cytonemes take up **Wg** punctae from the wing primordium, and negatively regulate the expression of **Delta**, which is also localized in vesicles moving along myoblasts cytonemes that contribute to Notch activation in the ASP (Huang & Kornberg, 2015).

During development of *Drosophila* thoracic **mechanosensory bristles**, the ligand **Delta** is located at membrane processes of the sensory organ precursors (SOPs) cells of late third instar larval **wing imaginal discs.** These specialized filopodia are seen mostly at the basal side of the epithelium, but also along the apico-basal axis and regulate long-range Delta-Notch lateral inhibition (Joussineau et al., 2003). Similarly, using live imaging through a window in the pupal case to visualize the late development of the **notum**, dynamic basal actin-based filopodia were seen extending from membrane-bound **Delta**-expressing ligand mechanosensory organ precursor cells towards the neighboring **Notch** receptor-receiving epithelial cells. Interestingly, the dynamic interaction of Delta-Notch filopodia triggers the lateral inhibition of Delta and the activation of Notch signaling in an intermittent way, which results on a well-ordered pattern of gene expression leading to a precise **microchaete** spacing (Cohen et al., 2010).

Drosophila **pupal legs** also produce Epidermal Growth Factor Receptor (**EGFR**) signaling filopodia shown by live imaging of 24h APF pupae, in which the pupal case was removed. Spitz (Spi) ligand-producing cells, the socket cells, form dynamic planar polarized protrusions proximally oriented towards EGFR responding cells, the bract cells. This filopodia-mediated ligand-receptor direct contact activates an asymmetric EGFR cell signaling, resulting in spatially patterned cell fates (Peng et al., 2012).

2. 3. Hh signaling filopodia in Drosophila melanogaster

Like other signaling pathways, there are specific Hh signaling filopodia or cytonemes in several *Drosophila melanogaster* tissues.

Whole-mount live third instar larval **lymph gland** presents membrane protrusions in the posterior signaling center (PSC), essential for functions as a hematopoietic niche and crucial for the maintenance of blood cell precursors (Mandal et al., 2007). Actin immunostained filopodia were impaired in PSC that fail to express *hh* by knocking down the chromatin-remodeling complex members (Tokusumi et al., 2012).

In the **wing imaginal disc**, when overexpressing the Hh co-receptor Ihog in the Hh-sending cells, the lipid-modified Hh is localized on basolateral filopodia emerging from those cells and co-localize with Dlp and Disp (Callejo et al., 2011). In addition, Hh accumulates in Hh responding cells filopodia, where also Shf and Dally were shown accumulated (Bilioni et al., 2013).

In the the germline stem cells niche of the **ovary**, the supporting cap cells show Hh in filopodia-like structures oriented towards adjacent

escort cells where Hh is delivered to maintain the germline stem cell population (Rojas-Ríos et al., 2012).

In live **pupal abdominal histoblasts** Hh-producing cells emit filopodia with a reach-range that correlates with the Hh signaling gradient extension in space and time (Bischoff et al., 2013).

3. Structure and function of the Drosophila adhesion proteins Ihog, Boi and their vertebrate orthologs CDO and BOC

3. 1. Immunoglobulin superfamily

The Immunoglobulin superfamily comprises cell surface antigen receptors, co-receptors and adhesion proteins, which have in common the Immunoglobulin domains.

Due to the cytoneme stabilization mediated by its overexpression, in this work, we focus on the *Drosophila melanogaster* Interference hedgehog (**Ihog**) protein, which belongs to the Ihog subfamily, also comprised by Brother of Ihog (**Boi**) and the vertebrate members Cell adhesion molecule down-regulated by oncogenes (**CDO**) and Brother of CDO (**BOC**) (Yao et al., 2006).

3. 2. Structure and function of Ihog, Boi, CDO and BOC

Drosophila melanogaster **Ihog**, **Boi** and their vertebrate homologs **CDO** and **BOC** are single-pass type I transmembrane proteins of the Immunoglobulin superfamily with high sequence similarities. They are constituted by an extracellular part comprised of four (Ihog, Boi and BOC) or five (CDO) **Immunoglobulin (Ig) domains**, and two (Ihog and Boi: Fn1 and Fn2) or three (CDO and BOC: Fn1, Fn2 and Fn3) **Fibronectin type III (FNIII) domains**; a transmembrane domain

and an intracellular **cytoplasmic tail domain** with unknown structure and function (Figure I-5A; Kang et al. 2002; Yao et al. 2006).

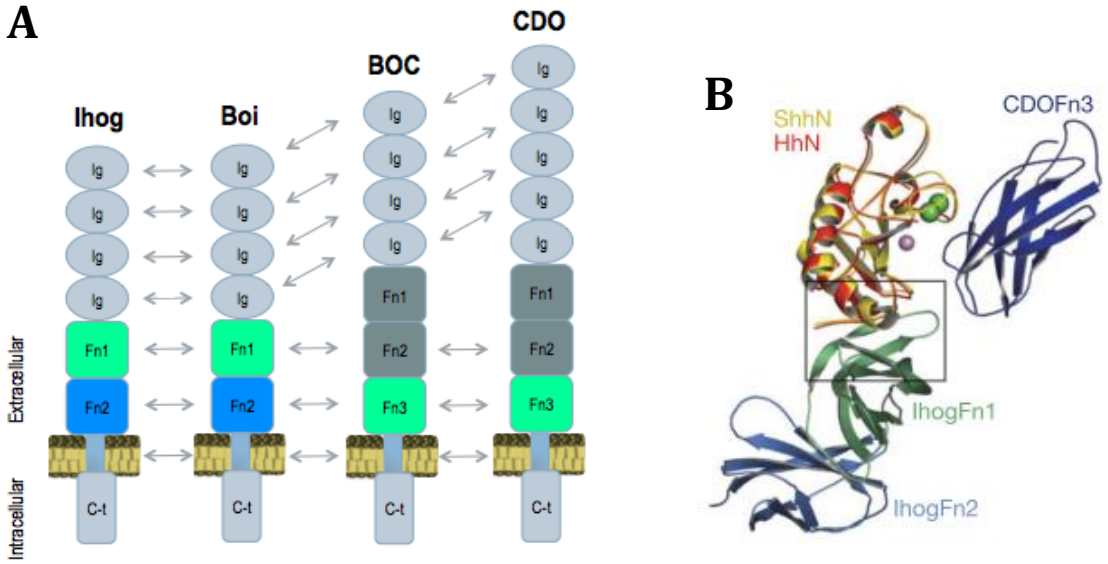

Figure I-5. Structure of the *Drosophila* adhesion proteins Ihog and Boi and its vertebrate orthologs CDO and BOC. **A)** Scheme depicting *Drosophila* Ihog and Boi and their vertebrate homologs BOC and CDO domains. Arrows indicate sequence similarities**.** Green indicates interaction with Hh ligands and blue with Ptc. **B)** Ihog-Hh and CDO-Shh different interactions (modified from McLellan et al., 2006).

Their interaction with the Hh ligands differs between orthologs (Figure I-5B). CDO interacts with Shh by a non-orthologous FNIII repeat (Fn3), which requires high levels of calcium (McLellan et al., 2008; Yao et al., 2006), while Ihog interacts with HhN by its first FNIII domain (Fn1) and requires heparin (McLellan et al., 2006; Yao et al., 2006). Ihog also interacts with Ptc by another FNIII domain, Fn2 (Zheng et al., 2010) and both FNIII domains (Fn1 and Fn2) have been demonstrated to be essential for Hh signaling in wing imaginal discs of flies (Zheng et al., 2010).

CDO and BOC function as co-receptors of Shh, being necessary for its long-range signaling (Allen et al., 2011; Kavran et al., 2010), as Ihog

and Boi for Hh in *Drosophila melanogaster* (Lum et al., 2003; Okada et al., 2006; Tenzen et al., 2006; Zhang et al., 2006). However, their expression differ from *Drosophila* orthologs, as they are only expressed in Shh-responding cells in the limb bud (Tenzen et al., 2006), while Ihog and Boi are expressed broadly in both the A and P compartments of wing imaginal discs of third instar larvae with a slight decrease at the AP compartment border (Bilioni et al., 2013; Camp et al., 2014; Yan et al., 2010; Zheng et al., 2010).

These proteins have redundant functions in Hh co-reception. Thus, *Drosophila melanogaster ihog*$^{-/-}$ or *boi*$^{-/-}$ and mice *cdo*$^{-/-}$ or *boc*$^{-/-}$ single mutants are viable, but result in mild effects: *ihog*$^{-/-}$ or *boi*$^{-/-}$ in Hh signaling *cdo*$^{-/-}$ in holoprosencephaly and *boc*$^{-/-}$ in axonal guidance, typical phenotypes of a reduced Shh signaling. Besides, *ihog*$^{-/-}$, *boi*$^{-/-}$ or *cdo*$^{-/-}$, *boc*$^{-/-}$ double mutants cause in all cases severe phenotypes (Allen et al., 2011; Camp et al., 2010; Izzi et al., 2011; Okada et al., 2006; Sanchez-Arrones et al., 2012; Tenzen et al., 2006; Yan et al., 2010; Zhang et al., 2011; Zhang et al., 2006; Zheng et al., 2010).

It has been described that Ihog interacts directly with the glypican Dally-like (Dlp), and with Hh and Ptc in the A compartment of wing imaginal discs (Kim et al., 2011; Yan et al., 2010; Yao et al., 2006). Indeed, Ihog is necessary for Ptc localization at the plasma membrane (Zheng et al., 2010) and required to maintain normal extracellular Hh levels in wing imaginal discs (Bilioni et al., 2013; Callejo et al., 2011; Yan et al., 2010). Ihog ectopically expressed is visualized on basolateral Hh signaling filopodia, or cytonemes (Bilioni et al., 2013; Bischoff et al., 2013; Callejo et al., 2011; Gradilla et al., 2014).

Objectives

The main goal of this work is to further analyze the contribution of specialized signaling filopodia (cytonemes) in Hh signaling pathway and gradient formation. For that purpose, we have used as paradigm the *in vivo* filopodia dynamics in the pupal abdominal histoblast cells during development. In addition, we have studied the genetic and molecular interactions between Hh signaling components and cytonemes in the third-instar larval wing imaginal disc epithelium. The following objectives were set out:

1. To analyze Hh cytoneme dynamics and their relationship with the morphogen gradient formation.
   1.1. To compare Hh-producing and Hh-receiving cells cytoneme dynamics.
   1.2. To study if the Hh ligand and the Ptc receptor are distributed on cytonemes.
   1.3 To analyze the response to Hh signaling activation using *ptc* expression as a readout.

2. To study Ihog function during wing disc and abdominal histoblasts development.
   2.1. To study Hh cytoneme dynamics under different conditions of gain-of-function or loss-of-function of Ihog.
   2.2. To characterize Ihog functional domains.
   2.3. To generate an Ihog transgenic line unable to interact with Hh.

3. To study Ihog possible interactions with proteins involved in both, the Hh signaling pathway and actin dynamics.

Materials and Methods

1. Drosophila melanogaster

1. 1. Drosophila melanogaster maintenance

Drosophila melanogaster stocks maintenance was done following the basic techniques described in Ashburner, 1989. Fly stocks were grown in a standard culture media containing glucose, yeast, agar, wheat, propionic acid and nipagin, and kept in incubation chambers with a controlled temperature (18ºC or 25ºC) and a relative humidity (60-75%). Fly crosses were kept at 18ºC until the desired time of expression induction.

1.2. Gal4/UAS/Gal80^{ts} system

Transient expression of most of the transgenic constructs used in this work was carried using the Gal4/UAS genetic system (Brand & Perrimon, 1993) together with the Gal4 repressor Gal80^{ts} (McGuire, 2003) in order to either over-express (Table MM-2) or down-regulate with RNA interference (RNAi) (Table MM-3) genes of interest in a spatio-temporal controlled manner. This is achieved making crosses between two transgenic lines: one containing the Gal4 sequence, which encodes the transcription factor Gal4 cloned downstream of a promoter of interest (Table MM-1) and the other transgenic line containing a gene cloned downstream of the UAS (Upstream Activation Sequence) sequence that the Gal4 will recognize and lead the expression of this gene (Figure MM-1). Therefore, the Gal4 protein will be produced in a specific region controlled by the upstream promoter, it will recognize and bind to the UAS sequence to activate the gene downstream in that specific region. At the permissive low temperatures (18ºC) the Gal4 repressor Gal80^{ts} is active, blocking the binding of the Gal4 protein to UAS sequences; though at restrictive high temperatures (29ºC) it is inactivated,

leading to Gal4-UAS binding and transcription of the gene downstream the UAS sequence. Consequently, fly progeny of the Gal4-UAS cross will express the gene of interest in a specific region and in a specific time of development.

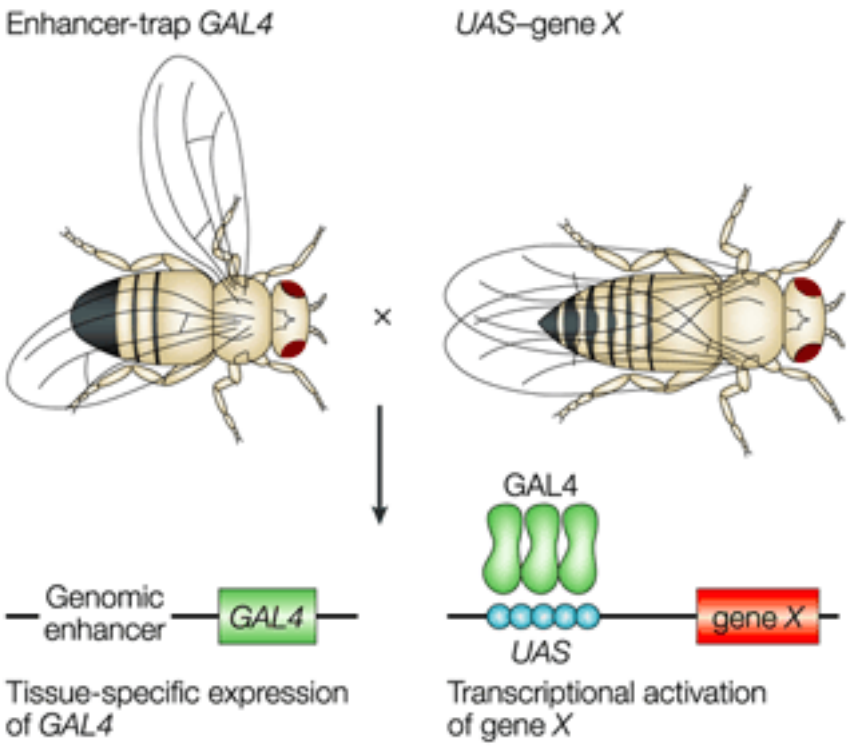

Figure MM-1. Gal4/UAS system. Cartoon depicting the Gal4/UAS system. Image taken from St Johnston 2002.

Table MM-1. Gal4/Gal80^{ts} lines

Genotype	Comments	Reference
tubGal80^{ts}	Gal80 termosensitive fused to *tubulin* promoter	BDSC
hh.Gal4	Gal4 fused to *hh* promoter	Tanimoto et al. 2000
ptc.Gal4	Gal4 fused to *ptc* promoter	Hinz et al. 1994
en.Gal4	Gal4 fused to *en* promoter, but expressed exclusively in the P compartment	Gift from Christian Dahman

Table MM-2. UAS-transgene lines for gain-of-function experiments

Genotype	Comments	Reference
UAS.GMA-GFP	Actin-binding domain of moesin fused to GFP	Bloor & Kiehart 2001
UAS.lifeact-GFP	Actin-binding peptide fused to GFP	BDSC 35544
UAS.lifeact-Ruby	Actin-binding peptide fused to Ruby	BDSC 35545
UAS.lifeact-RFP	Actin-binding peptide fused to RFP	BDSC 58716
UAS.CD4-GFP	CD4 fused to GFP	BDSC 35839
UAS.CD63-GFP	CD63 fused to GFP	Panáková et al. 2005
UAS.Flo2-RFP	*Flotillin 2 fused to RFP*	Bischoff et al. 2013
UAS.boi-YFP	Boi fused to YFP	Bilioni et al. 2013
UAS.ihog-YFP (1)	Ihog fused to YFP	Callejo et al. 2011
UAS.ihog-RFP	Ihog fused to RFP	Callejo et al. 2011
UAS.ihogΔIg-RFP (2)	Ihog Ig domains deleted, fused to RFP	Sánchez-Hernández 2013
UAS.ihogΔFN-RFP (1)	Ihog FN domains deleted, fused to RFP	Sánchez-Hernández 2013
UAS.ihogΔFn1	Ihog Fn1 domain deleted	Zheng et al. 2010
UAS.ihogFn2*	2 point mutations K653E and Q655E on Ihog Fn2-Ptc interacting region	Zheng et al. 2010
UAS.ihogΔFn2-HA	Ihog Fn2 domain deleted, fused to HA	Sánchez-Hernández (unpublished)
UAS.ihogΔCt-RFP (1)	Ihog Ct domain deleted, fused to RFP	Sánchez-Hernández 2013

(1) These constructs have an additional unintended point mutation (S697G) in the interdomain between the Fn2 and the transmembrane domains of Ihog, but it does not appear to affect Ihog function when comparing *UAS.ihog-YFP*-driven stabilization with a non-affected *UAS.ihog-RFP*.
(2) This construct has an additional unintended point mutation (D558G) in the Hh-interacting domain Fn1 of Ihog.

Table MM-3. UAS-RNAi lines for loss-of-function experiments

Genotype	Comments	Reference
UAS.Cpa-RNAi	RNAi against *Cpa*	VDRC 16731
UAS.Scar-RNAi	RNAi against *Scar*	BDSC 36121
UAS.Pico-RNAi	RNAi against *Pico*	VDRC 16371
UAS.Flo2-RNAi	RNAi against *Flo2*	VDRC 31525
UAS.αSMase-RNAi	RNAi against *αSMase*	BDSC 25283
UAS.Vps24-RNAi	RNAi against *Vps24*	BDSC 38281
UAS.Hrs-RNAi	RNAi against *Hrs*	BDSC 33900
UAS.TSG101-RNAi	RNAi against *TSG101*	BDSC 35710
UAS.CG31729-RNAi	RNAi against *CG31729*	VDRC 105987
UAS.Vps22 -RNAi	RNAi against *Vps22*	BDSC 38289
UAS.Ykt6-RNAi	RNAi against *Ykt6*	BDSC 38314
UAS.AnxB11-RNAi	RNAi against *AnxB11*	VDRC 29693
UAS.Vps4-RNAi	RNAi against *Vps4*	VDRC 105977
UAS.boi-RNAi	RNAi against *boi*	VDRC 108265
UAS.ihog-RNAi	RNAi against *ihog*	VDRC 102602

1. 3. Other Drosophila lines used in this work

Descriptions of mutations, insertions and transgenes are available at Fly Base (http://flybase.org).

The following tables contain the fly stocks used in this work: that carry fluorescent proteins fused to promoters or to the whole regulatory and coding sequences of a gene to visualize the endogenous-like expression of a gene or the protein product (Table MM-4), and mutant or the FRT lines used (Table MM-5).

Table MM-4. Wild type and endogenous-like fluorescent protein lines

Genotype	Comments	Reference
Bac-hh-GFP	Regulating and coding sequences of *hh* fused to GFP	Tom Kornberg (unpublished)
Bac-ptc-Cherry	Regulating and coding sequences of *ptc* fused to mRFPCherry	Tom Kornberg (unpublished)
ptc-trap-GFP	*ptc* pomoter fused to GFP	CB02030 FlyTrap

Table MM-5 Mutant / FRT lines

Genotype	Comments	Reference
hh^{ts2}	Mutant *hh* termosensitive allele	Ma et al. 1993
ptc^{16} FRT42D	Mutant *ptc* allele next to FRT42D	Capdevila et al. 1994
ubiRFPnls FRT42D	Ubiquitous nuclear RFP next to FRT42D	BDSC 35496

1. 4. The FLP/FRT system

The FLP/FRT system (Golic & Lindquist, 1989) consists in an enzyme flippase (FLP) that induces recombination between the FRTs (Flippase Recombination Target) sequences located either in the same chromosomal arm (cis-recombination) or in the same position of homologous chromosomal arms (trans-recombination, Figure MM-2).

Most of the gene mutants used in this work are lethal homozygous. Therefore, we study their mutant phenotype during development in mitotic recombinant clones. Only certain cell populations (clones) will have the mutation and some others will not, letting us compare wild type versus mutated territories. To induce random clones in the histoblasts nest tissue we heat shocked wandering third instar larvae just before becoming pupae for 1h at 37ºC, which is the temperature to activate the FLP. We used the nuclear *UbiRFP* and the *ptc^{16}* fly lines that carry the *FRT42D* in the same chromosomal position, so that the FLP recombines those chromosomes and give rise to *ptc^{16}* homozygous mutant clones (RFP negative) and wild-type *UbiRFP* homozygous clones (RFP positive) (Figure MM-2).

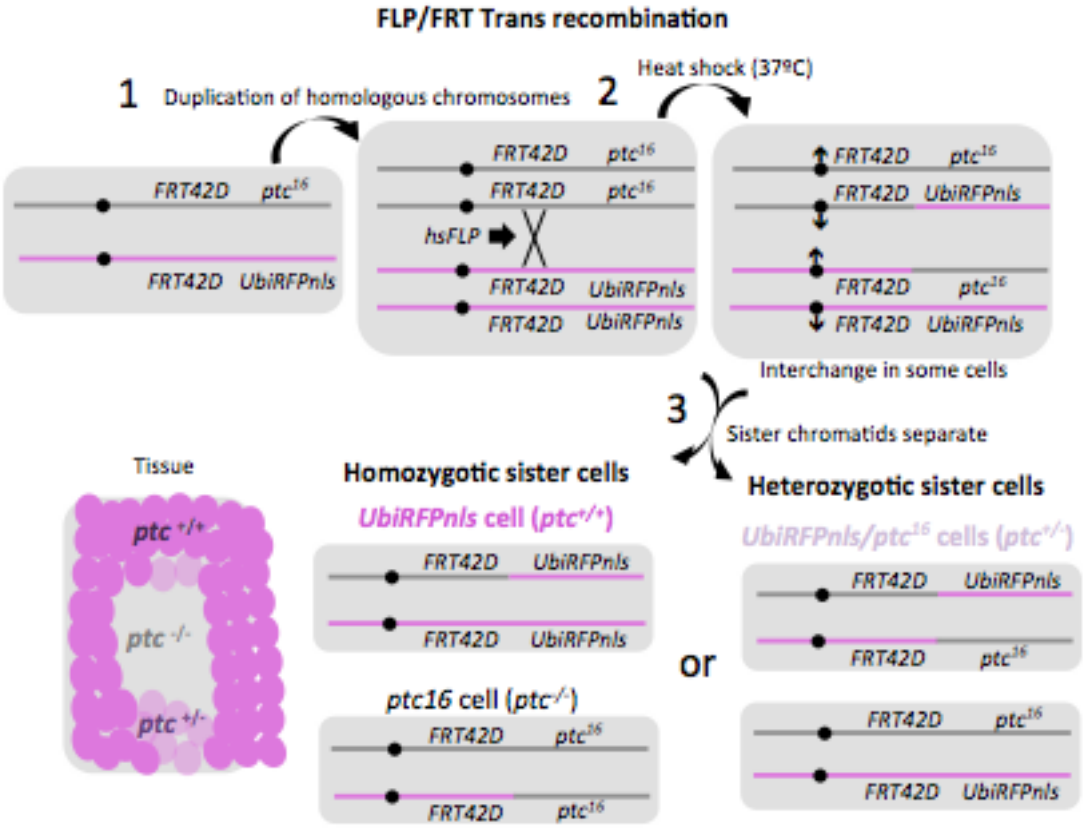

Figure MM-2. FLP/FRT trans recombination to induce mitotic clones. Cartoon explaining *ptc*^{16} clones using FLP/FRT system.

2. Analysis on fixed wing imaginal discs

2. 1. Immunohistochemistry of wing imaginal discs

Immunostaining of wing imaginal discs is performed in dissected third instar larvae and turned indise-out body, so that wing imaginal discs are exposed. After larvae dissection on ice-cold PBS to minimize cellular stress, we fix them 30 minutes on 4% paraformaldehyde in PBS 1X at room temperature (RT), wash them three times on PBT (PBS + Triton X-100 0,1%) for 15 minutes at RT, to permeabilize, blocking in 20mM glycine 30 minutes at RT and incubate with primary antibodies (Table MM-6) diluted in 2mM glycine overnight at 4ºC. After washing 15 minutes three times the primary antibodies with

PBT, discs were incubated with secondary antibodies (Table MM-7) diluted on PBT during 1 hour at RT on darkness. Finally, the samples were washed 3 times with PBT and 3 times with PBS 15 minutes each at RT and finally, wing imaginal discs were mounted on mounting medium Vectashield (Vector Laboratories).

Fixed and stained wing imaginal discs tissues were imaged using a LSM710 confocal microscope (Zeiss).

Table MM-6: Primary antibodies used in this work.

Antigen	Immunized animal	Working dilution	Reference
Hh	Rabbit	1:500	Bilioni et al., 2013
Ptc	Mouse	1:150	Capdevila & Guerrero, 1994
Ci	Rat	1:20	Gift from B. Holmgren
βPS	Mouse	1:50	DSHB CF.6G11

Table MM-7: Secondary antibodies used in this work.

Antigen	Immunized animal	Working dilution	Reference
Alexa 488	Rabbit/Mouse/Rat	1:400	ThermoFischer
Alexa 594	Rabbit/Mouse/Rat	1:400	ThermoFischer
Alexa 647	Rabbit/Mouse/Rat	1:400	ThermoFischer
Pacific Blue	Rabbit/Mouse	1:400	ThermoFischer

2. 2. Quantification of cytonemes and gradient extent in wing discs

Cytoneme and gradient extent were determined as described in Bischoff et al., 2013. To quantify the maximum extent of cytonemes, we measured the extent of the ten longest protrusions in the wing pouch, from the A/P border to the tip, using the ImageJ line tool. The

average extent of the ten longest cytonemes was used for the quantitative analysis. For gradient extent, an area of five cell diameters in height and 120 µm in length, covering the gradient and the A/P border in Ptc-promoter–trap::GFP images, was cropped out to calculate the plot profile using ImageJ.

3. Analysis of cytoneme dynamics

3. 1. In vivo imaging of pupal abdominal histoblasts

Live imaging of pupal abdominal histoblasts was performed using a chamber as described in Seijo-Barandiarán et al. 2015. We always used pupae of around 30h APF, when Hh morphogenetic gradient is being formed, to visualize Hh signaling filopodia from histoblasts of dorsal abdominal segment A2 moving towards the midline. These filopodia were filmed using a vertical laser scanning confocal microscope (Zeiss LSM710) at a room temperature. 40x oil immersion objectives where used taking Z-stacks in around 30 µm tissue thickness with a step size of 1 µm and time intervals of 2 minutes for all movies except for the *ptc*^{16} clone experiment, taken every 30 seconds. All imaged pupae developed into pharate adults and hatched normally.

3. 2. Manual tracking of cytonemes

Cytonemes were tracked using MTrackJ plugin of ImageJ (https://imagescience.org/meijering/software/mtrackj/). We took the base (track#1) and the tip (track#2) point coordinates of each cytoneme (cluster) and colored them by cluster, so that each cytoneme would be in a different color. Cytonemes were analyzed in a 30 minutes time-window in all movies, unless specified. We discarded those cytonemes that were not perfectly visible within the

whole 30 minutes movies because of the tissue movement or of the interference of the surrounding dying larval epithelial cells (as shown in Movie MM-1B). The tracking was done in a region of 49 μm x 76 μm for GMA cytoneme dynamics comparison between different genotypes in either Hh-producing or Hh-receiving cells; and in a region of 79 μm x 116 μm for the *ptc*^{16} mutant clone experiment, where only cytonemes from the *ptc* mutant and the wild-type territories delimited by the references shown in Movie MM-1C and Figure S-1 were used for statistical analysis.

3. 3. Data analysis of cytoneme dynamics

Using the (x, y) coordinates of the base and tip points of each filopodium given by the MTrackJ results; we calculated the elongation velocity, the retraction velocity and the lifetime as described below in 2.4.

We also calculated filopodium extent through this formula:

Filopodium extent (E): $E = \sqrt{(x_{tip} - x_{base})^2 + (y_{tip} - y_{base})^2}$

3. 4. Description of cytoneme dynamic models

We have distinguished two populations of cytoneme dynamics behavior (Figure R-5) in terms of how elongation or retraction velocities occur respect to the maximum extent of the cytoneme. Constant velocities to reach the maximum extent are measured as triangle-like (t), while velocities that reach an extent distinct but close to the maximum extent are classified as trapezoid-like (T). In this last situation, the maximum extent is included in a "stationary" phase where not much elongation or retraction occurs, where small cytonemes extent change rates are oscillating close to zero.

Therefore, we could have populations of cytonemes that behave as a triangle (elongating and retracting as a triangle, "tt"), as a trapezoid (elongating and retracting as a trapezoid, "TT"), or as a mixture of both (elongating as a triangle and retracting as a trapezoid, "tT"; or viceversa, "Tt"). For unknown elongation or retraction we have named it as "x".

The parameters measured are explained below using the triangle and trapezoid models.

2 phases triangle dynamics model:

Filopodia dynamics can be described with two phases: elongation and retraction (Figure R-5A).

In this model, the base of the triangle represents the filopodium lifetime; the elongation velocity (Ve) and the retraction velocity (Vr) correspond to the slopes of the triangle, that have been calculated from the experimental data connecting the filopodium origin and end with the maximum extent, respectively. The filopodium origin (and end) has been taken in the previous (and next) frame of the recorded data.

3 phases trapezoid dynamics model:

Filopodia dynamics can be described with three phases: elongation, stationary and retraction (Figure R-5B).

In this model, the base represents the filopodium lifetime, the slopes of the left and right sides of the trapezoid are the elongation velocity (Ve) and retraction velocity (Vr) respectively, which have been calculated respect to the stationary phase as follows:

The stationary phase is characterized by two main parameters: the average extent (Es) and average velocity (Vs), where Es is the

filopodium extent at the half lifetime, and Vs is the average of the velocities at the stationary phase.
The left trapezoid side is drawn by connecting the filopodium origin with the intersection point with Vs, which corresponds to the first experimental point equal or greater than Es. Equally, the right trapezoid side is drawn by connecting the filopodium end with the intersection point with Vs, which corresponds to the last experimental point equal or greater than Es.

To determine whether the elongation type is triangle or trapezoid, we first measured the stationary average extension velocity (Vse) as the average of the individual elongation velocities in the stationary phase. Then, if the first elongation velocity is larger than two times Vse, the filopodium elongates as a triangle. Otherwise, it elongates as a trapezoid. We used an equivalent criterion for the retraction after measuring the stationary average retraction velocity (Vsr) as the average of the individual retraction velocities in the stationary phase.

3. 5. Statistical analysis of cytoneme dynamics

We used R (http://www.R-project.org) to perform the Shapiro-Wilk normality test to address whether data followed a standard normal distribution. As data do not follow a normal distribution, we proceed to make a Mann-Whitney-Wilcoxon test of homogeneity of variances by pairwise comparisons using Wilcoxon rank sum test to test for significant differences between genotypes.

For statistical analysis of cytoneme dynamics comparing different genotypes expressed in Hh-producing or Hh-receiving cells we used the "N" numbers of cytonemes in all movies of each experiment, included in Table MM-8.

Table MM-8. Number of cytonemes and pupae filmed by genotype

Genotype	# Pupae	#Cytonemes (*)
ptc.Gal4>UAS.GMA-GFP 24h	4	104 (72 Ve, 94 Vr)
hh.Gal4>UAS.GMA-GFP 24h	4	100 (79 Ve, 82 Vr)
ptc.Gal4>UAS.GMA-GFP, UAS.ihog-RFP 24h	*4*	47 (28 Ve, 36 Vr)
hh.Gal4>UAS.GMA-GFP, UAS.ihog-RFP 24h	*4*	75 (30 Ve, 18 Vr)
ptc.Gal4>UAS.GMA-GFP 48h	1	18 (16 Ve, 17 Vr)
ptc.Gal4>UAS.GMA-GFP, UAS.ihog-RNAi, UAS.boi-RNAi 48h	2	31 (23 Ve, 21 Vr)
hh.Gal4>UAS.GMA-GFP 48h	2	56 (42 Ve, 47 Vr)
hh.Gal4>UAS.GMA-GFP, UAS.ihog-RNAi,UAS.boi-RNAi 48h	2	89 (60 Ve, 74 Vr)
hh.Gal4>UAS.GMA-GFP+UAS.ihogΔIg-RFP 24h	5	38 (22 Ve, 22 Vr)
hh.Gal4>UAS.GMA-GFP+UAS.ihogΔFN-RFP 24h	6	108 (80 Ve, 108 Vr)
hh.Gal4>UAS.GMA-GFP+UAS.ihogΔCt-RFP 24h	3	24 (0 Ve, 0 Vr)
hh.Gal4>UAS.GMA-GFP+UAS.ihogΔFn2-HA 24h	4	134 (105 Ve, 109 Vr)
hh.Gal4>UAS.GMA-GFP+UAS.ihogFn2* 24h	4	75 (9 Ve, 26 Vr)
ptc.Gal4>UAS.GMA-GFP+UAS.ihogΔIg-RFP 24h	4	33 (24 Ve, 30 Vr)
ptc.Gal4>UAS.GMA-GFP+UAS.ihogΔFN-RFP 24h	4	39 (32 Ve, 34 Vr)
ptc.Gal4>UAS.GMA-GFP+UAS.ihogΔCt-RFP 24h	4	57 (20 Ve, 28 Vr)
ptc.Gal4>UAS.GMA-GFP+UAS.ihogΔFn2-HA 24h	4	108 (96 Ve, 84 Vr)
ptc.Gal4>UAS.GMA-GFP+UAS.ihogFn2* 24h	2	25 (15 Ve, 11 Vr)

(*) Total measured cytonemes were used for maximum extent and lifetime values, while only cytonemes with recorded elongation or retraction phases during the filmed time period were used for statistical analysis of elongation (Ve) and retraction (Vr) velocities.

For statistical analysis of Emax of Hh-producing cytoneme dynamics either crossing *ptc*$^{-/-}$ mutant or wild-type territories we compared 23 cytonemes crossing *ptc*$^{-/-}$ mutant clone territory with 29 cytonemes crossing wild-type territory of 1 pupa. For statistical analysis of Ve and Vr we used that data from 17 cytonemes crossing wild-type territory and 14 cytonemes crossing *ptc*$^{-/-}$ mutant territory, in all cases cytonemes have an elongation and a retraction phase.

4. ihogFn1* variant with impaired Hh interaction

4. 1. Mutagenesis

In order to obtain a *Drosophila* transgenic line of Ihog with impaired interaction with Hh (*UAS.ihogFn1*Hh*), we have induced three aminoacid changes by point mutations in the *ihog* complementary DNA (cDNA), at three sites of the first FNIII domain (Fn1) that make hydrogen bonds with Hh (Figure MM-3; McLellan et al. 2006).

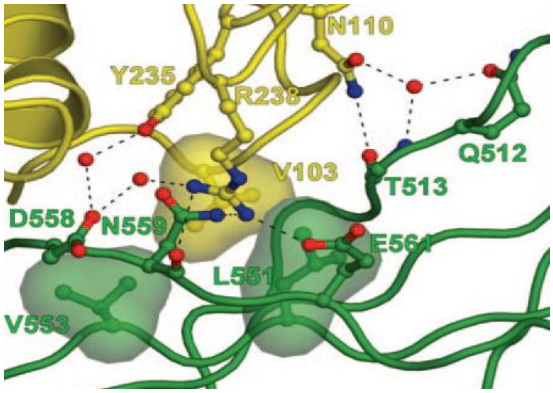

Figure MM-3. Fn1 domain of Ihog interacts with Hh. Image depicting the Hh-Ihog interactions. Hh residues are represented in yellow and IhogFn1 residues in green. Red spheres represent bridging waters and dashed lines represent hydrogen bonds. Image taken from McLellan et al. 2006.

With the expertise advice of the bioinformatics facility of the CBMSO, we have chosen the following three point mutations in order to impair Hh-Ihog interaction but not alter Ihog structure:

D558N (GAC→AAC) changing aspartic acid by asparagine

N559S (AAT→GTA) changing asparagine by serine

E561Q (GAA→CAA) changing glutamic acid by glutamine

Mutagenesis was done by Polymerase chain reaction (PCR) using the cDNA of *ihog* cloned before in the pENTRY vector (Gateway®, Invitrogen) in our laboratory (Callejo et al., 2011). PCR was done with forward primer designed including the three nucleotides changes and the rest of the sequence aligns with *ihog* sequence, while reverse primer is designed containing the exact sequence of *ihog* that aligns with the complementary strand. Therefore, PCR product must be the entire *pENTRY-ihog* sequence containing the three point mutations.

Primer sequences are:
Forward: 5′ TCCAACAATAACAGTAAGCAAAGTAATACCTCG 3′
Reverse: 5′ GTAAACGGCTAGGATGCGGAAACGATAGGTGTG 3′
Nucleotide changes are underlined.

Primers were first phosphorylated by the enzyme T4PNK (Takara 2021K) during 1h at 37ºC. The reaction was posteriorly inactivated at 65ºC during 20 minutes.

PCR conditions: 1 cycle of 5 minutes at 95ºC for denaturalization of *pENTRY-ihog*; 35 cycles that consist in denaturalization 45 seconds at 95ºC, primers alignment during 90 seconds at 55ºC, and extension during 10 minutes at 72ºC; and a final cycle of 15 minutes extension at 72ºC. We use the PFU polymerase kit (BioTools 10512).

PCR product is subjected to digestion with the enzyme DpnI (Takara 1235A) in TBuffer during 1h at 37ºC to eliminate methylated DNA template and keep only the PCR product. Then we circularized the PCR product binding the phosphorylated ends using the enzyme T4 DNA ligase (Promega M1804) overnight at 4ºC. Finally, this DNA was transformed in DH5α bacteria and grown in LB kanamycin, due to *pENTRY* resistance to kanamycin. Then we isolated the plasmid

*pENTRY-ihogFn1*Hh* with Viogene® kit and verified the mutations by sequencing in the facility of "Parque Científico" of the University.

In order to verify the whole sequence of *ihog* in the mutated plasmid *pENTRY-ihogFn1*Hh* we used the following primers:
1- "forFN" 5' CAAGCAGATTCAGGAACCCC 3' (binding sites: 1317-1336 of *ihog*, after the fourth Ig domain sequence)
2- "F630" 5' TCTTTTTCTAAGCAATGTATCCTCC 3' (binding sites: 630-654 of *ihog*, after the second Ig domain sequence)
3- "F1521" 5' CGCAAGAACTGGCAGAC 3' (binding sites: 1521-1538 of *ihog*, before Fn1 sequences known to interact with Hh)
4- "M13Rv" 5' CAGGAAACAGCTATGAC 3' (recognizes the attL2 sequence of *pENTRY* that aligns with the complementary strand)
5- "M13Fw" 5' GTAAAACGACGGCCAG 3' (recognizes before the attL1 sequence of *pENTRY*)

After sequence verification, the mutated DNA of *ihog* has been changed from the *pENTRY* to the *pDESTINATION* vector by "LR" reaction using the enzyme Clonase II (Gateway®, Invitrogen). To get our Ihog variant fused to RFP in its C terminus, we are using the *pDESTINATION* with the RFP tag (*pTWR*, Gateway®, Invitrogen).

This construct has been transformed in DH5α bacteria and grown in LB with ampiciline, due to *pTWR* resistance to ampiciline. The sequence has been verified for further injection in *Drosophila* embryos by the transgenesis facility of CBMSO to get the transgenic fly line of *UAS-ihogFn1*-RFP*.

4. 2. Analysis in silico of Hh-Ihog interaction

With the aim to analyze *in silico* if changes for *UAS.ihogFn1*Hh* could modify Ihog-Hh interaction, the bioinformatic facility of the CBMSO performed an analysis using MM/GBSA to probe the energy of Hh interaction in 250 samples taken every 20 ns for the wild type Ihog and for the Ihog variant containing the three point mutations described in 3.1.

Results

1. Dynamics of Hh cytonemes and its relationship with the Hh morphogenetic gradient formation.

Studies in fixed samples of *Drosophila melanogaster* larval wing imaginal discs showed that actin-based signaling filopodia (cytonemes) located in the basal surface of Hh-producing cells carry Hh along them towards Hh-receiving cells (Callejo et al., 2011; Bilioni et al., 2013; Bischoff et al., 2013). Likewise, Hh-receiving cells present basal cytonemes towards Hh-producing cells, in which the Hh ligand is also visualized. Additionally, different proteins involved in Hh signaling, such as Disp, Dlp, Dally and Shf, have been shown located along these specialized filopodia in fixed tissues but most of them are only visualized by *ihog* overexpression (Callejo et al., 2011; Bilioni et al., 2013; Bischoff et al., 2013).

In this work, we have mainly analyzed *in vivo* the dynamics of Hh signaling filopodia emanating from either the signal-producing or signal-receiving cells of pupal abdominal histoblasts attempted to elucidate their role in Hh morphogenetic gradient formation. We have also analyzed fixed wing imaginal discs that allowed us to visualize Hh signaling components in cytonemes by immunohistochemistry experiments.

1.1. Actin dynamics and exosomes machinery regulate Hh signaling.

The way dually lipidated Hh is being transported in aqueous extracellular environment is under debate (reviewed in Simon et al. 2016). Our laboratory suggests Hh transports via multivesicular

bodies (MVBs) through actin-based filopodia (cytonemes). To test this hypothesis, we carried on disturbance of components of the actin polimerization and vesicular traffick machineries in order to test for effects in the formation of Hh morphogenetic gradient.

For that purpose, we have used **RNA-mediated interference (RNAi)** against the following **actin-binding proteins**: the **Cpa** subunit of the Capping protein (CP), which inhibitis addition or loss of actin monomers to actin filaments by restricting its accessibility (Cooper & Sept, 2008); **Scar/WAVE** involved in the generation of filopodia (Kunda et al., 2003); **Pico**, which interacts with Ena/VASP actin regulators for emission of lamellipodia (Lyulcheva et al., 2008). RNAi knockdown of all these proteins in the **P compartment** significatively **shortened cytoneme and Hh gradient extent** compared to controls with and without co-expression of fluorescently labelled Ihog (Figure R-1a–d,g–j; Figure R-2a,b; Bischoff et al., 2013). Likewise, knockdown of the scaffold component of lipid raft microdomains Flotillin 2 (Flo2) in P compartment cells led to the same phenotype (Figure R-1f,l; Figure R-2a,b; Bischoff et al., 2013) opposite to its ectopic expression, which produced longer cytonemes and extended Hh gradient (Figure R-1e,k; Figure R-2a,b; Bischoff et al., 2013). This agrees with the observation that overexpression of Flo2 induces filopodia-like protrusions in various cell lines (Neumann-Giesen et al., 2004).

An interesting result was that in all cases, **ectopic** expression of ***ihog*** in the **P compartment** led to a **shortening** of the Hh signaling **gradient**, as shown with the construct of the *ptc* promoter fused to the Green Fluorescent Protein (Ptc-promoter–trap::GFP) (Figure R-2d; Bischoff et al., 2013).

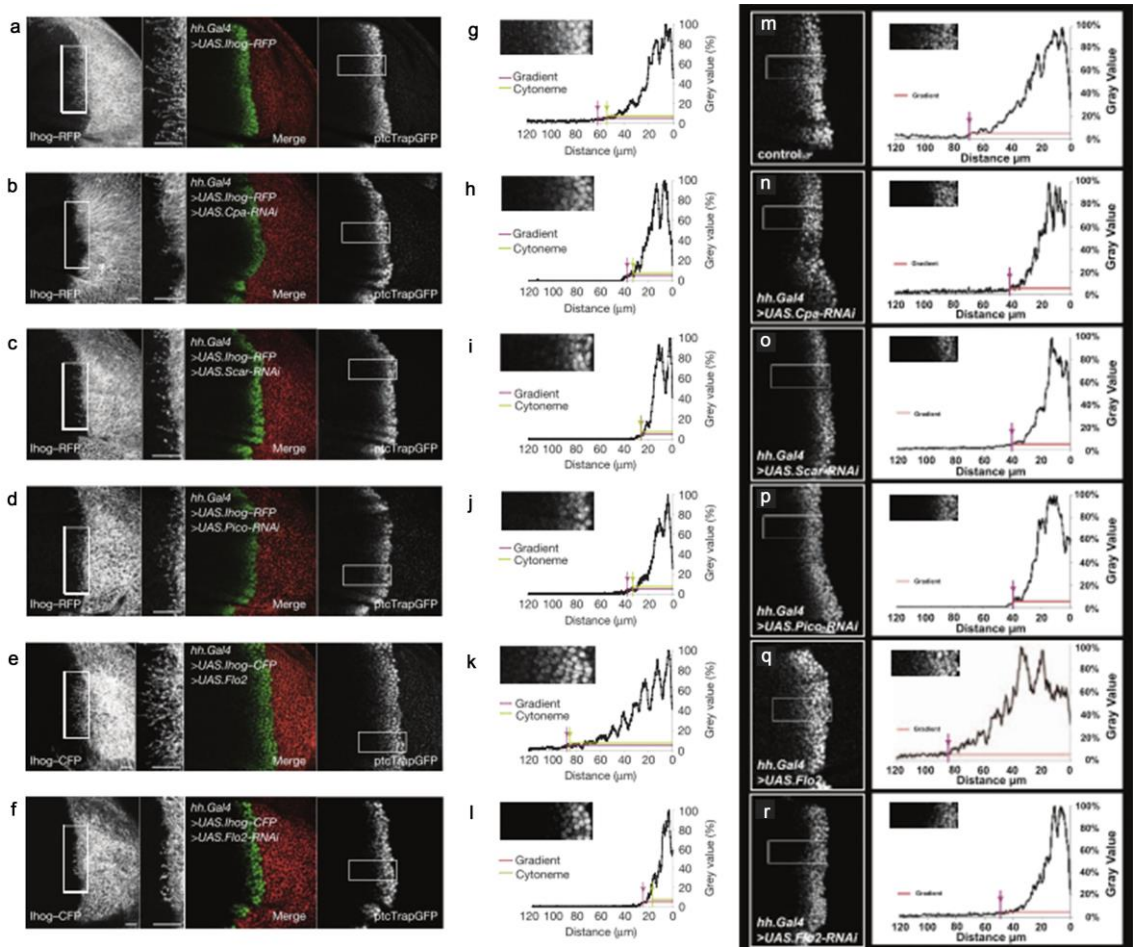

Figure R-1. Interfering with actin-binding proteins affects Hh cytonemes and gradient extension. **a-f:.** Confocal images of fixed larval wing discs expressing Ihog-RFP in Hh-sending cells (hh.Gal4) as a control (a) or co-expressing RNAi- or UAS- constructs (b-f). (b) Cpa-RNAi and Ihog–RFP. (c) Scar-RNAi and Ihog–RFP. (d) Pico-RNAi and Ihog–RFP. (e) UAS.Flo2 and Ihog–CFP. (f) Flo2-RNAi and Ihog–YFP. In all of them, left panel shows basal view of Ihog and detail showing cytonemes in the adjacent panel; the Hh activity gradient is visualized using Ptc-promoter–trap::GFP on the right panel; and merge of both channels is shown in the centre. Scale bars: 20µm. In the RNAi wing discs (b–d,f), both the cytonemes and the gradient are shorter than in the control (a). In UAS.Flo2 wing discs (e), the cytonemes and gradient are longer than in the control (a). **g-l:** Quantification of gradient extent in the wing discs shown in a–f using profile plots. The graphs depict the vertically averaged pixel intensities along the horizontal (A–P) axis of the detail of the Ptc-promoter–trap::GFP image shown in the top left corner. The red arrows indicate the extent of the gradient and green arrows show the average extent of cytonemes. Scale bars: 20µm. **m-r:** Hh signaling gradient by Ptc-promotor-trap::GFP expression in Control (**m**) and interference in P compartment with *Cpa* (**n**) *Scar*. (**o**) *Pico* (**p**) *Flo2* (**r**) or overexpressing *Flo2* (**q**) without overexpression of *ihog*. Left panels show the Hh signaling gradient and right panels the quantification of gradient extent using profile plots. In the RNAi expressing wing discs (n-p,r), the gradient is shorter than in the control (m). In *UAS.Flo2* wing discs (q), the gradient is longer than in the control (m). In all images, anterior is to the left. Images modified from Bischoff et al., 2013.

Remarkably, there is a **strong positive correlation between cytoneme reach and gradient extent** in all experiments (Figure R-2c), which strongly suggests that cytonemes play a role in Hh gradient establishment.

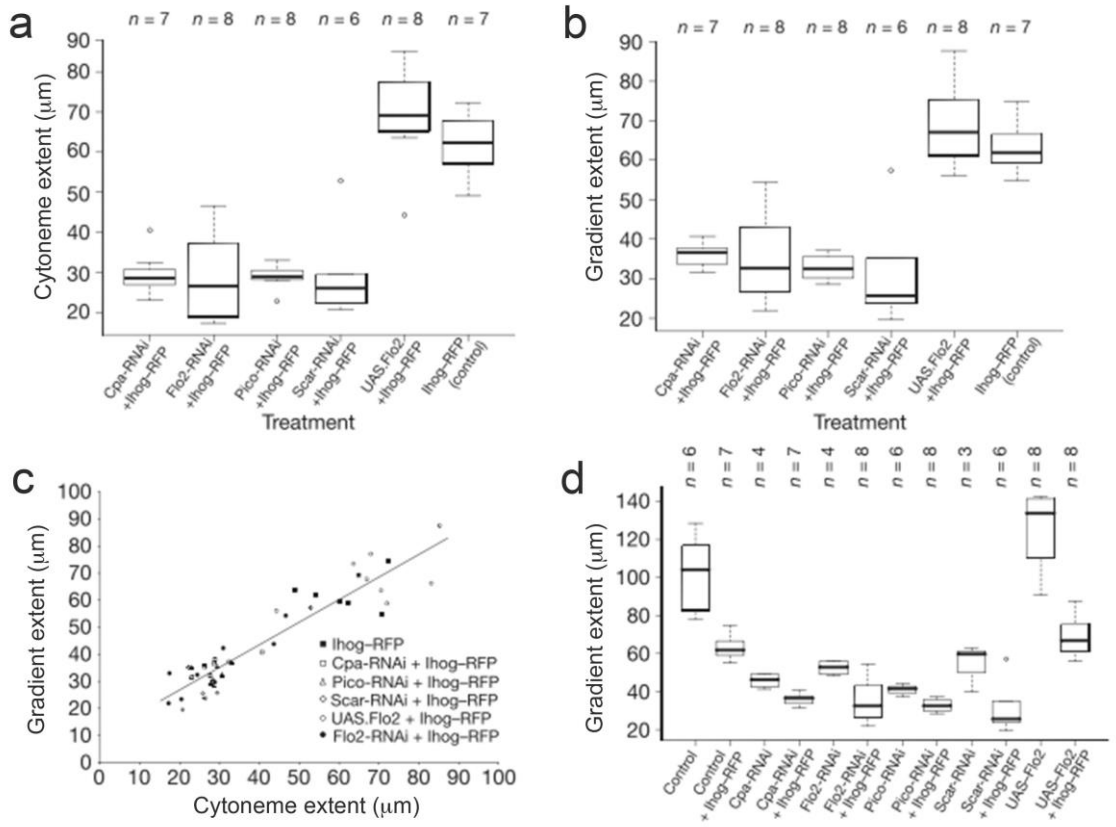

Figure R-2. Interfering with actin-binding proteins affects Hh cytonemes and gradient extension in wing imaginal discs. (**a**–**c**) Statistical analysis of the effect of interfering with the function of actin-binding proteins. (**a**) Box plots comparing cytoneme extent between control discs and treatments affecting cytoneme formation under *ihog* overexpression conditions in the Hh-producing cells. The boxes show the median and the interquartile range. The whiskers show the minima/maxima, or 1.5 times the interquartile range if outliers are present. Four RNAi treatments reduced cytoneme extent significantly compared with *UAS.Ihog–RFP* (Kruskal–Wallis test, $P<0.001$ and pairwise Wilcoxon rank sum test, $P<0.01$). Overexpression of Flo2 increased cytoneme extent in some individuals, but with no overall significant difference from *UAS.Ihog–RFP*. (**b**) Box plots comparing gradient extent between control discs and treatments. As for cytoneme extent, there were significant differences between *UAS.Ihog–RFP* and the four RNAi treatments (Kruskal–Wallis test, $P<0.001$ and pairwise Wilcoxon rank sum test, $P<0.01$). The longest gradients were obtained in *Flo2* overexpression. (**c**) Scatter plot of gradient extent against cytoneme extent, showing strong correlation (Spearman's $\rho = 0.89$, $n = 44$ wing discs; $P<0.001$). (**d**) Box plot showing gradient extent in control discs, *RNAi* treatments and *UAS.Flo2* treatment when co-expressed with *UAS.Ihog–RFP* or expressed alone in Hh-producing cells. Expression of *UAS.Ihog–RFP* shortens the gradient (Wilcoxon rank sum test; $P<0.001$). As for *ihog* overexpression experiments (**b**), there are significant differences between the wild type and treatments without *ihog* overexpression (Kruskal–Wallis test; $P<0.001$ and Wilcoxon rank sum test; $P<0.05$). Images modified from Bischoff et al., 2013.

Next, we **interfered** with components of the endosomal sorting complexes required for transport **(ESCRT) machinery** (reviewed in Raposo & Stoorvogel 2013): **ESCRT-0** component **Hrs** (Hepatocyte growth factor–associated tyrosine kinase) involved in the formation of MVBs; **ESCRT-I** component **TSG101** involved also in the production of MVBs acting as a bridge between the ESCRT-0 and ESCRT-II complexes; **ESCRT-II** component **Vps22** involved in the formation of MVBs and delivery of ubiquitin tagged proteins to the endosome; **ESCRT-III** component **Vps24** involved in protein sorting into the MVBs. We also interfere with **Vps4**, involved in the stripping of ESCRT components; the ESCRT-independent sorting protein **αSMase** (Trajkovic et al., 2008); the *Drosophila* homologous for the P4-ATPase (**CG31729**), TAT-5 in C. elegans shown to regulate the budding of exovesicles (EVs) from the plasma membrane (Wehman et al., 2011); and the SNARE (Soluble NSF Attachment Protein Receptor) complex component **Ykt6**, known to be involved in the release of EVs containing Wingless (Wg) (Gross et al., 2012).

All these RNA interference experiments **altered expression** of the Hh targets **Ptc** (Figure R-3a–d) and **Ci** (Figure R-3e–h), indicating a role of vesicular traffic in short-range and long-range Hh signaling (Gradilla et al., 2014).

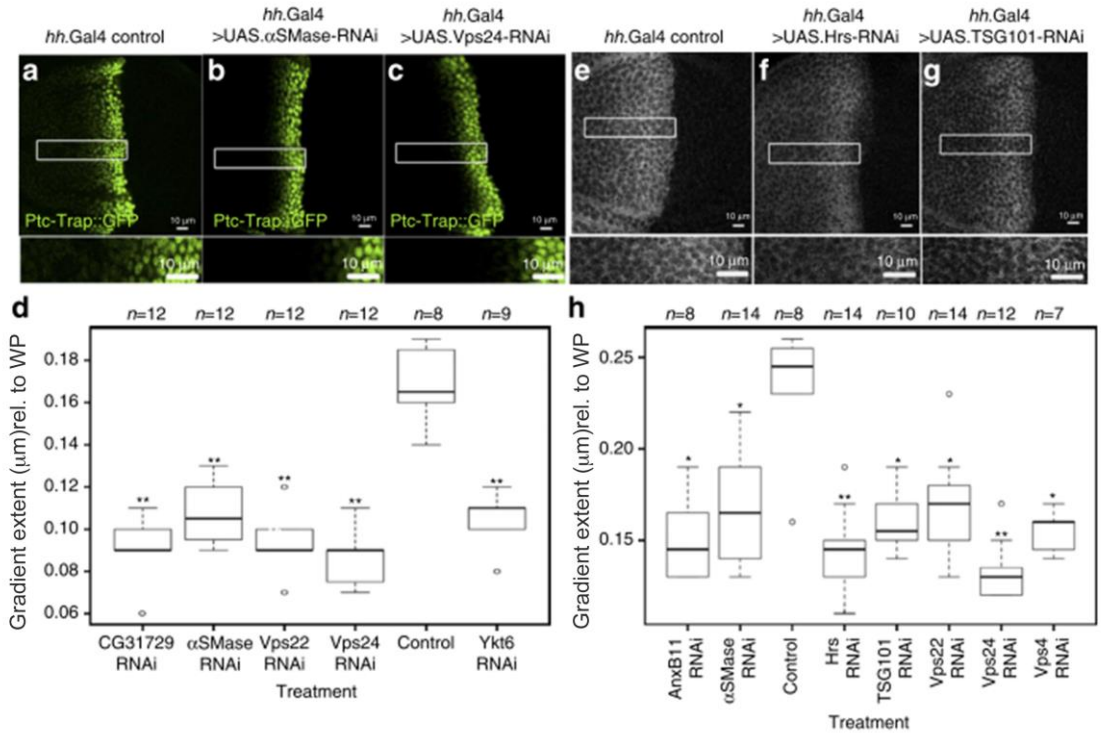

Figure R-3. Interfering with vesicular traffic proteins affects Hh gradient extension. **a–h**: Hh signaling in wing discs expressing RNAi treatments in the P compartment (**b–d,f–h**) and control (**a,e**), visualized in the A compartment using the Ptc-promotor-Trap::GFP reporter (**a–d**) and immunolabeling for the long-range target Ci (**e–h**). Detail shown at the bottom and anterior is to the left. Note in RNAi wing discs (**b–d,f–h**) that gradients are shorter than in controls (**a,e**). Scale bars: 10 µm. **d,h**: Box plots comparing gradient extent relative to the wing pouch (WP) length, between control discs and treatments for each reporter. (**i–l**). Significance levels for pairwise tests (Tukey HSD or Wilcoxon, depending on Normality of data): $^{+}$P<0.1, *P<0.05,**P<0.01, ***P<0.001. Images modified from Gradilla et al., 2014.

1.2. Hh-producing and Hh-receiving cells emit similar dynamic cytonemes

Live imaging of *Drosophila melanogaster* pupal abdominal histoblasts revealed that P compartment **Hh-producing cells** produce **highly dynamic filopodia** oriented **towards** the A compartment **Hh-receiving cells**, easily visualized when expressing the Green Fluorescent Protein (GFP) fused to the actin-binding domain of moesin (**GMA**) (Figure R-4B; Movie R-1A). These GMA-labeled filopodia are **less dynamic** when co-expressing **Ihog** (Figure R-4D; Movie R-1B), stabilized for up to 9.5h (Bischoff et al., 2013).

Similarly, **Hh-receiving** abdominal histoblast **cells** produce **highly dynamic protrusions** oriented **towards** the **Hh-producing cells** visualized with GMA (Figure R-4A; Movie R-2A). The GMA-labeled filopodia are **less dynamic** when they co-express **Ihog** (Figure R-4C; Movie R-2B), as was previously described when co-expressing Ihog in the Hh-producing histoblasts.

Performing a detailed analysis of filopodia dynamics, we have been able to distinguish two different **dynamic behaviors**: one of filopodia elongating and retracting at constant velocities, which we have classified as "**triangle dynamics**" and another one with a "stationary" interphase between the elongation and retraction phases, which we have classified as "**trapezoid dynamics**" (Figure R-5; see Materials and methods).

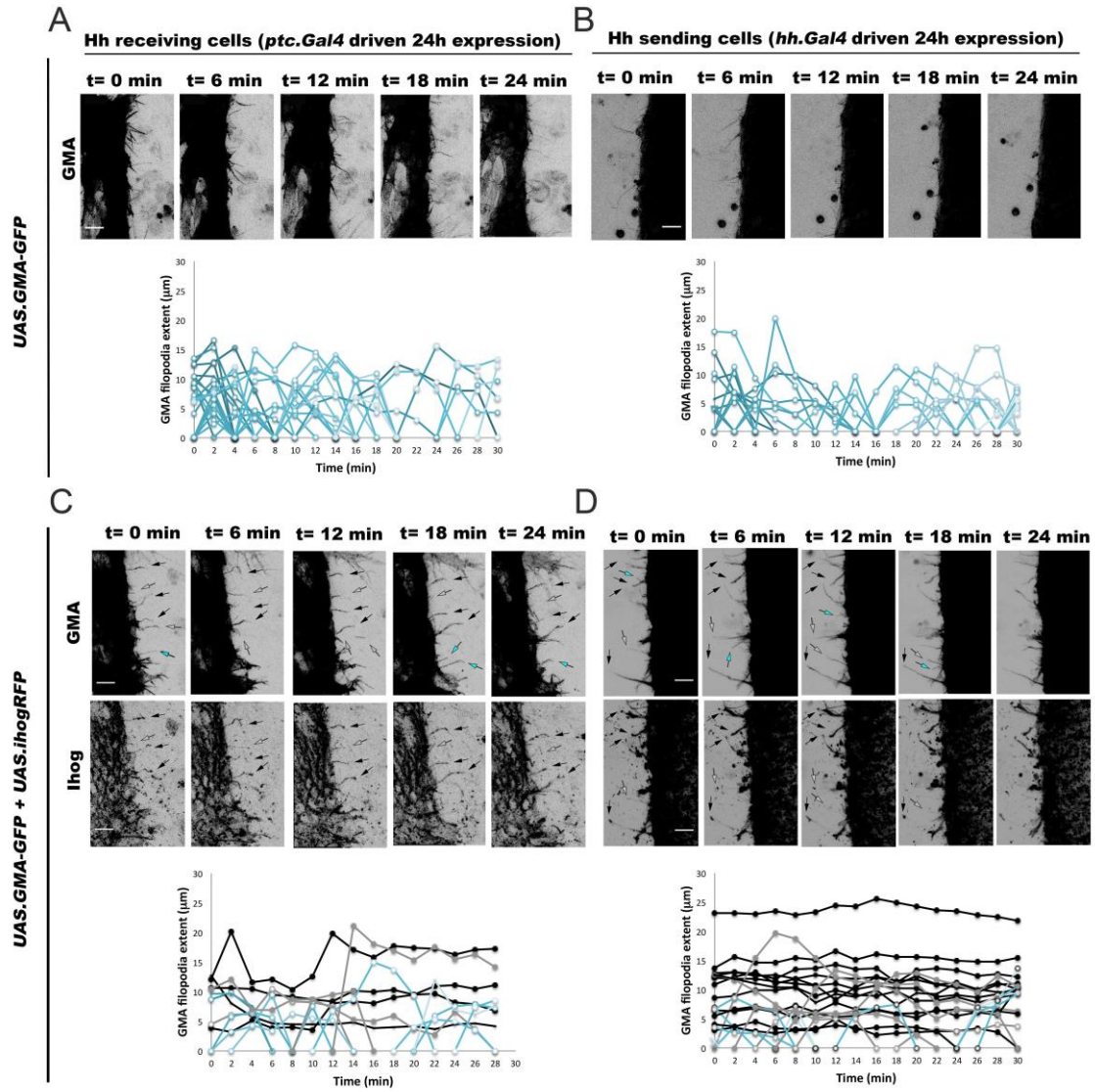

Figure R-4. Hh-producing and Hh-receiving histoblasts emit similar dynamic cytonemes. Five time frames from Movie R-1 and Movie R-2 are shown on the upper part of B,D and A,C, respectively. Hh-producing cells (B, D) and Hh-receiving cells (A, C) show highly dynamic cytonemes expressing GMA (top panels of A and B) and more stabilized cytonemes co-expressing GMA (top panels of C and D) with Ihog (bottom panels of C and D). Scale bars represent 10 µm. Graphs representing GMA cytonemes extent over time are shown in the bottom part of A, B, C and D. Notice that cytonemes with high levels of Ihog (black arrows on pictures) are more stable (black curves on graphs) than those with lower levels (grey arrows and grey curves) or in absence (cyan arrows and cyan curves) of Ihog.

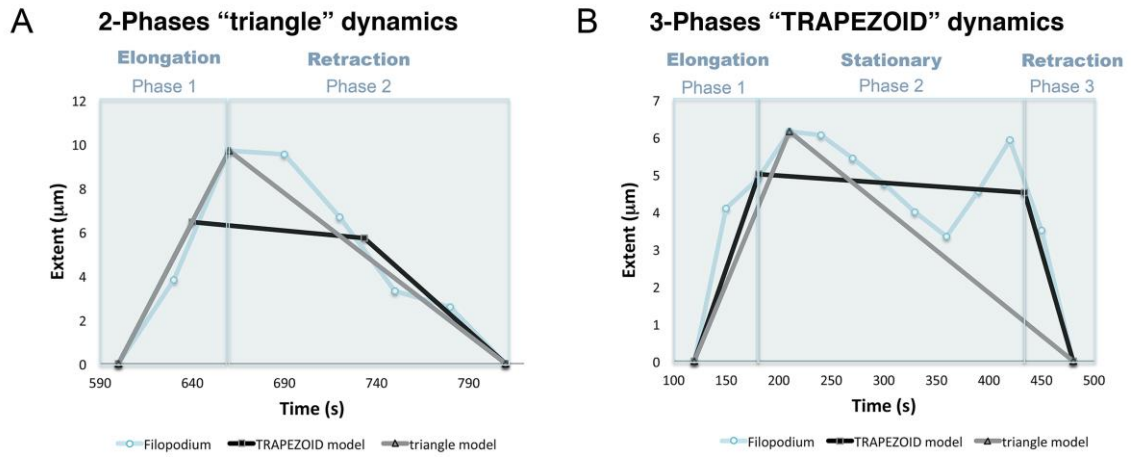

Figure R-5. Cytoneme dynamics models. **A: 2-Phases "triangle" dynamics.** Experimental data obtained from a filopodium extent over time is represented on light blue; its TRAPEZOID model curve is represented in black and its triangle model curve on grey. Notice that the 2-Phases filopodium dynamics are more similar to the triangle model with an elongation and retraction phase thatn to the TRAPEZOID model. **B: 3-Phases "TRAPEZOID" dynamics.** Data obtained from from a filopodium extent over time is represented on light blue; its TRAPEZOID model curve is represented on black and its triangle model curve on grey. Notice that the 3-Phases filopodium dynamics are more similar to the TRAPEZOID model with a stationary phase between the elongation and retraction phases than to the triangle model.

Both signal and receptor histoblast cells emit dynamic protrusions with similar percentages of triangle and trapezoid dynamics, they are distributed overall the A/P axis and are oriented towards A or P cells (from A or P cells, respectively) in a range between -90ºC to 90ºC, being 0ºC straight towards A or P cells (Figure S-2 compare A with B). Ectopic expression of *ihog* does not change distribution of filopodia or their angles, but does change their dynamics, as **Ihog-coated filopodia** behave more **like trapezoids** with a "stationary" phase between elongation and retraction phases in either Hh-sending or Hh-receiving cells, compared to non-overexpressing *ihog* cells (Figure S-2, compare C and D with A and B).

Expressing GMA in either Hh-producing or Hh-receiving cells, filopodia have **similar values** of average **maximum extent**, **lifetime**, **elongation** (Ve) and **retraction** (Vr) **velocities** with no statistical significant differences between signal-receptor cells (Figure R-6; Table R-1). The maximum extent of filopodia is similar with or without co-expressing *ihog* (Figure R-6A). Besides, this overexpression changes filopodia dynamics. Filopodia **lifetime** values are **higher** for filopodia with **high levels of Ihog** than those with low levels (Figure R-6B). However, in our 30 minutes recording, some filopodia with high levels of Ihog are very stable and we cannot visualize their elongation and retraction phases. Therefore, we could only compare elongation and retraction velocities for those with normal or moderate levels of Ihog. These velocities are similar for Hh-producing and for Hh-receiving cells filopodia (Figure R-6C).

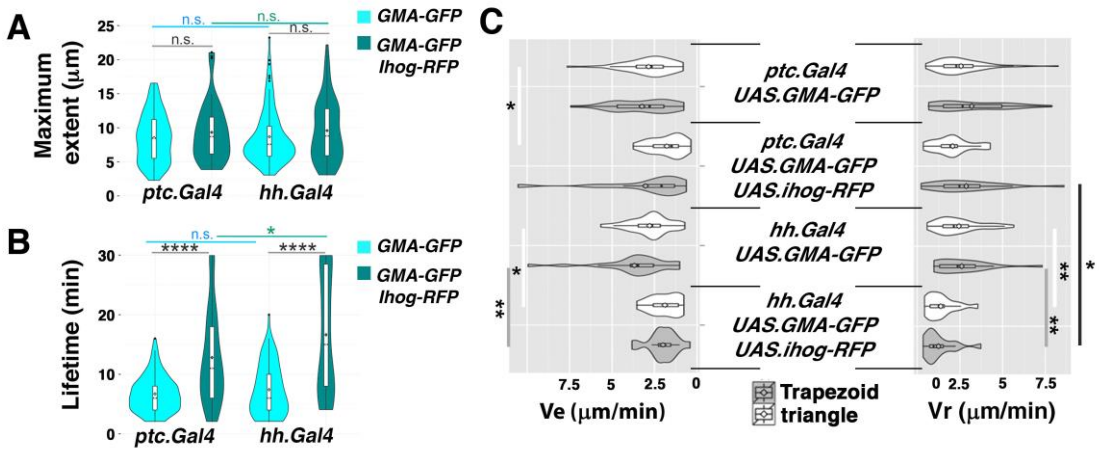

Figure R-6. Hh-producing and Hh-receiving cells cytonemes have similar dynamics. Statistical analysis of cytoneme dynamics of Hh-sending (*hh.Gal4* driver) and Hh-receiving (*ptc.Gal4* driver) cells expressing *GMA* or co-expressing *GMA* and *ihog*. Violin plots represent cytoneme maximum extent (**A**), lifetime (**B**) and elongation (Ve) and retraction (Vr) velocities (**C**) measurements. Colored diamonds indicate the mean of the data and black lines the median. Notice that there are no significant differences in maximum extent, but there are differences in lifetime and Ve or Vr values comparing non-overexpressing with overexpressing *ihog* experiments. n.s.: not significant, * $p<0.05$, ** $p<0.01$, *** $p<10^{-3}$, **** $p<10^{-4}$.

	Hh-receiving cells (*ptc.Gal4*)		Hh-producing cells (*hh.Gal4*)	
	GMA	GMA + Ihog	GMA	GMA + Ihog
Emax µm	8.68 ± 3.95	9.33 ± 4.20	8.54 ± 3.56	10.03 ± 5.15
Lifetime min	7.42 ± 4.22	15.66 ± 9.98	6.96 ± 3.90	20.93 ± 10.85
Ve (t) µm/min	2.79 ± 1.14	1.78 ± 0.98	2.85 ± 1.40	1.89 ± 0.88
Ve (T) µm/min	3.69 ± 2.10	3.03 ± 2.80	3.24 ± 1.73	2.00 ± 0.85
Vr (t) µm/min	2.44 ± 1.28	2.08 ± 1.13	2.56 ± 1.40	1.38 ± 0.85
Vr (T) µm/min	2.61 ± 1.59	2.87 ± 1.95	3.19 ± 2.04	1.24 ± 0.91

Table R-1. Hh-producing and Hh-receiving GMA filopodia dynamics. Mean ± standard deviation values for maximum extent (Emax), lifetime, elongation (Ve) and retraction (Vr) velocities from *ptc.Gal4>UAS.GMA-GFP* (N=104 filopodia of 4 movies), *ptc.Gal4>UAS.GMA-GFP, UAS.ihog-RFP* (47 filopodia of 4 movies), *hh.Gal4>UAS.GMA-GFP,* (N= 100 filopodia of 4 movies) and *hh.Gal4>UAS.GMA-GFP, UAS.ihog-RFP* (75 filopodia of 4 movies) . t:triangle. T.trapezoid.

These results demonstrate that Hh-producing and Hh-receiving cells emit **similar dynamic filopodia** which are **more stable** with ectopic **Ihog**, allowing better visualization of these kind of filopodia in fixed samples. Although the extent of filopodia was the same with or without ectopic Ihog.

1.3. Hh ligand and receptor localize along cytonemes.

Next we set out to **test** whether **Hh** or its receptor **Ptc** could be visualized ***in vivo*** along **cytonemes**, as in other signaling pathways ligands, receptors and other signaling components were shown in vesicles moving along these specialized filopodia (reviewed in Roy & Kornberg 2015; Pröls et al. 2016; Gradilla and Guerrero, 2013). So far, *Drosophila* Hh ligand has been shown in **fixed** tissues, such as in cytonemes of the germline stem cells niche of the **ovary** (Rojas-Ríos et al., 2012) and in cytonemes of **wing imaginal discs** (Callejo et

al., 2011; Bilioni et al., 2013; Bischoff et al., 2013; Gradilla et al., 2014), although it has not been shown *in vivo*. Shh has been visualized in vesicles moving along cytonemes *in vivo* in chick limb bud (Sanders et al., 2013), so we tested if Drosophila Hh also localizes in vesicles moving along cytonemes *in vivo*.

Hh-producing cells expressing a peptide marker of filamentous actin (F-actin) fused to RFP (Lifeact-RFP), which does not interfere with actin dynamics (Riedl et al., 2010), produce highly dynamic basal filopodia (Figure R-7E-F, arrow; Movie R-3A). Using a construct containing the regulatory and coding sequences of *hh* fused to GFP (*Bac-hh-GFP*) we noticed that **Hh** was on **punctate-structures** that **move fast** (Figure R-7E, arrow; Movie R-3A') along the **apico-basal surface** of these cells (Movie R-4A') and can be **localized at filopodial tips** (Figure R-7B, arrowhead; Movie R-4A; Movie R-5). **Ectopic** expression of ***ihog*** in Hh-producing cells leads to more stabilized filopodia (Figure R-7I, arrows; Movie R-3B), as previously shown (Figure R-4; Figure R-6; Movie R-1; Movie R-2; Table R-1; Bischoff et al. 2013). In this situation, **Hh accumulates at the plasma membrane** and **along the stabilized basal filopodia** (Figure R-7I-J, arrows; Movie R-3B'; Movie R-4B').

Hh-receiving cells expressing Lifeact-RFP do not highly accumulate Hh on their membranes, but **Hh localizes** at the apico-basal surface of membranes of Hh-producing cells and **along filopodia-like structures oriented in the A-P axis at the basal surface** (Figure R-7C-D, arrowheads; Movie R-6A-A'), where dynamic filopodia are formed (Figure R-7C, arrows; Movie R-7A-A'). **Overexpressing *ihog*** in Hh-receiving cells **accumulate** the **Hh** ligand along their **membranes** (Figure R-7G-H; Movie R-6B-B'), even at higher levels

along **stabilized basal filopodia** protruding from Hh-receiving cells (Figure R-7G-H; Movie R-7B-B').

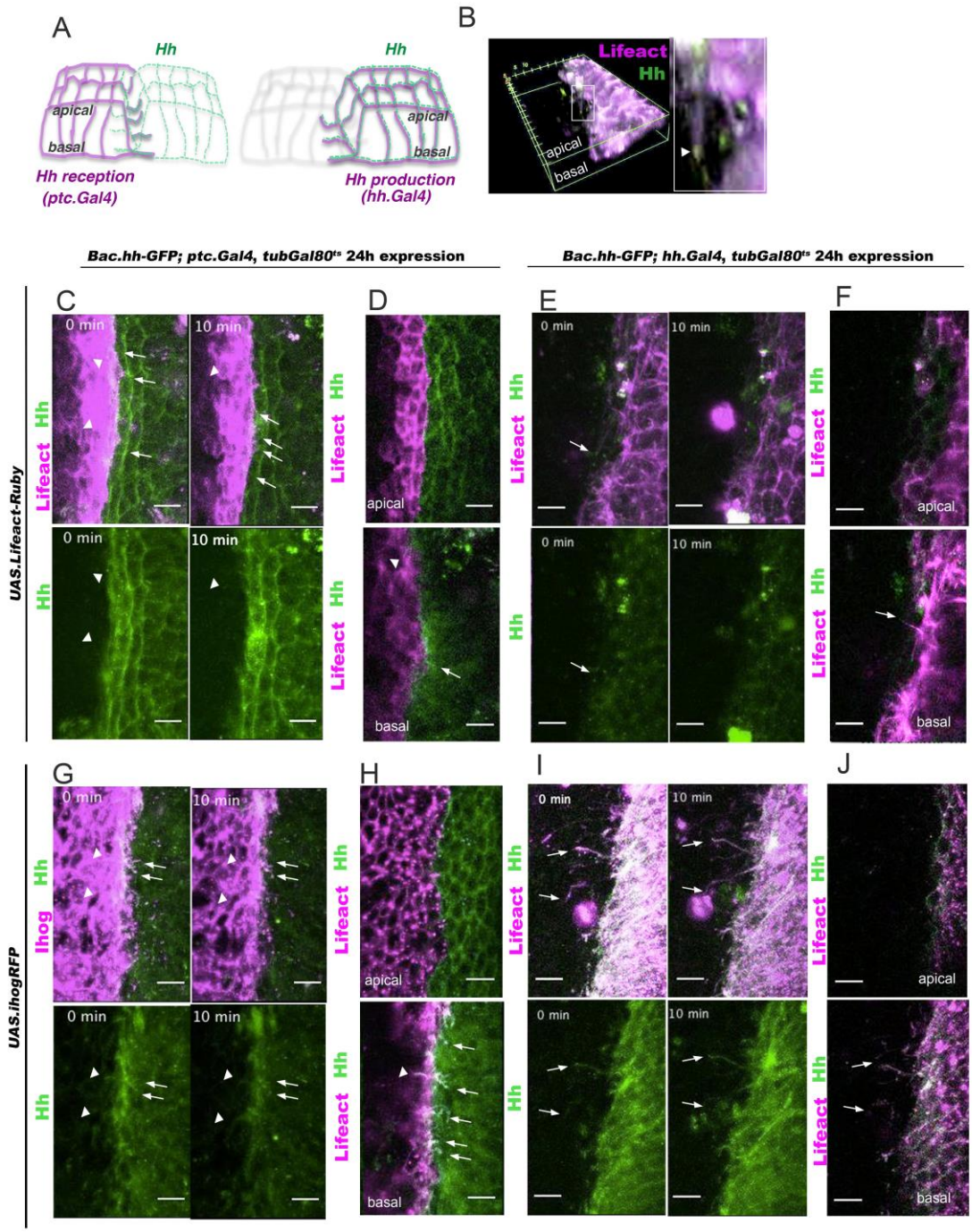

Figure R-7. Hh ligand localization along basolateral cytonemes. **A:** Drawings depicting the interaction of basal Hh-receiving cell cytonemes (magenta) with Hh-producing cell cytonemes (left drawing) and the Hh (green) transport along cytonemes of Hh-sending cells (magenta, right drawing). **B:** 3D view taken from Movie R-5 and inset showing Hh in a cytoneme tip (arrowhead) of Hh-sending histoblasts expressing *lifeact-RFP.* **C, E, G, I:** Two time frames from Movie R-3 and Movie R-7 showing Hh along cytonemes that it is highly accumulated when

overexpressing Ihog. **D, F, G, J**: Apical and basal planes taken from Movie R-4 and Movie R-6. Hh accumulation on cytonemes is visualized on basal planes. White arrows indicate cytonemes and arrowheads indicate Hh on filopodia-like structures from Hh-sending cells towards Hh-receiving cells. All scale bars indicate 10 μm.

Ptc is localized on **punctate structures** along the **apical and lateral surfaces** of **Hh-receiving histoblasts** that express Lifeact (Movie R-8A), GMA (Movie R-8B), CD4 (Movie R-8C) or Ihog (Movie R-8D). These live imaging experiments did not allow us to locate Ptc along basal filopodia, probably due to Ptc rapid internalization from the plasma membrane, as we could see it along **basal filopodia when impairing its internalization** in wing imaginal discs (González-Méndez et al 2017).

Altogether, these results indicate that **Hh** and its receptor **Ptc** are localized along **specialized signaling filopodia** and that **Hh**, but **not Ptc**, **accumulates** in **Ihog**-driven **stabilized filopodia**.

1.4. Hh and Ptc are transported in exosomes along cytonemes

By expressing *ihog* and the exosomal and multivesicular marker *CD63* in Hh-producing cells of wing discs and staining with anti-Hh, we observed **Hh co-localizing with Ihog and CD63** in **vesicle-like structures** in fixed wing imaginal discs (Figure R-8C, arrowheads; Gradilla et al. 2014). Additionally, the membrane marker CD4, CD63 and Ihog were present at punctate-like structures moving along filopodia in live Hh-producing histoblasts (Gradilla et al., 2014).

As shown above, Ptc is localized at punctate structures throughout the apical and basolateral surfaces (Movie R-8), so we wonder if Ptc could be also transported on exosomes along filopodia. A controlled expression of CD63 in the Hh-receiving cells and in a *Bac-ptc-Cherry* (a construct containing the whole regulatory and coding sequences of *ptc* fused to mRFPCherry) background expressing *ptc* in an endogenous-like way, **Ptc and CD63 co-localize at punctate-like structures** along the **apico-basolateral surfaces** and also along basal filopodia-like structures (Figure R-8A, arrowheads and arrows; Movie R-9). These vesicle-like structures **move very fast** throughout the whole tissue mainly in the Hh-receiving cells being difficult to visualize within cytonemes, but some of them could be perceived **along basal dynamic filopodia** (Figure R-8A, arrowheads and arrows; Movie R-10). Co-expression of *ihog* and *CD63* in these Hh-receiving cells revealed a **rapid movement of CD63-coated vesicles moving along the Ihog-driven stabilized filopodia** (Figure R-8B, arrowheads and arrows; Movie R-11), which also appeared in the whole Hh-receiving tissue (Figure R-8B, Movie R-12).

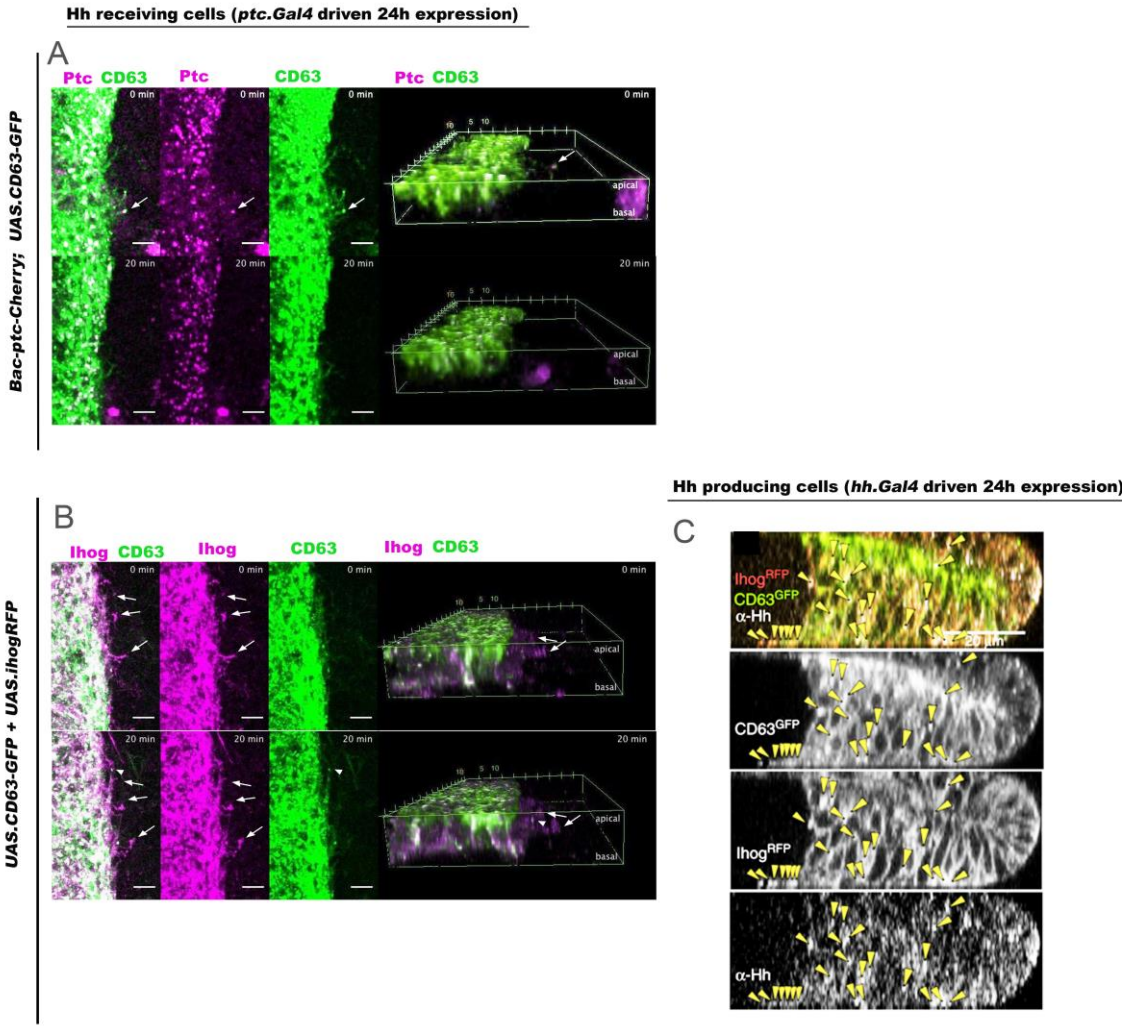

Figure R-8. Hh and Ptc localization in MVBs along basolateral cytonemes. **A:** Two time frames of Z-projection (left) and 3D view (right) of Movie R-10. Ptc-Cherry is localized on vesicle-like structures together with CD63-GFP expressed on Hh-receiving cells along filopodia-like dynamic structures on the basal surface of abdominal histoblast epithelia. **B:** Two time frames of Z-projection (left) and 3D view (right) of Movie R-11. Ihog and CD63 co-localize in punctate-structures along stabilized cytonemes on basal surface of abdominal histoblast epithelia **C:** Orthogonal slice of a wing disc co-expressing *ihog-RFP* and *CD63-GFP* in Hh-producing cells. Endogenous Hh localizes at punctate structures (yellow arrowheads) together with Ihog and CD63 in the P compartment and in basal cytonemes emanating from P towards A compartment cells. Image C was taken from Gradilla et al., 2014.

1.5. Cytoneme dynamics on Hh ligand and receptor mutants

As we have shown the ligand Hh and the receptor Ptc are localized along specialized filopodia, we wanted to analyze if filopodia dynamics are impaired upon their absence.

Using the *hh* thermosensitive allele (***hh^{ts2}***) to **eliminate Hh function** (Ma et al., 1993), **cells overexpressing *ihog* still form filopodia** with similar dynamics to those overexpressing *ihog* in a wild type background; being **stabilized** along the 30-minutes abdominal histoblasts movies (Figure R-9A; Movie R-13). Therefore, **Hh** does **not** seem to be **necessary** for the **cytoneme formation and/or for the regulation of their dynamics**.

Subsequently, we tested if **Ptc absence** could impair the formation or the dynamics of Hh signaling filopodia, or if Hh-sending cells could still form filopodia to transport Hh across *ptc$^{-/-}$* clones. It has been described that *ptc$^{-/-}$* clones located at the A/P compartment border cannot internalize Hh, but Hh signal transmission towards more anterior wild type Hh-receiving cells is not impeeded (Chen & Struhl, 1996). **P compartment abdominal histoblasts** expressing GMA **emit filopodia that cross a *ptc$^{-/-}$* clone** and bridge the more A compartment cells (Figure R-9B; Figure S-1A; Movie R-14). These signaling filopodia have **similar dynamics** (maximum extent, lifetime and elongation and retraction velocities) **when crossing wild type or *ptc$^{-/-}$* mutant Hh-receiving territories** (Figure R-10; Figure S-1B; Table R-2) and they also show similarly distribution along the AP compartment border (Figure S-1B). Therefore**, Hh signaling filopodia dynamics is independent of the Ptc presence**.

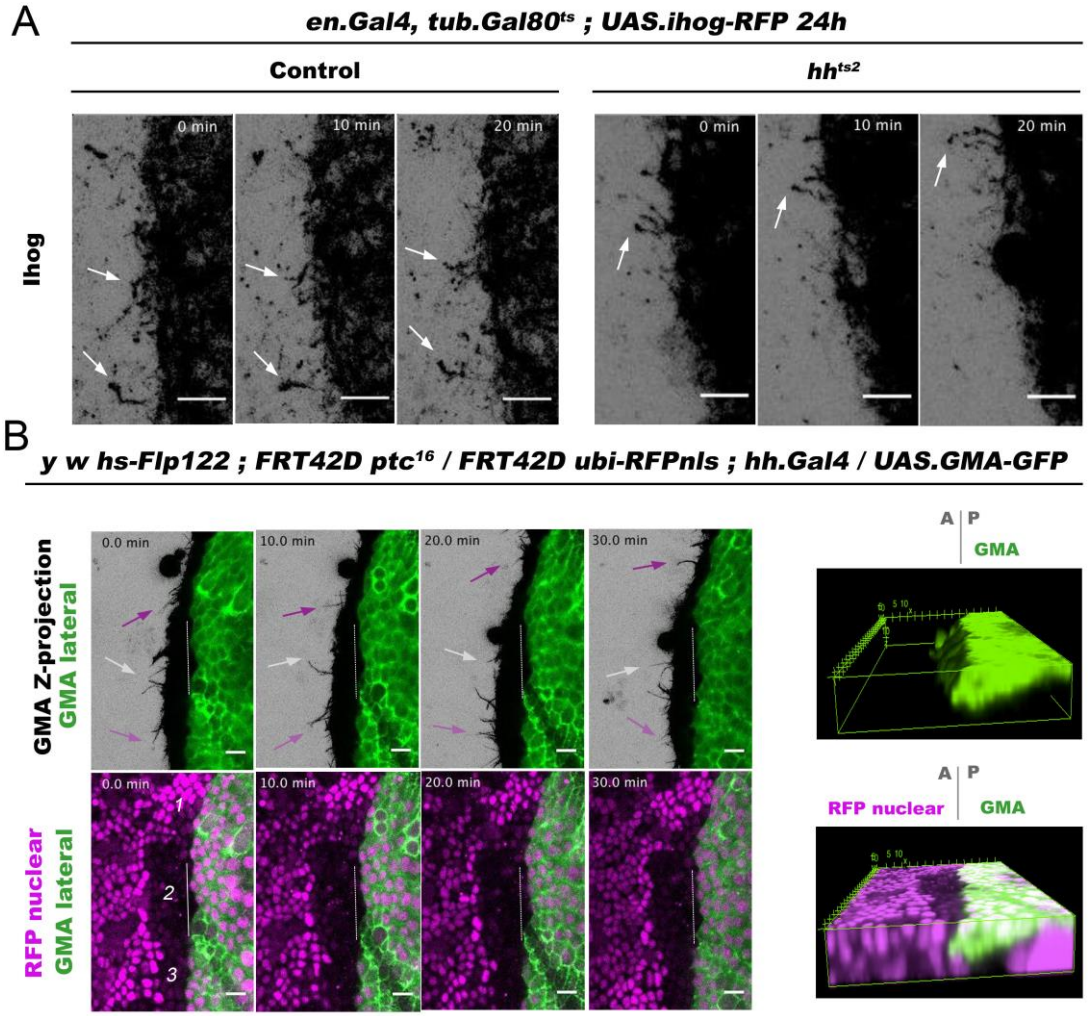

Figure R-9. Absence of Hh or Ptc does not interfere with cytoneme dynamics. **A: Absence of Hh does not affect ectopic Ihog-driven cytoneme stabilization.** Hh-producing abdominal histoblasts cytonemes (white arrows) are stabilized overexpressing *ihog* in the presence (Control) or absence of Hh (*hh*^{ts2}). Three time frames of Movie R-13 are shown. Arrows indicate 10 μm. **B: Absence of Ptc does not affect Hh-sending cytoneme dynamics.** Four time frames of Movie R-14 are shown on the left, displaying a lateral view of GMA to easily visualize the cell perimeter together with a z-projection of GMA (top panels) or with a lateral view of nuclear RFP (bottom panels). White dotted lines mark the region of the A/P border just next to the A compartment cells which are mutant for *ptc* (absence of nuclear RFP). Scale bars indicate 10 μm. Hh-producing abdominal histoblasts expressing GMA emit cytonemes which can cross either wild type (region 1, magenta nuclei), or *ptc* mutant (region 2, absence of magenta nuclei), or *ptc*$^{+/-}$ heterozygous (region 3, lower levels of magenta nuclei) territories. 3D views showing nuclear RFP (magenta) and GMA-GFP (green). Notice the absence of RFP nuclear (absence of magenta) indicating a *ptc* mutant clone territory and tissue invasion at basolateral surface from the P to the A compartment.

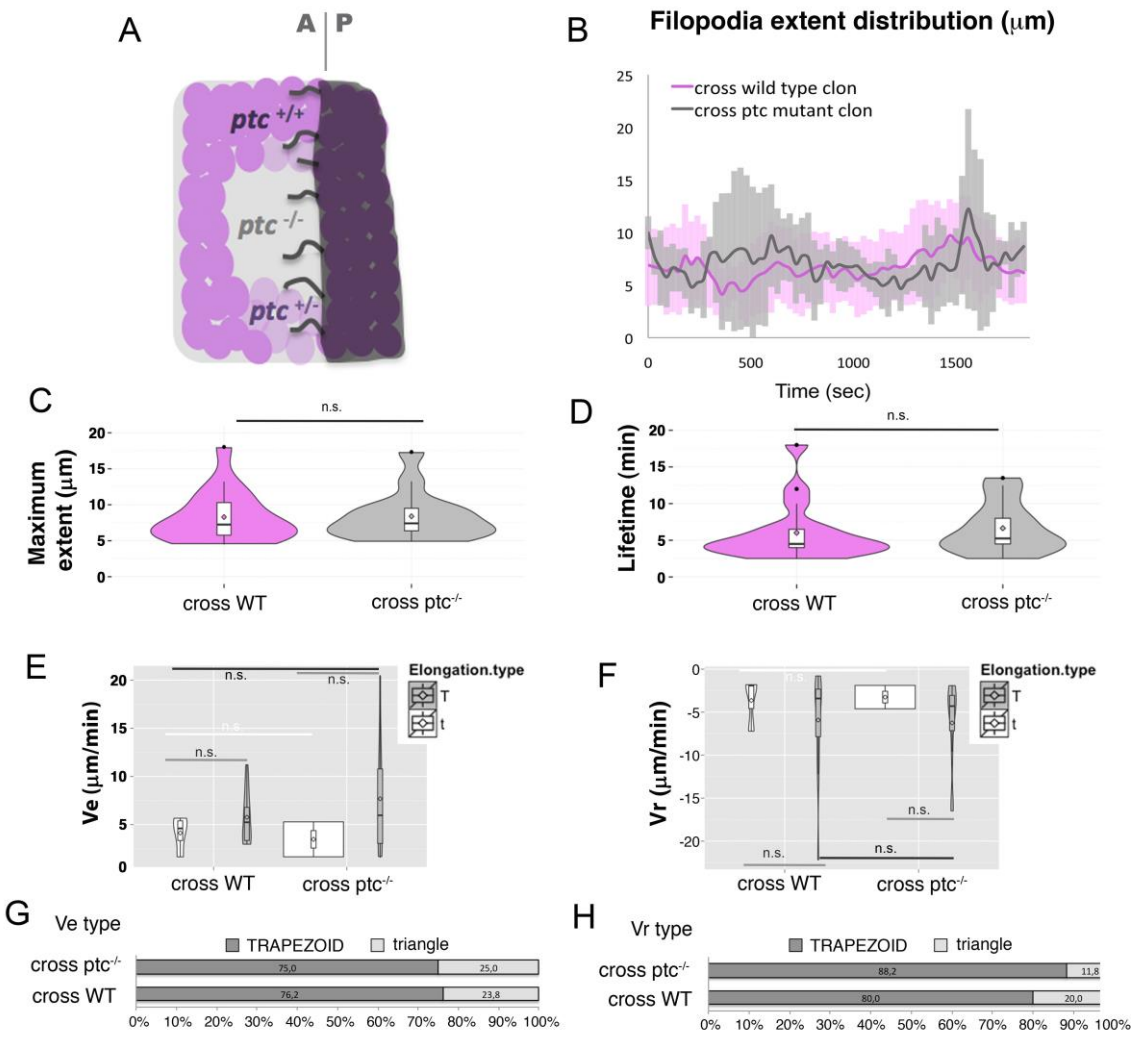

Figure R-10. Hh-producing abdominal histoblasts emit cytonemes able to cross *ptc* mutant clones with similar dynamics than those crossing wild type territories. **A:** Scheme depicting Hh-producing histoblasts that emit cytonemes (grey) that cross the A/P compartment border towards *ptc* mutant territory ($ptc^{-/-}$), wild-type territory ($ptc^{+/+}$) and heterozygous territory ($ptc^{+/-}$). **B:** Graph represents extent distribution over time of GMA-GFP cytonemes emanating from Hh-producing cells. Notice that there is no difference between cytonemes crossing a wild-type (magenta) or a *ptc* mutant clone (grey) territories. **C-F:** Violin plots representing the cytoneme maximum extent (C), lifetime (D), elongation velocity (Ve, E) and retraction velocity (Vr, F). Notice that there are not significant differences between cytonemes crossing *ptc* mutant or wild-type territories (n.s.). T: trapezoid. t: triangle. **G-H:** Percentage graphs representing the type of elongation (G) or retraction (H) velocities of cytonemes crossing *ptc* mutant ($ptc^{-/-}$) or wild-type (WT) territories. Notice that there are not differences.

	Cross WT territory	Cross *ptc*$^{-/-}$ territory
Emax µm	8.29 ± 3.53	8.40 ± 3.41
Lifetime min	6.03 ± 3.97	6.64 ± 3.45
Ve (t) µm/min	4.13 ± 1.84	3.47 ± 2.57
Ve (T) µm/min	5.76 ± 2.70	7.68 ± 5.68
Vr (t) µm/min	3.64 ± 3.12	3.25 ± 1.92
Vr (T) µm/min	5.91 ± 5.89	6.25 ± 5.05

Table R-2. GMA filopodia dynamics crossing *ptc*$^{-/-}$ and wt territories. Mean ± standard deviation values for maximum extent (Emax), lifetime, elongation (Ve) and retraction (Vr) velocities from N= 29 filopodia crossing wild-type (WT) anterior territory and N= 23 filopodia crossing *ptc*$^{-/-}$ territory.

Taken together, these results clearly indicate that **network of dynamic signaling filopodia** are formed **independently** of the **presence** of either the **Hh** ligand or the **Ptc** receptor.

2. Ihog role during wing disc and abdominal histoblasts development.

During wing development, **Ihog and Boi are redundant for Hh reception** (Zheng et al., 2010) and also for the **normal Hh extracellular levels** in Hh-producing cells (Yan et al., 2010). They are expressed **ubiquitously in the wing disc with decrease levels at the A/P compartment border** and **Ihog** mainly localizes to **basolateral** plasma membranes, while **Boi** does it mainly at **apical and lateral** surfaces (Bilioni et al., 2013; Zheng et al., 2010). Hh-producing cells expressing ***ihog*** **or** ***boi*** extend **lateral or basal filopodia** where Ihog or Boi are found, respectively (Bilioni et al., 2013). Hence, we wanted to **study Hh signaling filopodia *in vivo*** under *ihog* and *boi* gain- and loss-of-function conditions to analyze their possible role in the regulation of cytoneme dynamics and if they are also redundant for that specific role as they do for Hh reception.

2.1. Role of Ihog and Boi in Hh signaling cytoneme dynamics

Ectopic expression of *ihog* gives rise to better visualization of basolateral Hh signaling filopodia, or cytonemes, in either Hh-sending or Hh-receiving cells of *Drosophila* wing imaginal discs (Bilioni et al., 2013; Callejo et al., 2011), which is due to the stabilization of cytoneme dynamics (Figure R-4; Figure R-6; Table R-1; Movie R-1; Movie R-2; Bischoff et al. 2013) .

Next we tested whether Boi also has a role in cytoneme dynamics or if this role is exclusive of Ihog. Abdominal **Hh-sending histoblasts** expressing *boi* emit basolateral **Boi-labeled cytonemes** (Figure R-11D; Movie R-15A), which are **highly dynamic** (Figure R-11C; Movie R-16A), while the co-expression of ***boi* and *ihog*** leads to **more stable** (Figure R-11G; Movie R-16B) **basolateral cytonemes** (Figure R-11H; Movie R-15B). **Hh-receiving cells** expressing ***boi*** also emit **dynamic basolateral cytonemes** (Figure R-11A-B; Movie R-17). The lack of sufficient live imaging data did not allow us to describe cytoneme dynamics when co-expressing ***ihog* and *boi*** in Hh-receiving cells, but using **fixed** samples of **wing imaginal discs** revealed that they also **co-localized in basal cytonemes** (Figure R-11E-F; Movie R-18).

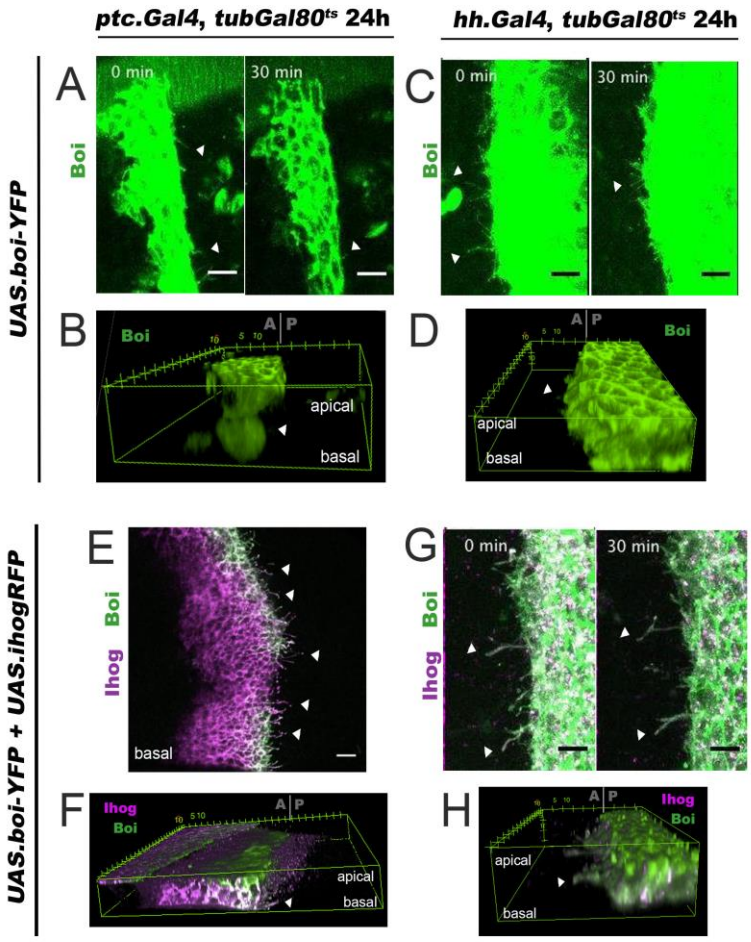

Figure R-11. Different roles of Ihog and Boi in cytoneme dynamics regulation. **A-D, G-H:** Two time frames (A, C, G) and 3D views (B, D, H) from Movie R-15 and Movie R-16 showing Boi-labelled dynamic cytonemes (white arrowheads in A-D) and Ihog-Boi co-labelled stabilized basal cytonemes (white arrowheads in G-H). **E-F:** Basal plane (E) and 3D-view (F) from Movie R-18 of a wing disc showing co-localization of Ihog and Boi in basal cytonemes of Hh-receiving cells.

To analyze if Boi has any influence on **ectopic Ihog-driven Hh filopodia stabilization**, we expressed the ribonucleic acid interference (RNAi) of *boi* during the whole development, together with *ihog-RFP* in Hh-producing cells. These histoblasts **still** emit **stabilized** Hh signaling filopodia in this ***boi*** **loss-of-function** situation (Figure R-12; Movie R-19).

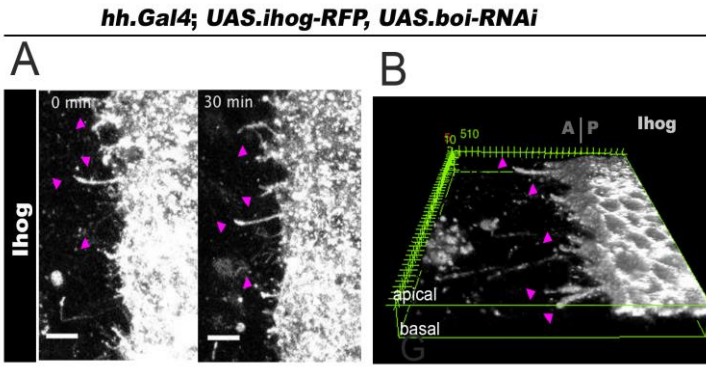

Figure R-12. Ihog-driven cytoneme stabilization is independent of Boi.
Two time frames from Movie R-19 (A) showing Ihog-driven stabilized cytonemes protruding from the basal plane, as shown in the 3D view (B), of Hh-producing cells that also express the RNAi against *boi*.

These results indicate that **ectopic** expression of **Ihog**, but **not** of **Boi**, leads to more **stable cytonemes**, although Ihog contributes to Boi accumulation in those stabilized basolateral cellular extensions.

Hh-sending or Hh-receiving histoblasts with **loss-of-function of both *ihog* and *boi* still emit dynamic filopodia** (Figure R-13; Movie R-20 with **similar values** of average maximum **extent**, **lifetime**, elongation (**Ve**) and retraction (**Vr**) velocities with apparently no statistical significant differences with their controls, although data were obtained from a low number of movies (Figure R-14; Table R-3). Further analysis would be needed to increase the number of movies and therefore the number of filopodia visualized for better statistical analysis. In addition, it would be necessary to investigate the role of *ihog* using null mutants for *ihog* or loss-of-function of *ihog* in either Hh-producing or Hh-receiving cells.

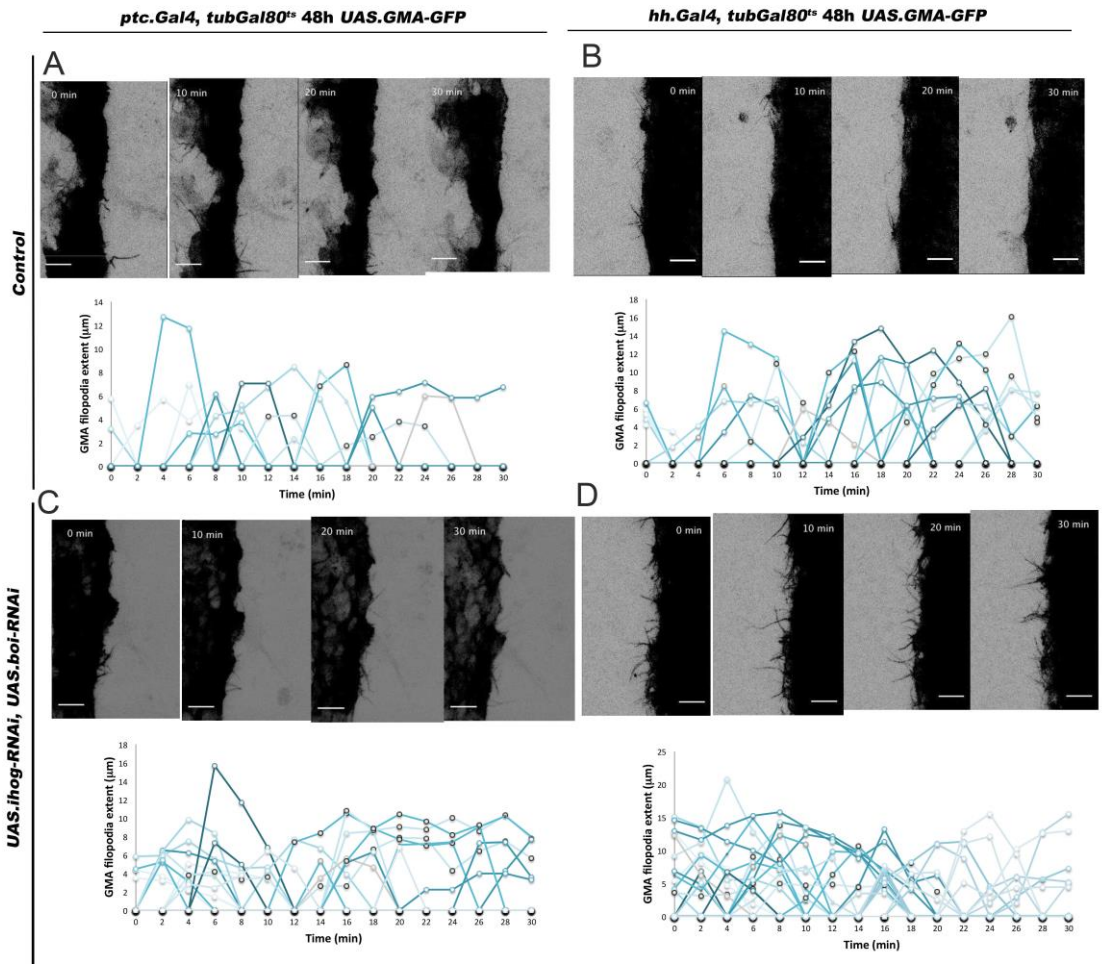

Figure R-13. Hh-producing or Hh-receiving histoblasts with a decrease function of both *ihog* and *boi* emit dynamic cytonemes. Four time frames from Movie R-20 are shown on the upper part of A, B, C and D. Hh-producing cells (B, D) and Hh-receiving cells (A, C) emit highly dynamic filopodia expressing GMA alone (A, B) or co-expressing RNAi against *ihog* and *boi* (C, D). Scale bars represent 10 µm. Graphs representing GMA filopodia extent over time are shown in the bottom part of A, B, C and D.

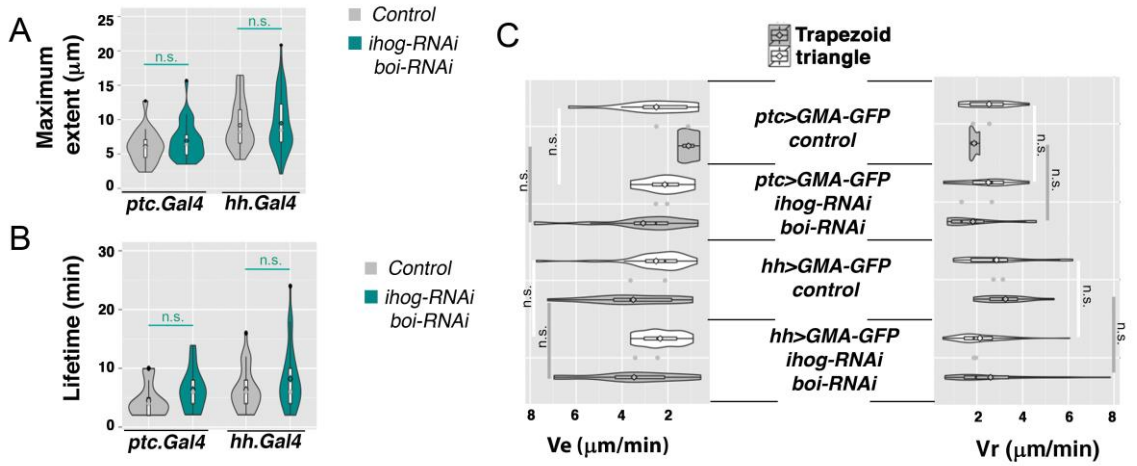

Figure R-14. Hh-producing or Hh-receiving histoblasts with a decrease function of both *ihog* and *boi* emit dynamic cytonemes. Statistical analysis of cytoneme dynamics of Hh-sending (*hh.Gal4*) and Hh-receiving (*ptc.Gal4*) cells expressing GMA or co-expressing GMA with RNAi against *ihog* and *boi*. Violin plots represent cytoneme maximum extent (**A**), lifetime (**B**) and elongation (Ve) and retraction (Vr) velocities (**C**) measurements. Colored diamonds indicate the mean of the data and black lines the median. Notice that there are not significant differences in maximum extent, lifetime, Ve and Vr values. n.s.: not significant.

	Hh-receiving cells (*ptc.Gal4*)		Hh-producing cells (hh.Gal4)	
	Control	*ihog boi RNAis*	Control	*ihog boi RNAis*
Emax (µm)	6.13 ± 2.44	6.91 ± 2.67	9.18 ± 3.39	9.48 ± 3.94
Lifetime (min)	4.53 ± 2.77	6.35 ± 3.41	6.36 ± 3.52	8.22 ± 5.07
Ve t (µm/min)	2.51 ± 1.58	2.14 ± 0.89	2.52 ± 1.42	2.34 ± 0.83
Ve T (µm/min)	1.10 ± 0.48	3.08 ± 2.03	3.51 ± 1.80	3.48 ± 1.94
Vr t (µm/min)	2.54 ± 0.92	2.51 ± 1.13	2.86 ± 1.51	2.14 ± 1.03
Vr T (µm/min)	1.88 ± 0.23	1.83 ± 1.32	3.26 ± 1.01	2.60 ± 1.91

Table R-3. GMA filopodia dynamics under *ihog* and *boi* decreased function. Mean ± standard deviation values of maximum extent (Emax), lifetime, elongation (Ve) and retraction (Vr) velocities from *ptc.Gal4>UAS.GMA-GFP* (N=18 filopodia of 1 movie), *ptc.Gal4>UAS.GMA-GFP,UAS.ihog-RNAi UAS.boi-RNAi* (N=31 filopodia of 2 movies), *hh.Gal4>UAS.GMA-GFP* (N=56 filopodia of 2 movies) and *hh.Gal4>UAS.GMA-GFP,UAS.ihog-RNAi,UAS.boi-RNAi* (N=89 filopodia of 2 movies). t:triangle. T:trapezoid.

2.2. Characterization of Ihog functional domains and their role in Hh signaling

As mentioned before, cytonemes are easily visualized basolaterally in wing imaginal discs epithelia overexpressing *ihog* (Bilioni et al., 2013; Callejo et al., 2011), due to its stabilizing effect on cytoneme dynamics (Figure R-4; Figure R-6; Table R-1; Movie R-1; Movie R-2; Bischoff et al. 2013). Then, we wanted to know which of the functional domains of Ihog (Figure I-5A) were involved in the regulation of cytoneme dynamics.

To study the role of the *ihog* functional domains, UAS transgenic *Drosophila* lines were made by tagging the C-terminus of Ihog deleted in its different domains with the red fluorescent protein (RFP): *UAS.ihogΔIg-RFP*, without the four Ig domains; *UAS.ihogΔFN-RFP*, without the two FNIII domains; and *UAS.ihogΔCt-RFP*, without the C-terminus domain (Sánchez-Hernández 2013). David Sánchez-Hernández thesis showed that expressing Ihog without Ig domains in Hh-sending cells of the wing imaginal disc, cytonemes appeared similar to those observed when expressing the wild type Ihog. However, deleting the C-terminus domain, cytonemes appeared to be more numerous and longer; meanwhile deleting both FNIII domains, cytonemes were not easily visualized, suggesting a possible role of FNIII domains in regulating cytoneme dynamics. David Sánchez-Hernández also analyzed cytonemes that expressed a construct of Ihog without the Fn1 domain (*UAS.ihog.ΔFn1*), which contains the Hh interacting region (Zheng et al., 2010), and another one with two point mutations in Fn2 domain (*UAS.ihog.Fn2**), described to block its interaction with Ptc (Zheng et al., 2010). *UAS.ihog.ΔFn1* expression in Hh-sending cells showed apparently fewer and shorter

cytonemes, while cytonemes of cells expressing *UAS.ihog.Fn2** were apparently more abundant and longer (Sánchez-Hernández, 2013). Therefore he proposed that Fn1 domain could be responsible for the regulation of cytoneme dynamics.

2.2.1. Role of Ihog functional domains in cytoneme dynamics

To examine whether FN domains are responsible of Ihog-mediated cytoneme stabilization and whether other domains have any role in cytoneme behavior, we used the *in vivo* pupal abdominal histoblasts epithelia. We analyzed cytoneme behavior by ectopic expression in Hh-producing or in Hh-receiving histoblasts of *GMA* together with the wild type *ihog* or with the different *ihog* mutant variants deleted in specific Ihog domains.

Co-expression of *GMA-GFP* with different ***ihog* constructs** revealed that **deleting** the **Ig domains** or the **C-terminus domain does not affect** Ihog-driven **cytoneme stability** either in Hh-producing cells (Figure R-15B,F; Movie R-21A-A''; Movie R-21C-C'') or in Hh-receiving cells (Figure R-15A,E; Movie R-22A-A''; Movie R-22C-C''). The **absence of both FNIII domains** does change the normal cytoneme stability driven by Ihog, turning them **more dynamic** (Figure R-15C-D; Movie R-21B-B''; Movie R-22B-B'') when compared to those co-expressing *GMA* and wild type *ihog* (Figure R-4C-D; Movie R-1B-B''; Movie R-2B-B''). Likewise, the **absence** of only the **Fn2** domain gives rise to more **dynamic cytonemes** (Figure R-15G-H; Movie R-23A,C), while the **Fn2*** construct produces **stabilized** cytonemes (Figure R-15I-J; Movie R-23B,D).

Next we analyzed the **maximum extent** of cytonemes using different Ihog mutant variants. This analysis revealed **no** statistical significant **differences** between wild type *ihog* and ***ihogΔIg* or *ihogFn2**** constructs. The co-expression of *GMA* and ***ihogΔFn2* in**

Hh-receiving cells produces cytonemes with a **shorter extent range** than *GMA* expression alone or together with wild type *ihog,* while the co-expression of the constructs **without both FNIII domains or** without the **C-terminus domain** in **Hh-secreting cells** produces cytonemes with a **longer extent range** (Figure R-16A; Table R-4; Table R-5).

As shown before, overexpression of *ihog* produces more stable cytonemes with longer lifetime values (Figure R-4; Figure R-6; Table R-1; Movie R-1; Movie R-2; Bischoff et al. 2013). We then analyzed the dynamics of the Ihog mutant variants. For image analysis, our statistical parameters were set according to our short 30 minutes movies, where we measured the **lifetimes** of the dynamic cytonemes in this time period. For the apparently static cytonemes, we assigned the fixed value of 30 minutes as their real lifetime exceeds our timeframe recorded. **Hh-receiving** cytonemes expressing ***ihogΔIg*** have **variable** values of lifetime, being, in average, **shorter** than cytonemes of overexpressed wild type ***ihog***. The constructs of *ihog* **without Fn2 or without both FNIII domains** produce cytonemes with statistically significant **shorter lifetimes** compared to those overexpressing *ihog* and have not significant differences compared to those non-overexpressing *ihog*; while the construct ***ihogFn2**** produces cytonemes with **similar** lifetimes compared to those overexpressing ***ihog***. These results support the hypothesis that in general the **FNIII domains, but not the Fn2 region that specifically interact with Ptc, are responsible for Ihog-driven cytoneme stabilization**. Finally, cytonemes expressing the ***ihogΔCt*** construct have lifetimes **similar** to those overexpressing wild type ***ihog*** and therefore, have significantly higher lifetimes than without *ihog* overexpression (Figure R-16A; Table R-4; Table R-5).

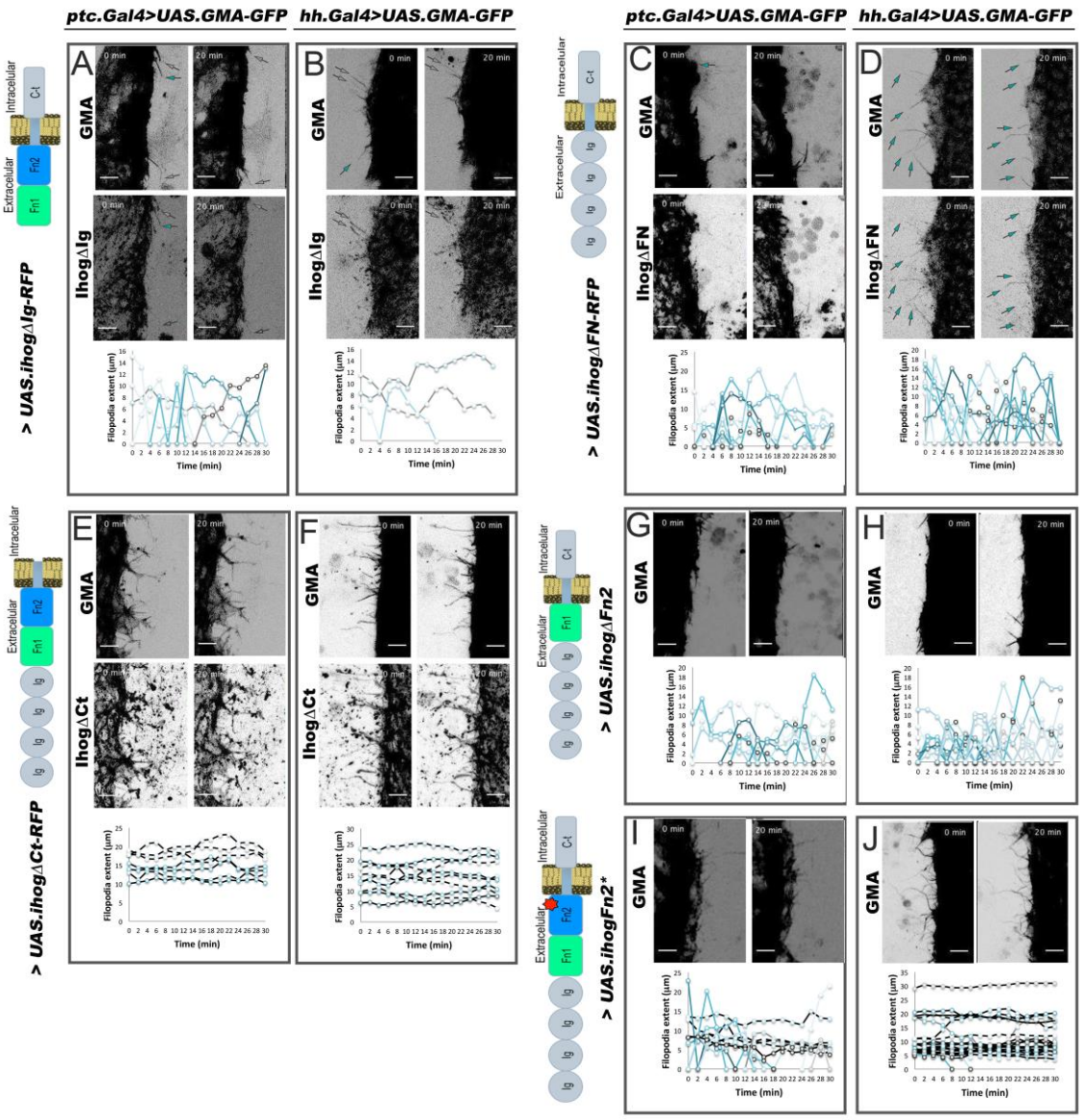

Figure R-15. Ihog domains function in cytoneme dynamics. Two time frames from Movie R-21, Movie R-22 and Movie R-23 are shown on the upper and middle part of A-J. Histoblasts expressing the different Ihog mutant constructs in Hh-producing cells (B, D, F, H, J) or Hh-receiving cells (A, C, E, G, I). Scale bars represent 10 µm. Cartoons of each mutant Ihog are depicted on the left. Graphs representing GMA filopodia extent over time are shown in the bottom part of A-J. Histoblasts expressing Ihog without Ig domains (IhogΔIg) mainly produce stabilized cytonemes, but also a few more dynamic (A-B); Histoblasts expressing Ihog without FNIII domains (IhogΔFN) produce dynamic cytonemes (C-D); histoblasts expressing Ihog without the C-terminus (IhogΔCt) produce stabilized cytonemes (E-F); histoblasts expressing Ihog without the second FNIII domain (IhogΔFn2) produce dynamic cytonemes (G-H); and histoblasts expressing Ihog with two point mutations in the second FNIII domain that block Ptc interaction (IhogFn2*) produce stabilized cytonemes (I-J).

Statistical analysis and values of **elongation** (Ve) and **retraction** (Vr) velocities for the different constructs are shown in Figure R-16B and Table R-4, Table R-5, respectively. Interestingly, cytonemes with **elongations and retractions** in **triangle-like behavior** are significantly **slower** overexpressing the ***ihogΔFn2*** construct in **Hh-receiving cells** compared to non-overexpressing *ihog* and to those overexpressing the *ihogΔFN* construct. Additionally, *ihogΔFn2* cytoneme **retraction** is **also slower** than *ihogΔFN* when expressed in **Hh-producing cells**. The analysis of the **trapezoid-like elongation** showed that cytonemes were **slower** expressing ***ihogΔFn2*** **in Hh-producing** cells compared **to expressing *ihogΔFN*, which elongates faster than overexpressing *ihog***. In the contrary, *ihogFn2** overexpression has not significant differences in those velocities compared to those of *ihog* overexpression. These results indicate again that FNIII domains regulate Ihog-driven cytoneme stabilization independent of its interaction with Ptc. They also indicate that the Fn1 domain could have a dominant role in cytoneme dynamics regulation, because there is a clear difference between deleting both FNIII domains (higher velocities, more dynamic) and deleting only the Fn2 domain (slower velocities, more stable), although further analysis would be needed to elucidate the independent role Fn1 and Fn2 domains in cytoneme dynamics. In addition, it would be necessary to measure elongation and retraction velocities of the more stable cytonemes in longer record movies and therefore to calculate their real lifetime.

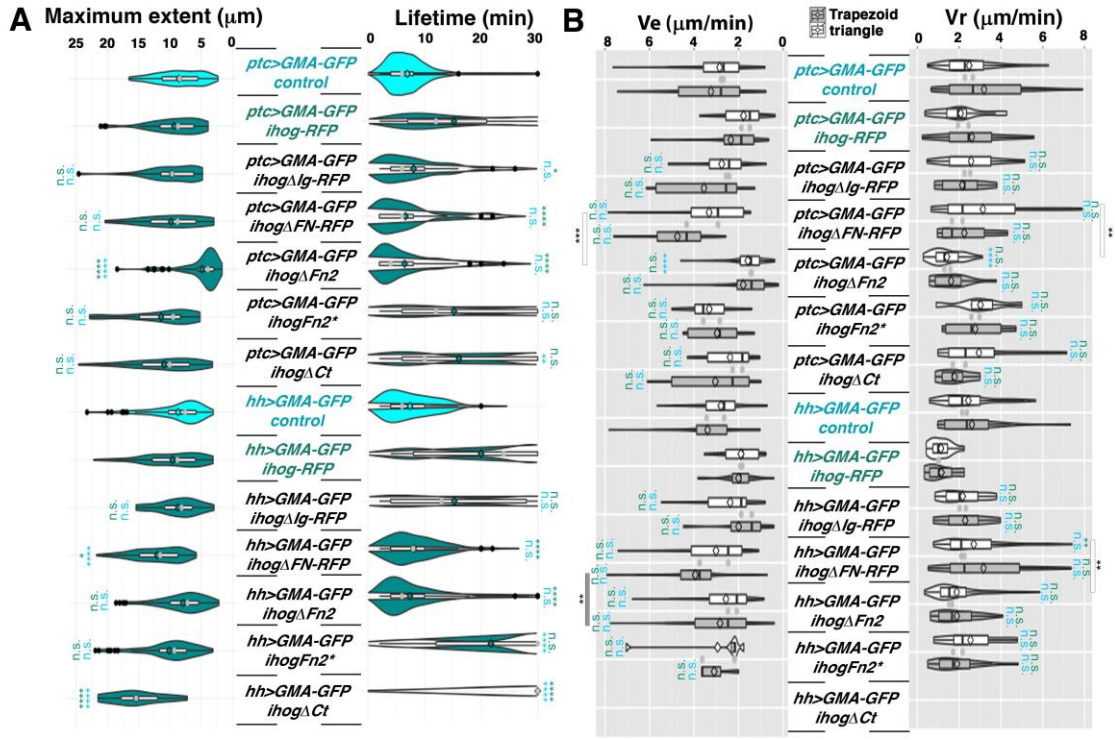

Figure R-16. Statistical analysis of cytoneme dynamics expressing the different Ihog constructs. Statistical analysis of cytoneme dynamics of Hh-sending (*hh.Gal4*) and Hh-receiving (*ptc.Gal4*) histoblasts expressing *GMA-GFP* as a control (cyan) or co-expressing *GMA-GFP* with *ihog-RFP* (dark cyan) or with the different *ihog* mutant constructs. Violin plots represent cytoneme maximum extent and lifetime (**A**) and elongation (Ve) and retraction (Vr) velocities (**B**) measurements. Colored diamonds indicate the mean of the data and black lines the median. n.s.: not significant, * $p<0.05$, ** $p<0.01$, *** $p<10^{-3}$, **** $p<10^{-4}$.

	Hh-producing cells (*hh.Gal4*) driven 24h expression of *GMA*				
	+ ihogΔIg	*+ ihogΔFN*	*+ ihogΔCt*	*+ ihogΔFn2*	*+ ihogFn2**
Emax (µm)	8.72 ± 3.35	12.15 ± 4.01	17.05 ± 6.16	7.91 ± 3.55	10.65 ± 5.30
Lifetime (min)	15.26 ± 11.26	8.05 ± 4.40	30 ± 0	7.40 ± 5.46	21.73 ± 10.64
Ve t (µm/min)	2.38 ± 1.36	3.01 ± 1.56	N/A	2.56 ± 1.37	2.94 ± 2.02
Ve T (µm/min)	2.00 ± 1.51	4.10 ± 1.89	N/A	2.98 ± 1.79	3.10 ± 0.96
Vr t (µm/min)	2.17 ± 0.98	2.91 ± 1.94	N/A	1.89 ± 1.15	2.54 ± 1.43
Vr T (µm/min)	2.29 ± 1.17	3.31 ± 2.21	N/A	1.89 ± 0.97	1.90 ± 1.11

Table R-4. Dynamics of filopodia co-expressing Ihog domain mutants and GMA in Hh-producing histoblasts. Mean ± standard deviation values of maximum extent (Emax), lifetime, elongation (Ve) and retraction (Vr) velocities from *hh.Gal4>UAS.GMA-GFP+UAS.ihogΔIg-RFP* (N=38 filopodia of 5 movies), *hh.Gal4>UAS.GMA-GFP+UAS.ihogΔFN-RFP* (N=108 filopodia of 6 movies), *hh.Gal4>UAS.GMA-GFP+UAS.ihogΔCt-RFP* (N=24 filopodia of 3 movies), *hh.Gal4>UAS.GMA-GFP+UAS.ihogΔFn2-HA* (N=134 filopodia of 4 movies) and *hh.Gal4>UAS.GMA-GFP+UAS.ihogFn2** (N=75 filopodia of 5 movies). t:triangle. T:trapezoid.

	Hh-receiving cells (*ptc.Gal4*) driven 24h expression of *GMA*				
	+ ihogΔIg	*+ ihogΔFN*	*+ ihogΔCt*	*+ ihogΔFn2*	*+ ihogFn2**
Emax (µm)	9.67 ± 4.28	9.82 ± 4.69	11.19 ± 5.52	4.85 ± 2.94	11.39 ± 5.48
Lifetime (min)	8.06 ± 6.0	6.62 ± 5.71	16.07 ± 11.78	6.46 ± 4.91	15.2 ± 11.39
Ve t (µm/min)	2.76 ± 1.27	3.32 ± 1.88	3.23 ± 2.80	1.58 ± 0.85	3.32 ± 1.19
Ve T (µm/min)	4.59 ± 3.23	4.75 ± 1.67	3.05 ± 1.96	1.79 ± 1.45	2.97 ± 1.30
Vr t (µm/min)	2.57 ± 1.32	3.14 ± 2.22	3,63 ± 2.70	1.42 ± 0.71	4.23 ± 3.43
Vr T (µm/min)	2.15 ± 1.12	2.25 ± 1.33	1.78 ± 0.76	1.61 ± 0.88	2.77 ± 1.76

Table R-5. Dynamics of filopodia co-expressing Ihog domain mutants and GMA in Hh-receiving histoblasts. Mean ± standard deviation values of maximum extent (Emax), lifetime, elongation (Ve) and retraction (Vr) velocities from *ptc.Gal4>UAS.GMA-GFP+UAS.ihogΔIg-RFP* (N=33 filopodia of 4 movies), *ptc.Gal4>UAS.GMA-GFP+UAS.ihogΔFN-RFP* (N=39 filopodia of 4 movies), *ptc.Gal4>UAS.GMA-GFP+UAS.ihogΔCt-RFP* (N=57 filopodia of 4 movies), *ptc.Gal4>UAS.GMA-GFP+UAS.ihogΔFn2-HA* (N=108 filopodia of 4 movies) and *ptc.Gal4>UAS.GMA-GFP+UAS.ihogFn2** (N=25 filopodia of 2 movies). t:triangle. T:trapezoid.

2.2.2. Role of Ihog functional domains on Hh accumulation

As the overexpression of *ihog* leads to Hh accumulation (Yan et al. 2010; Callejo et al. 2011; Bilioni et al. 2013; Figure R-7I-J, arrows; Movie R-3B'; Movie R-4B'), we then wanted to know which of the Ihog functional domains might be responsible for that Hh accumulation.

Expressing the *ihog* mutants fused to RFP, we visualized **Hh accumulated along stabilized filopodia** in ***UAS.ihogΔCt-RFP*** (Figure R17-C; Movie R-24C-C'; N=3), but **not in *UAS.ihogΔIg-RFP*** (Figure R-17A; Movie R-24A-A'; N=5). However, we have recently found out that this *UAS.ihogΔIg-RFP* mutant has an unintended **point mutation** in one of the predicted Hh-interacting aminoacids of Ihog. Thus, we cannot determine whether this effect on Hh stability is due to this additional mutation in the Fn1 or due to the lack of Ig domains. To better assess if Ig domains are involved in Hh accumulation, we have generated a new *ihogΔIg* mutant without the point mutation in the Fn1 domain but still waiting for the transgenic flies.

Additionally, when expressing ***UAS.ihogΔFN-RFP*** (Figure R-17B; Movie R-24B-B'; N=6) **Hh did not accumulated** in dynamic filopodia. Thus, we wondered if the essential domain responsible of Hh accumulation was the Fn1, as this domain contains the Hh interacting sequences, or if the Fn2 also influences Hh accumulation indirectly. We have transgenic flies that express Ihog mutants for either Fn1 or Fn2 domains but they are not tagged to RFP, so we could not visualize Ihog-labeling cytonemes *in vivo*. Besides, expressing the ***UAS.ihogΔFn1*** (Figure R-17D; Movie R-25A; N=5) we could **not** see **Hh accumulation** on filopodia-like structures as

expected. We have also observed that the expression of ***UAS.ihogΔFn2-HA*** (Figure R-17E; Movie R-25B; N=3) **neither accumulate Hh**. In the case of ***UAS.ihogFn2**** (Figure R-17F; Movie R-25C; N=6) despite the absence of Ptc interacting sequences, there was **Hh accumulation along stabilized filopodia-like structures**, indicating that an unknown different role of the Fn2 domain might regulate Hh accumulation along cytonemes as well as their dynamics.

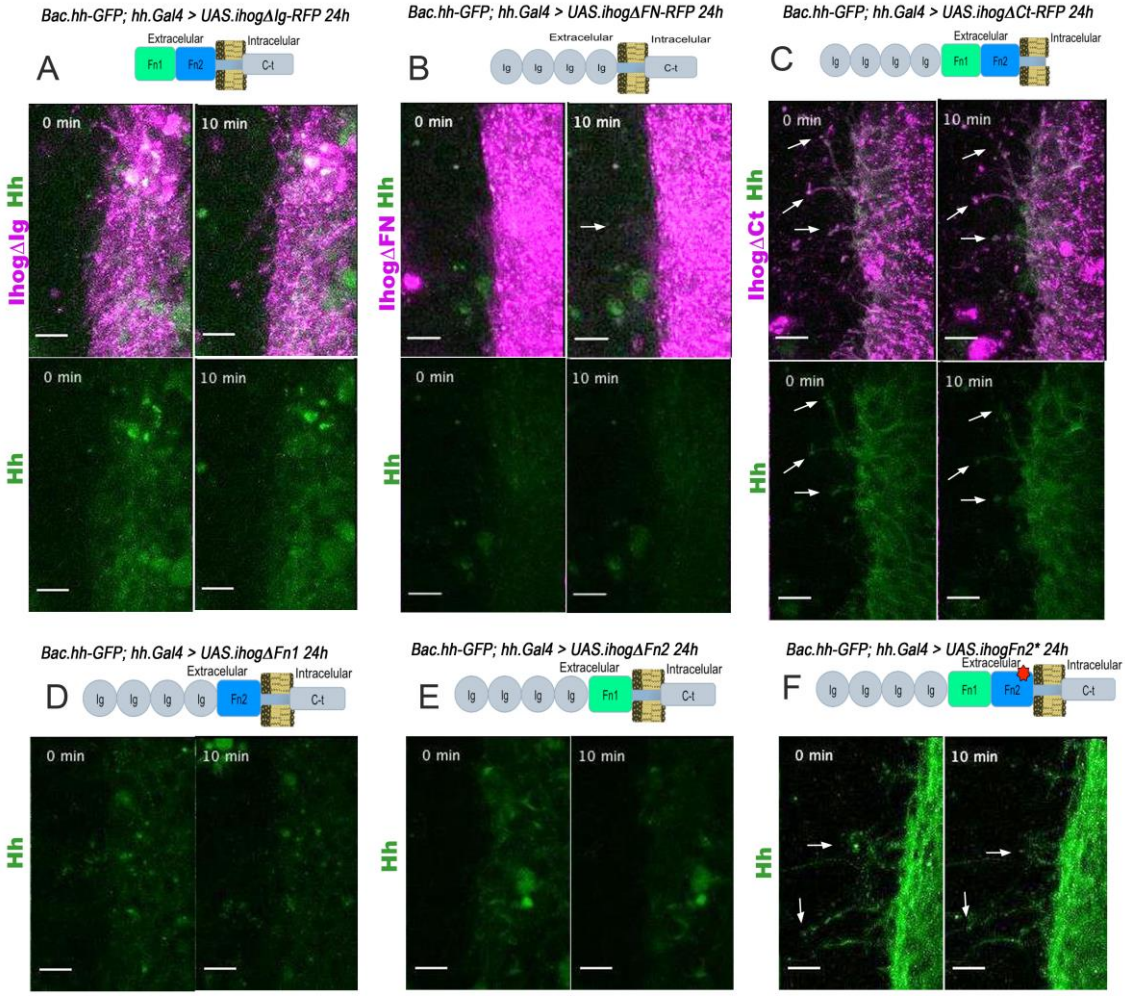

Figure R-17. Role of Ihog domains in Hh accumulation. Two time frames of Movie R-24 (A-C) or Movie R-25 (D-F) showing Hh levels when expressing different Ihog constructs in the Hh-producing cells. Scale bars represent 10 μm. Schemes of each Ihog mutant are depicted on the upper part. Expression of Ihog without Ig domains (IhogΔIg) does not accumulate Hh (A), neither the expression of Ihog without FNIII domains (IhogΔFN, B) or without one of the two FNIII domains (D, E), while the expression of Ihog without the C-terminus (IhogΔCt, C) or Ihog with two point mutations in the second FNIII domain to block Ptc interaction (IhogFn2*, F) accumulate Hh along stabilized cytonemes.

2.2.3. Role of Ihog functional domains in Hh response

Next, we analyzed the effect of the different Ihog mutant constructs in Hh gradient by expressing them in Hh-producing histoblasts. We used *lifetact* expression as a control. We also used a fly line that has the GFP fused to the promoter of *ptc* (*ptc-trap-GFP*) as a read out of Hh gradient (Figure R-18).

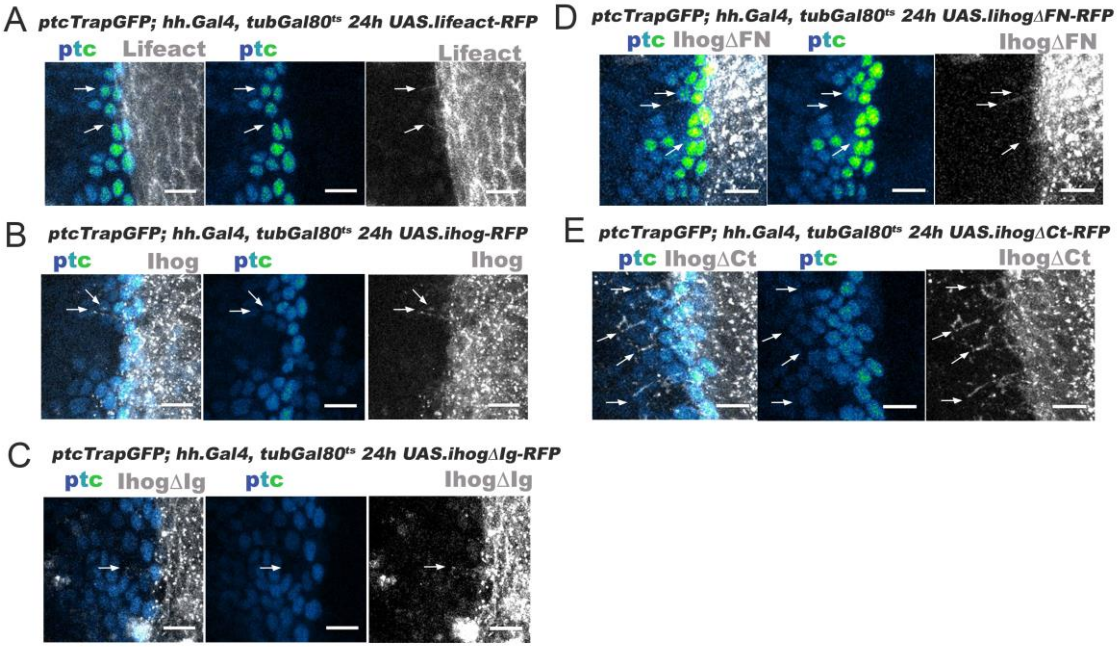

Figure R-18. Role of Ihog domains in Hh response. Confocal images of abdominal histoblasts expressing Lifeact-RFP (A), Ihog-RFP (B) or the different Ihog constructs (C-E) in the Hh-producing cells (gray) and an enhancer reporter ptcTrapGFP (Fire to Green Lookup table), which shows Hh signaling activity in a graded manner (more green color indicates high fluorescence intensity, while more blue indicates low fluorescence intensity). Scale bars represent 10 μm. Arrows indicate cytonemes. Overexpression of normal Ihog (B) reduces Hh signaling activity compared to that of Lifeact expression (A). Expression of Ihog without Ig domains (IhogΔIg) produces a flat gradient of *ptcTrapGFP* expression (C). Expression of Ihog without FNIII domains (IhogΔFN) produces a gradient similar to that of expressing Lifeact (D compared to A). Expression of Ihog without the C-terminus (IhogΔCt) results in a wider range of medium levels of *ptcTrapGFP* reported expression (E). Notice that in all cases, except for *UAS.ihogΔIg-RFP* and *UAS.ihogΔCt-RFP* cytoneme extension correlate with the highest levels of *ptcTrapGFP* expression (arrows).

The overexpression of *UAS.ihog-RFP* in the P compartment cells resulted in a shorter Hh gradient compared to overespression of *UAS.lifeact-RFP*, as shown by lower levels of *ptc* expression that go from blue to green color as they increase intensity (Figure R-18, compare A with B). This role of Ihog in controlling the Hh gradient has been previously described (Bilioni et al., 2013).

Expressing the **Ihog construct without the Ig domains**, Hh **signaling response** appeared to be **lower** creating a flatter gradient (Figure R-18C), while deleting FNIII domains or the C-terminus domain resulted in a normalized *ptc* gradient (Figure R-18D-E). In the case of ***UAS.ihogΔFN-RFP*, *ptc*** expression **levels** were higher in the first two rows of A compartment cells, **as in the control** (Figure R-18D, compare with A), while ***UAS.ihogΔCt-RFP*** produced a **wider range of medium levels of *ptc* expression**, compared to the control (Figure R-18E, compare with A and B).

Interestingly, in **all cases except for *UAS.ihogΔIg-RFP* and *UAS.ihogΔCt-RFP,* cytoneme extension correlates with the highest levels of *ptc* expression** (Figure R-18, arrows), as shown before in our study on the role of cytonemes in Hh signaling gradient establishment (Bischoff et al., 2013). However, longer time movies (overnight) would be needed to elucidate the role of Ihog domains in Hh gradient establishment in real time.

2.3. IhogFn1* does not interact in silico with Hh.

In order to analyze the Hh-Ihog interaction *in vivo* we decided to produce a fly line that expresses an Ihog protein unable to interact with Hh. We have induced **three point mutations in the first FNIII domain of Ihog (Fn1)** (Figure R-19A, arrows) on residues known to interact with Hh by hydrogen bonds (Figure MM-3; McLellan et al. 2006). To date, we still do not have the fly transgenic line so we are still awaiting to determine the biological function of this Ihog mutant protein. Nevertheless, ***in silico*** analysis of **Hh-Ihog interaction** showed a clear negative effect when using the **mutant IhogFn1*Hh with a significant interaction decrease** when compared to the control (Figure R-19B-C).

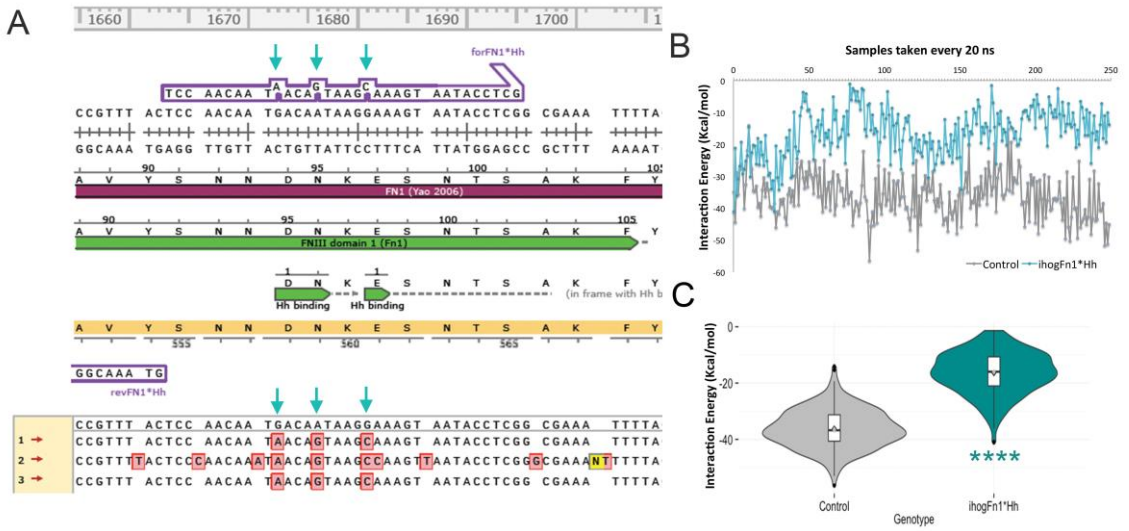

Figure R-19. Ihogfn1* point mutations affect Ihog-Hh interaction *in silico*. **A: Mutagenesis of IhogFn1.** Part of *ihog* sequence showing the first FNIII domain (Fn1) and three sequence alignments, using primers 1 to 3 as shown in Materials and Methods, to verify the three point mutations (D558N, N559S and E561Q indicated by cyan arrows) of the *pENTRY-ihogFn1*Hh* construct. Notice that the forward primer used for mutagenesis (forFn1*Hh, violet) has the three nucleotides changes (cyan arrows). **B-C: Ihog-Hh interaction *in silico*.** Graph representing the Hh-Ihog energy interaction of 250 samples taken every 20 ns with MM/GBSA for wild type Ihog and for the construct with the three point mutations in Fn1 (B). The statistical analysis is represented by violin plots (C). **** $p<10^{-4}$.

3. Integrins accumulate in A/P border by Ihog FNIII domains

Finally, analysis of the wild type levels of the *Drosophila* β-chain of integrins (βPS) show a generalized expression in the wing disc with slightly lower levels at the dorso-ventral and antero-posterior compartment borders (Figure R-20A, N=31 wing discs).

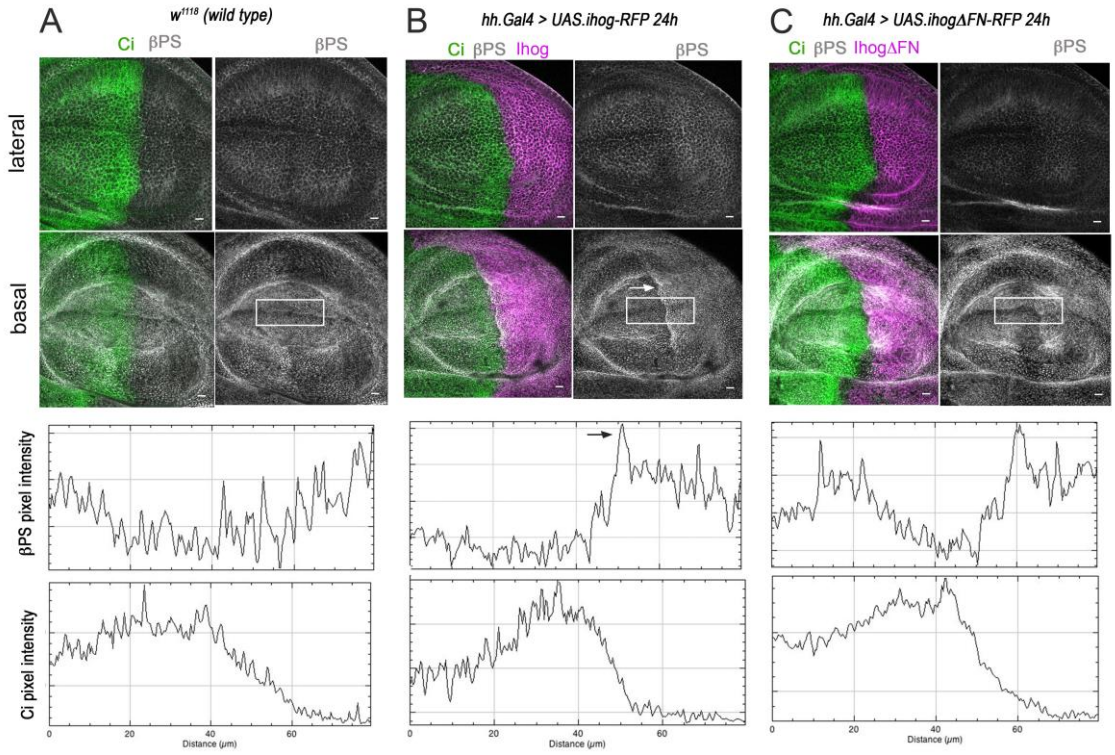

Figure R-20. The FNIII domains of Ihog regulate β-integrin levels at the A/P compartment border. Upper panels show confocal images of larval wing imaginal discs immunostained for Ci to mark A compartment and for βPS to show integrins localization in wild type (A), in ectopic Ihog (B) and in ectopic Ihog without the FNIII domains (C). Lower panels show relative intensity of Ci and βPS. Notice that ectopic Ihog drives accumulation of βPS in the A/P border (white arrow in the image and black arrow in the graph), while the construct without the FNIII domains does not accumulate βPS, showing a pattern more similar to that of the wild type.

Overexpressing ***ihog*** in the **P compartment** of wing imaginal discs, **βPS accumulates** in the whole compartment with a **significant rise along the A/P border** (Figure R-20B, arrow, N=35 wing discs). Overexpressing ***ihogΔFN*** still accumulates βPS in P compartment, but

not along the A/P compartment border (Figure R-20C, N=22 wing discs), indicating that **FNIII domains of Ihog have a specific interaction with integrins along the A/P compartment border**, but this interaction is dispensable for Ihog-integrins cis interaction within the Hh-producing cells. It is an urgent need to elucidate the Ihog-Integrins interaction and its possible role in the regulation of cytoneme dynamics.

Discussion

Hh signaling is regulated by both cytoneme and exosome production

The lipid modified Hh morphogen is anchored to membranes and unable to freely diffuse through the extracellular matrix. Thus, the mechanism for Hh distribution to receiving cells is still under debate (reviewed in Simon et al. 2016). Several models for Hh transport have been proposed; mediated by lipoproteins (Callejo et al., 2006; Panáková et al., 2005); in soluble multimers, forming micelles with inwards lipophilic residues (Gallet et al., 2006); or as budding fragments from the plasma membrane (Matusek et al., 2014). Our laboratory has proposed a transport mechanism via multivesicular bodies (MVBs) moving along actin-based filopodia or cytonemes (Callejo et al. 2011; Bilioni et al. 2013; Bischoff et al. 2013; Gradilla et al. 2014); where Hh is finally presented to the receiving cells within exosomes.

Functionally, we have previously demonstrated a **correlation** between cytonemes reach range and Hh signaling gradient extension (Figure R-2, Bischoff et al. 2013) while a similar observation has been described for Wnt/β-catenin signaling in zebrafish (Stanganello et al., 2015). In addition, we have also shown that Hh signaling is dependent on **actin** dynamic modulators (Figure R-1; Figure R-2; Bischoff et al. 2013) as well as on the **exosome formation** machinery (Figure-R3; Gradilla et al. 2014) supporting a cytoneme mediated mechanism for Hh distribution.

In more recent observations, we have determined that cytonemes from signal-receiving and signal-producing cells are polarized and form direct contact in specific sites along cytoneme length (González-Méndez et al, 2017). These contact sites, where ligand and receptor

complex localize, may facilitate morphogen reception. Furthermore, we demonstrate that other key pathway elements, the Hh co-receptor Interference hedgehog (Ihog) and the glypicans, have a crucial role during cytoneme-mediated cell-cell interaction (González-Méndez et al., 2017).

Hh and Ptc are transported on MVBs along cytonemes

There are several examples of **ligands and receptors** from different signaling pathways shown to be transported in **vesicles moving along specialized filopodia** (reviewed in Roy & Kornberg 2015; Pröls et al. 2016; Gradilla and Guerrero, 2013). To date, it has only been described Hh ligand *in vivo* moving along signaling filopodia in *Drosophila* in this thesis. Beesides, Hh has been shown in **fixed** and stained tissues, such as in cytonemes of the germline stem cells niche of the **ovary** (Rojas-Ríos et al., 2012) and in cytonemes of **wing imaginal discs** (Callejo et al., 2011; Bilioni et al., 2013; Bischoff et al., 2013; Gradilla et al., 2014).

In this thesis, we show that indeed the **Hh ligand** localizes ***in vivo*** in **vesicle-like structures** through the apico-basal surface of abdominal histoblasts and along **filopodia** (Figure R-7; Movie R-3; Movie R-4; Movie R-5). In addition, both **Hh** and the co-receptor **Ihog co-localize** with the **exosomal marker CD63** in vesicle-like structures moving throughout cytonemes (Figure R-8; Gradilla et al. 2014); while **ectopic Ihog drives Hh accumulation** at the plasma membrane and along the stabilized basal filopodia in both Hh-presenting and Hh-responding cells (Figure R-7; Movie R-3; Movie R-4; Movie R-5).

On the other hand, we have also observed ***in vivo*** presence of the **receptor Ptc in vesicle-like structures**, **co-localizing** with the

exosome marker **CD63** and along the apical and lateral surfaces of Hh-receiving histoblasts. However, unlike Hh, **Ptc does not accumulate in Ihog-driven stabilized cytonemes**, probably due to its **fast internalization**, as Ptc can be visualized along filopodia when freezing Ptc entrance in dynamin mutants (González-Méndez et al 2017). Moreover, live imaging movies have also allowed detection of **Ptc-CD63 along basal filopodia-like structures** in absence of Ihog overexpression (Figure R-8; Movie R-9; Movie R-10).

These results indicate that both the receptor Ptc and ligand Hh probably suffer a recycling process to form MVBs and then be externalized for Hh reception (González-Méndez et al., in preparation; Callejo et al. 2011; Gradilla et al. 2014). It might be indeed possible that Ptc and Hh vesicles make direct contact at specific sites along cytoneme length (González-Méndez et al., in preparation; González-Méndez et al., 2017).

Filopodia dynamics for Hh signaling

To date, most studies on signaling filopodia dynamics do not include detailed description of the parameters definition process. Here, we have performed a **thorough analysis of cytonemes dynamics** using live imaging and a **representative model with two distinct behaviors**: **triangle-like dynamics** of filopodia elongating and retracting at constant velocities; and **trapezoid-like dynamics** with a "stationary" interphase between the elongation and retraction phases (Figure R-5; see Materials and methods).

Interestingly, both **Hh-producing and Hh-receiving cells** emit **cytonemes** with **similar dynamics**; both becoming more stable when ectopically expressing ***ihog***, getting closer to the **trapezoid** class with a "stationary" phase between elongation and retraction

phases (Figure R-4; Figure R-6; Movie R-1; Movie R-2; Table R-1; Bischoff et al. 2013). This effect then would explain the **better visualization of cytonemes** in ectopic Ihog **fixed** samples (Bilioni et al., 2013; Bischoff et al., 2013; Callejo et al., 2011).

Filopodia extent

Our live imaging studies reveal that *Drosophila* abdominal histoblasts emit **Hh signaling filopodia** that reach **maximum extents** of 8.68 ± 3.95 μm in Hh-receiving cells and 8.54 ± 3.56 μm in Hh-producing cells. These data **resembles** meassurements of other relatively short signaling filopodia in **mouse**: the **FGFR2** and the **ErbB3** receptor cells of preimplantation embryo blastocists (3-8 μm) (Salas-Vidal & Lomelí, 2004); mouse embryo actin-based filopodia between cells of the late morula stage (10.9 ± 0.8 μm) (Fierro-González, White, Silva, & Plachta, 2013); and mesenchymal cultured cells C3H/10T1/2 transfected with Cdc42 (less than 10 μm) (Koizumi et al., 2012).

However, **larger signaling filopodia** (more than 10 μm) have also been described: the **FGFR2** and **ErbB3** receptor cells of **mouse** preimplantation embryo blastocists, with filopodia up to 34.6 μm (Salas-Vidal & Lomelí, 2004); **Shh** specialized filopodia in **chick** limb bud, up to 150 μm (Sanders et al., 2013); **zebrafish** epiblast cell **Wnt8a**, from 16.6 μm to 50 μm. (Stanganello et al., 2015); **chick** embryo **Wnt** signaling dermomyotome, up to 20 μm (Sagar et al., 2015); air sac tracheoblasts, up to 50 μm (Sato & Kornberg, 2002); the **LgR4/Lgr5** transfected **human** HEK cell line exceeding 80 μm (Snyder et al., 2015); and **RhoD** transfected **mouse** mesenchymal cultured cells C3H/10T1/2 that form dynamic short protrusions (less

than 20 μm) and immotile long protrusions (some more than 60 μm) (Koizumi et al., 2012).

Additionally, similar cytoneme maximum extent values are reached with ectopic Ihog: 10.03 ± 5.15 μm in Hh-producing cells and 9.33 ± 4.20 μm in Hh-receiving cells (average ± standard deviation). This indicates that although Ihog stabilizes cytonemes (Figure R-4; Figure R-6; Table R-1; Movie R-1; Movie R-2; Bischoff et al. 2013), the maximum extent values are not disturbed, unless using Ihog mutant variants. In the case of the expression of Ihog without the Fn2 domains, cytonemes show shorter maximum extent when expressed in Hh-receiving histoblasts. In the case of expressing Ihog without both FNIII domains or without the C-terminus domain, cytonemes show larger maximum extent when expressed in Hh-sending histoblasts. In these mutant variants still unknown interaction with actin-binding proteins could account for the changes in the extent values.

Filopodia dynamics

Regarding filopodia dynamics, our *in vivo* data in abdominal histoblasts reveal that Hh signaling GMA-labelled filopodia have **lifetime** values of 7.42 ± 4.22 min (average ± standard deviation) in Hh-receiving cells and 6.96 ± 3.90 min in Hh-producing cells; **triangle-like elongation velocities** of 2.79 ± 1.14 μm/min in Hh-receiving cells and 2.85 ± 1.40 μm/min in Hh-producing cells; **trapezoid-like elongation velocities** of 3.69 ± 2.10 μm/min in Hh-receiving cells and 3.24 ± 1.73 μm/min in Hh-producing cells; **triangle-like retraction velocities** of 2.44 ± 1.28 μm/min in Hh-receiving cells and 2.56 ± 1.40 μm/min in Hh-producing cells; and **trapezoid-like retraction velocities** of 2.61 ± 1.59 μm/min in Hh-

receiving cells and 3.19 ± 2.04 μm/min in Hh-producing cells. These **velocity values are similar to those of chick embryo Wnt signaling filopodia** between dermomyotome and ectoderm, which extend at an average rate of 2.23 μm/min and retract at an average rate of 4.13 μm/min (Sagar et al., 2015). Yet again, **faster elongation rates** have also been shown, **Shh** specialized filopodia in **chick** limb bud with a maximum elongation rate of 9 μm/min (Sanders et al., 2013), and **zebrafish** epiblast cell **Wnt8a** filopodia extensions displaying an average velocity of 6.6 ± 0.06 μm/min. Interestingly, despite the difference in velocity the latest zebrafish extensions elongate in a process that **last less than 10 min** (Stanganello et al., 2015), **consistent with our lifetime values**.

Cytoneme dynamics are independent of Hh and Ptc

An outstanding question concerning cytoneme formation and dynamics is their relation to ligand and/or receptor presence. It has been previously published that membrane CD8 labeled **filopodia** were **not altered after Hh induction** by heat-shock (Roy et al., 2011). Here we verified that in the **absence of the ligand Hh**, **ectopic Ihog still drives cytonemes stabilization** (Figure R-9; Movie R-13), suggesting that Hh is not necessary for cytoneme formation neither for regulation of their dynamics. Additionally, **Hh-producing cells** still emit **cytonemes** with **similar dynamics** when **crossing** either **wild type** or ***ptc* mutant** Hh-receiving territories (Figure R-9; Figure R-10, Movie R-14), indicating that Hh signaling filopodia dynamics are independent of the receptor Ptc. Thus, we can conclude that the existence of a **network of dynamic Hh signaling filopodia** in *Drosophila* abdominal tissue is **independent** of both the **ligand** and the **receptor** presence.

Ihog and Boi function in Hh signaling filopodia dynamics

On the other hand, in the case of the Hh co-receptors **Ihog and Boi, which seem to be functionally redundant** (Zheng et al., 2010), **are not in regards to Hh signaling filopodia dynamics**, as Ihog (Figure R-4; Figure R-6; Table R-1; Movie R-1; Movie R-2; Bischoff et al. 2013), but not Boi (Figure R-11; Movie R-17) drives cytoneme stabilization in a Boi-independent manner (Figure R-12; Movie R-19). Nevertheless, loss-of-function of both Ihog and Boi does not impair cytoneme formation (Figure R-13; Movie R-20). Overall, these data indicate a specific role of Ihog in regulating filopodia dynamics, although further research would be needed to elucidate the specific Ihog function, such as performing live imaging of *ihog* null mutants. In contrast, in the **chick limb bud** the cytoneme **stabilizing effect** is attributed to the ectopic espression of **BOC** (Sanders et al., 2013), the Boi homologue, as well as to the ectopic Ihog homologue CDO (data not shown in Sanders et al., 2013).

On the other hand, we have also observed that ectopic Ihog can recruit Boi to basal stabilized cytonemes (Figure R-11; Movie R-15; Movie R-16; Movie R-18), although the *Drosophila* Boi is preferentially located at apical and lateral surfaces (Bilioni et al., 2013; Zheng et al., 2010). Thus, it would be interesting to further investigate in detail the Ihog-Boi interaction and analyze the role of this interaction on Hh signaling pathway regulation.

Intriguingly, Ihog is widely expressed in both the A and P compartments of wing imaginal discs of third instar larvae with a slight decrease at the AP compartment border, just where it acts as a co-receptor of Hh (Zheng et al., 2010; Yan et al., 2010; Bilioni et al., 2013; Camp et al., 2014). One possibility to explain this decrease of

Ihog at the AP compartment border could be to facilitate the dynamic behavior of cytonemes, according to our results that high levels of Ihog lead to more stable cytonemes (Figure R-4; Figure R-6; Table R-1; Movie R-1; Movie R-2; Bischoff et al. 2013).

Role of Ihog functional domains in Hh signaling

In this thesis, we have next focused in further study of the co-receptor Ihog whose ectopic expression drives to a longer stationary phase and a trapezoid-like behavior within our particular model of filopodia dynamics (Figure S-2). Interestingly, the **absence of the Ihog FNIII domain**s lead to a triangle-like behavior or still a trapezoid-like behavior but with a significantly shorter stationary phase; getting **closer to wild type dynamics** regarding elongation and retraction velocities and thus reaching similar lifetimes to non-overexpressing *ihog* cytonemes (Figure R-15 compared to Figure R-4; Movie R-22, Movie R-23 and Movie R-24 compared to Movie R-1 and Movie R-2). These results clearly demonstrate that **FNIII domains are responsible of Ihog-driven cytoneme dynamics regulation**.

Surprisingly the construct ***ihogΔFn2*** produced filopodia with **slower elongation and retraction velocities** compared to non-overexpressing *ihog* or to the expression of ***ihogΔFN*** (Figure R-15; Table R-4; Table R-5). These data indicate that **Fn1 and Fn2 domains** could **regulate cytoneme dynamics in different ways**, probably having the Fn1 a dominant role in the regulation of cytoneme stability. Further analysis would be needed to address this hypothesis.

It is known that **FNIII domains** are essential for **Hh-Ihog and Ptc-Ihog interactions** (McLellan et al., 2006; Zheng et al., 2010). Remarkably, expression of the construct ***ihogFn2****, with an intact

domain but with two point mutations in Fn2 that **unable its interaction with Ptc**, produces cytonemes with **similar lifetime values** to those overexpressing wild type *ihog* (**stabilized cytonemes**) (Figure R-16; Table R-4; Table R-5). Thus, these results support the hypothesis **that FNIII domains, but not the Ptc interaction specific residues, are responsible for Ihog-driven cytoneme stabilization**.

Regarding **ligand interaction**, expression of Ihog lacking either or both of the FNIII domains (**Fn1 and Fn2**) leads to **less accumulation** of Hh compared to the wild type Ihog expression (Figure R-17; Movie R-26), indicating that both FNIII domains are also **responsible for Hh accumulation in cytonemes**. Cristal structure studies have indicated that Fn1 domain directly interacts with Hh (McLellan et al., 2006; Yao et al., 2006); but the interaction of Fn2 with Hh was unknown and it could be indirect. This **interaction** might be mediated by the FNIII domain with some component of the **ECM** (the proteoglycans Dally or Dlp) or with **integrins**. In strong support of this possibility, we have described that **Ihog without FNIII domains fails to accumulate the β-chain of integrins (βPS) at the A/P border**, which normally occurs by ectopic wild type Ihog (Figure R-20). In addition, the P compartment expression of FNIII deleted Ihog leads to a **Hh morphogenetic gradient similar to wild type** (Figure R-18) rather than the restriction effect normally carried by ectopic complete Ihog, probably due to the fact that **both cytoneme dynamics and Hh sequestration are restored to wild type conditions**.

Furthermore, the Ihog construct described as unable to interact with Ptc (***ihogFn2**)*** still **accumulates Hh** as wild type Ihog (Figure R-17; Movie R-26), indicating that the **Hh-Ihog interaction** is

independent of the specific **Fn2 region responsible for Ihog-Ptc interaction**.

As for the **Ig domains**, they could also have a role in **Hh recruitment** driven by Ihog (Yan et al. 2010; Callejo et al. 2011; Bilioni et al. 2013; Figure R-7I-J, arrows; Movie R-3B'; Movie R-4B'), since the construct ***UAS.ihogΔIg-RFP* does not accumulate Hh** (Figure R-17A; Movie R-25A-A'; N=5). Moreover, deleting Ig domains of Ihog leads to a **flat signaling response**, probably due to less Hh accumulation at the basal surface. However, this effect might result or partly result from a recently identified **unintended point mutation** in one of the predicted Hh interacting aminoacids. Future analysis of experiments using a new mutation-free *UAS.ihogΔIg-RFP* construct will clarify the role of Ihog Ig domains over the Hh accumulation effect.

Overall **ectopic Ihog** induces Hh attachment to membranes and cytonemes, also **reducing** the **Hh signaling responses** when expressed in **Hh-producing cells** (Bilioni et al. 2013; Bischoff et al. 2013; Figure R-18), probably due to less Hh signaling activity in Hh-receiving cells. Conversely, ectopic Ihog in **Hh-receiving cells** sequesters Hh and the **Hh gradient is extended** (González-Méndez et al., 2017) probably due to more Hh signaling activity in those Hh responding cells. Additionally, **cytoneme extent correlates with the responsive *ptc* gradient** (Figure R-18), in agreement with our previous study of Hh signaling gradient establishment regulated by cytonemes (Bischoff et al., 2013). Nonetheless, in the case of *UAS.ihogΔIg-RFP* and *UAS.ihogΔCt-RFP* expression the gradient-cytoneme extent correlation drifts apart. The ***UAS.ihogΔIg-RFP*** results in **flat *ptc* expression** could be simply consequence of **lacking Hh interaction** or other altered unknown Ig domains

interactions. As for the ***UAS.ihogΔCt-RFP*** *case,* a still **unidentified role** for this domain must be modifying the gradient.

Altogether, our results demonstrate that the **FNIII domains** of Ihog have a role both in **regulating Hh cytonemes dynamics and Hh levels**, as suggested by Sánchez-Hernández 2013. In addition, the **Ig and FNIII domains** could interact with **Shf** and/or with the glypican **Dally** to regulate **Hh retention** (Bilioni et al., 2013), as Shf and Dally interact with Ihog and are also required to maintain normal levels of Hh (Bilioni et al., 2013; Gorfinkiel et al., 2005; Sanchez-Hernandez et al., 2012). Preliminary immunohistochemistry and immunoprecipitation experiments indicate an Ihog-Shf interaction mediated by the Ig domains, and an Ihog-Dlp interaction mediated by the FNIII domains (data not shown). Further analysis of these Ihog interactions would be needed to better understand the role of each Ihog domains.

As a summary, we present a **model** (Figure D-1) in which **FNIII domains** of Ihog regulate actin-based **filopodia dynamics**. This might be mediated by the **interaction** of the FNIII domains with components of the **extracellular matrix** such as Dally or Dlp, or with **integrins**. Due to these interactions with the ECM, when Ihog levels are high, Ihog-coated filopodia could have added difficulties to elongate and retract, leading to more stable filopodia. While, by deleting the FNIII domains prevention of exceding cell-cell and cell-ECM interactions (of adhesion proteins) would allow normal cytoneme elongation and retraction. In addition to the extracellular dynamic control, **Ihog** could also act as a **bridge between actin binding proteins and adhesion proteins** further regulating filopodia intracellularly.

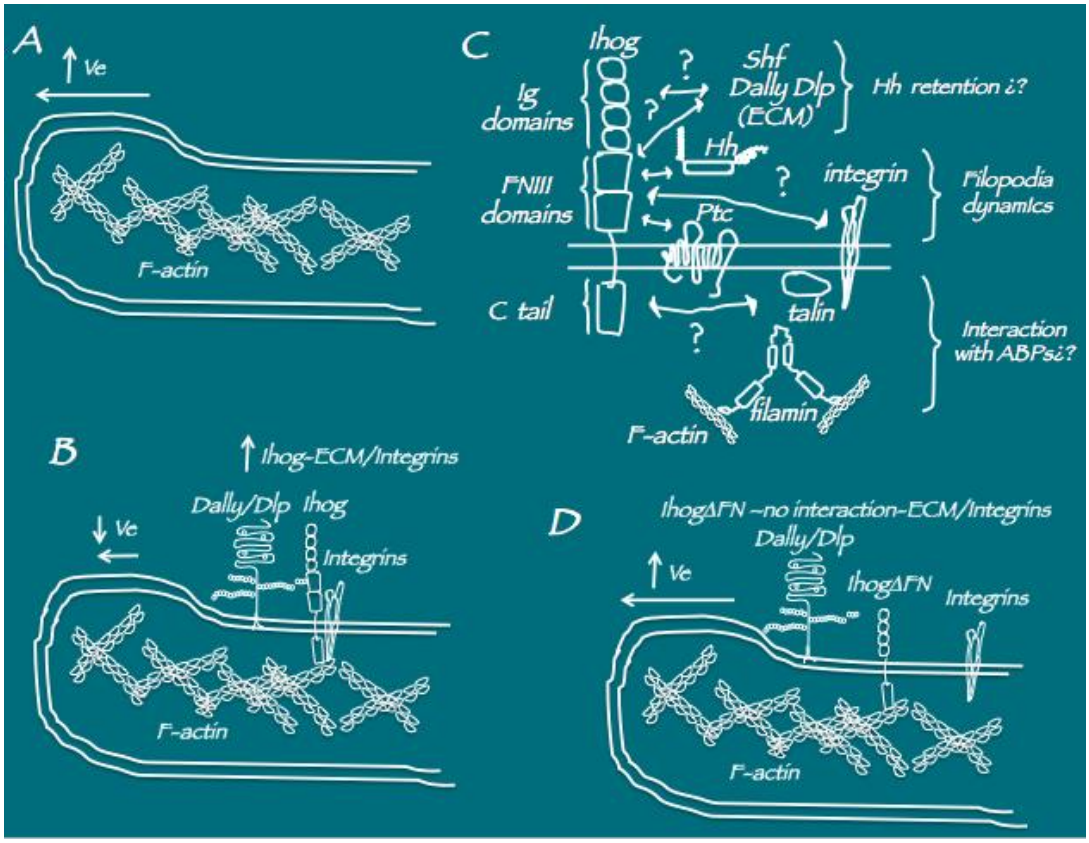

Figure D-1. Model for the functional domains of Ihog on Hh cytoneme dynamics.

A: Wild type filopodia. Scheme of wild type filopodia with normal extension velocity (Ve). **B: Ectopic Ihog filopodia.** Scheme of a cell filopodia overexpressing ihog, where the extra levels of Ihog interact with the ECM components Dally or Dlp, integrins and actin filaments, impairing normal filopodial movement by a reduced Ve. **C: Ihog domains interactions and function.** Scheme of the different domains of Ihog. Arrows indicate possible molecular interactions and question marks indicate unknown but possible interactions. **D: Ectopic IhogΔFN filopodia.** Scheme of a cell filopodia overexpressing an Ihog construct lacking the FNIII. This mutant form of Ihog probably does not interact with the ECM components Dally or Dlp, or with the integrins, leading to normal filopodial movement with a higher Ve than the case of ectopic wild type Ihog.

Conclusions

1. Specialized actin-based filopodia (cytonemes) and the exosome production machineries regulate Hedgehog (Hh) signaling. Mutant conditions affecting actin dynamics or exosome production affect the Hh gradient.

2. There is a strong correlation between cytoneme reach range and the extension of the Hh morphogenetic gradient.

3. The ligand Hh and the receptor Patched (Ptc) are localized in vesicle-like structures that co-localize with the exosomal and MVB marker CD63 in fixed samples and *in vivo*.

4. Hh localizes *in vivo* along dynamic Lifeact-labelled cytonemes and highly accumulates along ectopic Ihog-driven stabilized cytonemes located in the basolateral part of the pupal abdominal epithelium. Ptc does not accumulate *in vivo* in Ihog-driven stabilized cytonemes and it is more difficult to visualize along cytonemes due to its rapid endocytosis.

5. The existence of a network of dynamic cytonemes is independent of the presence of the Hh ligand and the Ptc receptor.

6. Cytonemes of abdominal histoblasts comprise two types of dynamic behaviors: triangle-like dynamics with constant elongation and retraction velocities and trapezoid-like dynamics with a stationary interphase between elongation and retraction phases.

7. The adhesion molecules and Hh co-receptors Ihog and Boi are both located in cytonemes, but only ectopic Ihog stabilizes them.

8. Ihog regulates cytoneme dynamics by disturbing the stationary phase of trapezoid-like dynamics. The two Fibronectin type III domains of Ihog are responsible for the cytoneme dynamics regulation.

9. Both Fibronectin type III domains are implicated in the extracellular Hh stability. The second FNIII domain of Ihog (Fn2) could be indirectly responsible of Ihog-driven Hh retention.

10. The two FNIII domains of Ihog have a specific role in regulating Ihog-integrins interaction along the A/P compartment border between Hh-producing and Hh-receiving cells.

Bibliography

Allen, B. L., Song, J. Y., Izzi, L., Althaus, I. W., Kang, J. S., Charron, F., Krauss, R. S. & McMahon, A. P. (2011). Overlapping roles and collective requirement for the coreceptors GAS1, CDO, and BOC in SHH pathway function. *Developmental Cell*, *20*(6), 775–787.

Ashburner, M. (1989). *Drosophila: A Laboratory Handbook*. *Plainview NY Cold Spring Harbor Laboratory Press*.

Basler, K., & Struhl, G. (1994). Compartment boundaries and the control of Drosophila limb pattern by hedgehog protein. *Nature*, *368*(6468), 208–14.

Bilioni, A., Sánchez-Hernández, D., Callejo, A., Gradilla, A. C., Ibáñez, C., Mollica, E., Rodríguez-Navas, M. C., Eléanor, S. & Guerrero, I. (2013). Balancing Hedgehog, a retention and release equilibrium given by Dally, Ihog, Boi and shifted/DmWif. *Developmental Biology*, *376*(2), 198–212.

Bischoff, M., Gradilla, A. C., Seijo, I., Andrés, G., Rodríguez-Navas, C., González-Méndez, L., & Guerrero, I. (2013). Cytonemes are required for the establishment of a normal Hedgehog morphogen gradient in Drosophila epithelia. *Nature Cell Biology*, *15*(11), 1269–81.

Bloor, J. W., & Kiehart, D. P. (2001). zipper Nonmuscle myosin-II functions downstream of PS2 integrin in *Drosophila* myogenesis and is necessary for myofibril formation. *Developmental Biology*, *239*, 215–228.

Brand, A. H., & Perrimon, N. (1993). Targeted gene expression as a means of altering cell fates and generating dominant phenotypes. *Development (Cambridge, England)*, *118*(2), 401–15.

Briscoe, J., & Therond, P. (2013). The mechanisms of Hedgehog signalling and its roles in development and disease. *Nat Rev Mol Cell Biol*, *14*, 416–429.

Burke, R., Nellen, D., Bellotto, M., Hafen, E., Senti, K. A, Dickson, B. J., & Basler, K. (1999). Dispatched, a novel sterol-sensing domain protein dedicated to the release of cholesterol-modified hedgehog from signaling cells. *Cell*, *99*(7), 803–815.

Callejo, A., Bilioni, A., Mollica, E., Gorfinkiel, N., Andrés, G., Ibáñez, C., Torroja, C., Doglio, L., Sierra, J. & Guerrero, I. (2011). Dispatched mediates Hedgehog basolateral release to form the long-range morphogenetic gradient in the Drosophila wing disk epithelium. *Proceedings of the National Academy of Sciences of the United States of America*, *108*(31), 12591–8.

Callejo, A., Torroja, C., Quijada, L., & Guerrero, I. (2006). Hedgehog lipid modifications are required for Hedgehog stabilization in the extracellular matrix. *Development (Cambridge, England)*, *133*, 471–483.

Camp, D., Currie, K., Labbé, A., van Meyel, D. J., & Charron, F. (2010). Ihog and Boi are essential for Hedgehog signaling in Drosophila. *Neural Development*, *5*(1), 28.

Camp, D., Haitian He, B., Li, S., Althaus, I. W., Holtz, A. M., Allen, B. L., Charron, F. & van Meyel, D. J. (2014). Ihog and Boi elicit Hh signaling via Ptc but do not aid Ptc in sequestering the Hh ligand. *Development (Cambridge, England)*, *141*(20), 3879–88.

Capdevila, J., Estrada, M. P., Sánchez-Herrero, E., & Guerrero, I. (1994). The Drosophila segment polarity gene patched interacts with decapentaplegic in wing development. *The EMBO Journal*, *13*(1), 71–82.

Capdevila, J., & Guerrero, I. (1994). Targeted expression of the signaling molecule decapentaplegic induces pattern duplications and growth alterations in Drosophila wings. *The EMBO Journal*, *13*(19), 4459–68.

Cardozo, M. J., Sánchez-Arrones, L., Sandonis, Á., Sánchez-Camacho, C., Gestri, G., Wilson, S. W., Guerrero, I. & Bovolenta, P. (2014). Cdon acts as a Hedgehog decoy receptor during proximal-distal patterning of the optic vesicle. *Nature Communications*, *5*(May), 4272.

Chamoun, Z., Mann, R. K., Nellen, D., von Kessler, D. P., Belloto, M., Beachy, P. A. & Basler, K. (2001). Skinny Hedgehog , an Acyltransferase Required for Palmitoylation and Activity of the Hedgehog Signal. *Science*, *293*(5537), 2080–2084.

Chen, M. H., Li, Y. J., Kawakami, T., Xu, S. M., & Chuang, P. T. (2004). Palmitoylation is required for the production of a soluble multimeric Hedgehog protein complex and long-range signaling in vertebrates. *Genes and Development*, *18*(6), 641–659.

Chen, Y., & Struhl, G. (1996). Dual roles for patched in sequestering and transducing Hedgehog. *Cell*, *87*(3), 553–563.

Cohen, M., Georgiou, M., Stevenson, N. L., Miodownik, M., & Baum, B. (2010). Dynamic Filopodia Transmit Intermittent Delta-Notch Signaling to Drive Pattern Refinement during Lateral Inhibition. *Developmental Cell*, *19*(1), 78–89.

Cooper, J. A., & Sept, D. (2008). New insights into mechanism and regulation of actin capping protein. *Int Rev Cell Mol Biol*, *267*, 183–206.

Desbordes, S. C., & Sanson, B. (2003). The glypican Dally-like is required for Hedgehog signalling in the embryonic epidermis of Drosophila. *Development (Cambridge, England)*, *130*(25), 6245–55.

Deshpande, G., Swanhart, L., Chiang, P., & Schedl, P. (2001). Hedgehog Signaling in Germ Cell Migration. *Cell*, *106*(6), 759–69.

Diaz-Benjumea, F. J., Cohen, B., & Cohen, S. M. (1994). Cell interaction between compartments establishes the proximal-distal axis of Drosophila legs. *Nature*, *372*(6502), 175–179.

Domínguez, M. (1999). Dual role for Hedgehog in the regulation of the proneural gene atonal during ommatidia development. *Development (Cambridge, England)*, *126*(11), 2345–2353.

Etheridge, L. A., Crawford, T. Q., Zhang, S., & Roelink, H. (2010). Evidence for a role of vertebrate Disp1 in long-range Shh signaling. *Development (Cambridge, England)*, *137*, 133–140.

Eugster, C., Panáková, D., Mahmoud, A., & Eaton, S. (2007). Lipoprotein-Heparan Sulfate Interactions in the Hh Pathway. *Developmental Cell*, *13*(1), 57–71.

Fierro-González, J. C., White, M. D., Silva, J. C., & Plachta, N. (2013). Cadherin-dependent filopodia control preimplantation embryo compaction. *Nature Cell Biology*, *15*(12), 1424–1433.

Gallet, A., Ruel, L., Staccini-Lavenant, L., & Thérond, P. P. (2006). Cholesterol modification is necessary for controlled planar long-range activity of Hedgehog in Drosophila epithelia. *Development (Cambridge, England)*, *133*(3), 407–18.

Garcia-Bellido, A., Ripoll, P., & Morata, G. (1973). Developmental Compartmentalisation of the Wing Disk of Drosophila. *Nature New Biology*, *245*(147), 251–253.

Glazer, L., & Shilo, B. Z. (2001). Hedgehog signaling patterns the tracheal branches. *Development (Cambridge, England)*, *128*(9), 1599–606.

Golic, K. G., & Lindquist, S. (1989). The FLP recombinase of yeast catalyzes site-specific recombination in the drosophila genome. *Cell*, *59*(3), 499–509.

Gomez, T. M., & Letourneau, P. C. (2014). Actin dynamics in growth cone motility and navigation. *Journal of Neurochemistry*, *129*(2), 221–234.

González-Méndez, L., Seijo-Barandiarán, I. and Guerrero, I. (2017) Cytoneme-mediated cell-cell contacts for Hedgehog reception. *eLIFE*. In press.

Goodrich, L. V, Johnson, R. L., Milenkovic, L., & Mcmahon, J. A. (1996). Conservation of the hedgehog ~ patched . s gnaling pathway from flies to mice : reduction of a mouse patched gene by Hedgehog. *Genes and Development*, *10*, 301–312.

Gorfinkiel, N., Sanchez, L., & Guerrero, I. (2003). Development of the Drosophila genital disc requires interactions between its segmental primordia. *Development*, *130*(2), 295–305.

Gorfinkiel, N., Sierra, J., Callejo, A., Ibañez, C., & Guerrero, I. (2005). The Drosophila ortholog of the human Wnt inhibitor factor shifted controls the diffusion of lipid-modified hedgehog. *Developmental Cell*, *8*(2), 241–253.

Gradilla, A.C., González, E., Seijo, I., Andrés, G., Bischoff, M., González-Mendez, L., Sánchez, V., Callejo, A., Ibáñez, C., Guerra, M., Ortigão-Farias, J. R., Sutherland, J. D., González, M., Barrio, R., Falcón-Pérez, J. M. & Guerrero, I. (2014). Exosomes as Hedgehog carriers in cytoneme-mediated transport and secretion. *Nature Communications*, *5*, 5649.

Gradilla, A. C., & Guerrero, I. (2013a). Cytoneme-mediated cell-to-cell signaling during development. *Cell and Tissue Research*, *352*(1), 59–66.

Gradilla, A. C., & Guerrero, I. (2013b). Hedgehog On The Move: A Precise Spatial Control Of Hedgehog Dispersion Shapes The Gradient. *Current Opinion in Genetics and Development*, *23*(4), 363–373.

Gross, J. C., Chaudhary, V., Bartscherer, K., & Boutros, M. (2012). Active Wnt proteins are secreted on exosomes. *Nature Cell Biology*, *14*(10), 1036–1045.

Guerrero, I., & Chiang, C. (2007). A conserved mechanism of Hedgehog gradient formation by lipid modifications. *Trends in Cell Biology*, *17*(1), 1–5.

Guerrero, I., & Kornberg, T. B. (2014). Hedgehog and its circuitous journey from producing to target cells. *Seminars in Cell and Developmental Biology*, *33*, 52–62.

Hamada, H., Watanabe, M., Lau, H. E., Nishida, T., Hasegawa, T., Parichy, D. M., & Kondo, S. (2014). Involvement of Delta/Notch signaling in zebrafish adult pigment stripe patterning. *Development (Cambridge, England)*, *141*(2), 318–24.

Hinz, U., Giebel, B., & Campos-Ortega, J. (1994). The basic-helix-loop-helix domain of Drosophila lethal of scute protein is sufficient for proneural function and activates neurogenic genes. *Cell*, *76*(1), 77–87.

Holzer, T., Liffers, K., Rahm, K., Trageser, B., Özbek, S., & Gradl, D. (2012). Live imaging of active fluorophore labelled Wnt proteins. *FEBS Letters*, *586*(11), 1638–1644.

Hsiung, F., Ramírez-Weber, F.-A., Iwaki, D. D., & Kornberg, T. B. (2005). Dependence of Drosophila wing imaginal disc cytonemes on Decapentaplegic. *Nature*, *437*(7058), 560–563.

Huang, H., & Kornberg, T. B. (2015). Myoblast cytonemes mediate Wg signaling from the wing imaginal disc and Delta-Notch signaling to the air sac primordium. *eLife*, *4*, e06114.

Ingham, P. W., Mcmahon, A. P., Ingham, P. W., & Mcmahon, A. P. (2001). Hedgehog signaling in animal development : paradigms and principles Hedgehog signaling in animal development : paradigms and principles. *Genes and Development*, *15*(23), 3059–3087.

Ingham, P. W., Nakano, Y., & Seger, C. (2011). Mechanisms and functions of Hedgehog signalling across the metazoa. *Nature Reviews. Genetics*, *12*(6), 393–406.

Izzi, L., Lévesque, M., Morin, S., Laniel, D., Wilkes, B. C., Mille, F., Krauss, R. S., McMahon, A. P., Allen, B. L. & Charron, F. (2011). Boc and gas1 each form distinct shh receptor complexes with ptch1 and are required for shh-mediated cell proliferation. *Developmental Cell*, *20*(6), 788–801.

Joussineau, C. De, Soule´, J., Martin, M., Anguille, C., Philippe, M. & Daniel, A. (2003). Delta-promoted filopodia mediate long-range lateral inhibition in Drosophila. *Nature*, *426*(December), 555–559.

Kang, J., Mulieri, P. J., Hu, Y., Taliana, L., & Krauss, R. S. (2002). BOC , an Ig superfamily member , associates with CDO to positively regulate myogenic differentiation, *21*.

Kavran, J. M., Ward, M. D., Oladosu, O. O., Mulepati, S., & Leahy, D. J. (2010). All mammalian hedgehog proteins interact with cell adhesion molecule, down-regulated by oncogenes (CDO) and brother of CDO (BOC) in a conserved manner. *Journal of Biological Chemistry*, *285*(32), 24584–24590.

Kim, M.-S., Saunders, A. M., Hamaoka, B. Y., Beachy, P. A, & Leahy, D. J. (2011). Structure of the protein core of the glypican Dally-like and localization of a region important for hedgehog signaling. *Proceedings of the National Academy of Sciences of the United States of America*, *108*(32), 13112–13117.

Koizumi, K., Takano, K., Kaneyasu, A., Watanabe-Takano, H., Tokuda, E., Abe, T., Watanabe, N., Takenawa, T. & Endo, T. (2012). RhoD activated by fibroblast growth factor induces cytoneme-like cellular protrusions through mDia3C. *Molecular Biology of the Cell*, *23*(23), 4647–4661.

Kopp, A., & Duncan, I. (2002). Anteroposterior patterning in adult abdominal segments of Drosophila. *Developmental Biology*, *242*(1), 15–30.

Kopp, A., Muskavitch, M. A., & Duncan, I. (1997). The roles of hedgehog and engrailed in patterning adult abdominal segments of Drosophila. *Development (Cambridge, England)*, *124*(19), 3703–3714.

Kornberg, T. B., & Roy, S. (2014). Cytonemes as specialized signaling filopodia. *Development*, *141*(4), 729–736.

Kunda, P., Craig, G., Dominguez, V., & Baum, B. (2003). Abi, Sra1, and Kette Control the Stability and Localization of SCAR/WAVE to Regulate the Formation of Actin-Based Protrusions. *Current Biology*, *13*(21), 1867–1875.

Lee, J. J., Ekker, S. C., von Kessler, D. P., Porter, J. A., Sun, B. I., & Beachy, P. A. (1994). Autoproteolysis in hedgehog protein biogenesis. *Science (New York, N.Y.)*, *266*(5190), 1528–1537.

Lewis, P. M., Dunn, M. P., McMahon, J. A., Logan, M., Martin, J. F., St-Jacques, B., & McMahon, A. P. (2001). Cholesterol modification of sonic hedgehog is required for long-range signaling activity and effective modulation of signaling by Ptc1. *Cell*, *105*(5), 599–612.

Lidke, D. S., Lidke, K. A., Rieger, B., Jovin, T. M., & Arndt-Jovin, D. J. (2005). Reaching out for signals: Filopodia sense EGF and respond by directed retrograde transport of activated receptors. *Journal of Cell Biology*, *170*(4), 619–626.

Lum, L., Yao, S., Mozer, B., Rovescalli, A., Von Kessler, D., Nirenberg, M., & Beachy, P. A. (2003). Identification of Hedgehog Pathway Components by RNAi in Drosophila Cultured Cells. *Science*, *299*(5615), 2039–2045.

Luz, M., Spannl-Müller, S., Özhan, G., Kagermeier-Schenk, B., Rhinn, M., Weidinger, G., & Brand, M. (2014). Dynamic association with donor cell filopodia and lipid-modification are essential features of Wnt8a during patterning of the zebrafish neuroectoderm. *PLoS ONE*, *9*(1).

Lyulcheva, E., Taylor, E., Michael, M., Vehlow, A., Tan, S., Fletcher, A., Krause, M. & Bennett, D. (2008). Drosophila Pico and Its Mammalian Ortholog Lamellipodin Activate Serum Response Factor and Promote Cell Proliferation. *Developmental Cell*, *15*(5), 680–690.

Ma, C., Zhou, Y., Beachy, P. A., & Moses, K. (1993). The segment polarity gene hedgehog is required for progression of the morphogenetic furrow in the developing Drosophila eye. *Cell*, *75*(5), 927–938.

Madhavan, M. M., & Madhavan, K. (1980). Morphogenesis of the epidermis of adult abdomen of Drosophila. *Journal of Embryology and Experimental Morphology*, *60*, 1–31.

Mandal, L., Martinez-Agosto, J. A., Evans, C. J., Hartenstein, V., & Banerjee, U. (2007). A Hedgehog- and Antennapedia-dependent niche maintains Drosophila haematopoietic precursors. *Nature*, *446*(7133), 320–4.

Marigo, V., Scott, M. P., Johnson, R. L., Goodrich, L. V, & Tabin, C. J. (1996). Conservation in hedgehog signaling: induction of a chicken patched homolog by Sonic hedgehog in the developing limb. *Development (Cambridge, England)*, *122*(4), 1225–1233.

Matusek, T., Wendler, F., Polès, S., Pizette, S., D'Angelo, G., Fürthauer, M., & Thérond, P. P. (2014). The ESCRT machinery regulates the secretion and long-range activity of Hedgehog. *Nature*, *516*(7529), 99–103.

McGuire, S. E. (2003). Spatiotemporal Rescue of Memory Dysfunction in Drosophila. *Science*, *302*(5651), 1765–1768.

McLellan, J. S., Yao, S., Zheng, X., Geisbrecht, B. V, Ghirlando, R., Beachy, P. a, & Leahy, D. J. (2006). Structure of a heparin-dependent complex of Hedgehog and Ihog. *Proceedings of the National Academy of Sciences of the United States of America*, *103*(46), 17208–17213.

McLellan, J. S., Zheng, X., Hauk, G., Ghirlando, R., Beachy, P. A., & Leahy, D. J. (2008). The mode of Hedgehog binding to Ihog homologues is not conserved across different phyla. *Nature*, *455*(7215), 979–83.

Miller, J., Fraser, S. E., & McClay, D. (1995). Dynamics of thin filopodia during sea urchin gastrulation. *Development (Cambridge, England)*, *121*(8), 2501–2511.

Mullor, J. L., Calleja, M., Capdevila, J., & Guerrero, I. (1997). Hedgehog activity, independent of decapentaplegic, participates in wing disc patterning. *Development (Cambridge, England)*, *124*(6), 1227–1237.

Neumann-Giesen, C., Falkenbach, B., Beicht, P., Claasen, S., Luers, G., Stuermer, C. A., Herzog, V. & Tikkanen, R. (2004). Membrane and raft association of reggie-1/flotillin-2: role of myristoylation, palmitoylation and oligomerization and induction of filopodia by overexpression. *Biochem J*, *378*(Pt 2), 509–518.

Ninov, N., Chiarelli, D., & Martín-Blanco, E. (2007). Extrinsic and intrinsic mechanisms directing epithelial cell sheet replacement during Drosophila metamorphosis. *Development (Cambridge, England)*, *134*(2), 367–379.

Ninov, N., & Martín-Blanco, E. (2007). Live imaging of epidermal morphogenesis during the development of the adult abdominal epidermis of Drosophila. *Nature Protocols*, *2*, 3074–3080.

Nüsslein-Volhard, C., & Wieschaus, E. (1980). Mutations affecting segment number and polarity in Drosophila. *Nature*, *287*(5785), 795–801.

Ohlig, S., Farshi, P., Pickhinke, U., van den Boom, J., Höing, S., Jakuschev, S., Hoffmann, D., Dreier, R., Schöler, H. R., Dierker, T., Bordych, C. & Grobe, K. (2011). Sonic hedgehog shedding results in functional activation of the solubilized protein. *Developmental Cell*, *20*(6), 764–774.

Okada, A., Charron, F., Morin, S., Shin, D. S., Wong, K., Fabre, P. J., Tessier-Lavigne, M. & McConnell, S. K. (2006). Boc is a receptor for sonic hedgehog in the guidance of commissural axons. *Nature*, *444*(7117), 369–373.

Panáková, D., Sprong, H., Marois, E., Thiele, C., & Eaton, S. (2005). Lipoprotein particles are required for Hedgehog and Wingless signalling. *Nature*, *435*(7038), 58–65.

Pankratz, M. J., & Hoch, M. (1995). Control of epithelial morphogenesis by cell signaling and integrin molecules in the Drosophila foregut. *Development (Cambridge, England)*, *121*(6), 1885–98.

Peng, Y., Han, C., & Axelrod, J. D. (2012). Planar polarized protrusions break the symmetry of EGFR signaling during Drosophila bract cell fate induction. *Dev Cell*, *11*(23), 507–518.

Pepinsky, R. B., Zeng, C., Rayhorn, P., Baker, D. P., Williams, P., Bixler, S. A, Christine, M., Garber, E. A., Taylor, F. R., Elizabeth, A., Galdes, A., Wen, D., Williams, K. P., Ambrose, C. M., Miatkowski, K. & Wang, E. A. (1998). Identification of a Palmitic Acid-modified Form of Human Sonic hedgehog Identification of a Palmitic Acid-modified Form of Human Sonic hedgehog *. *The Journal of Biological Chemistry*, *273*(22), 14037–14045.

Peters, C., Wolf, A., Wagner, M., Kuhlmann, J., & Waldmann, H. (2004). The cholesterol membrane anchor of the Hedgehog protein confers stable membrane association to lipid-modified proteins. *Proceedings of the National Academy of Sciences of the United States of America*, *101*(23), 8531–8536.

Pocha, S. M., & Montell, D. J. (2014). Cellular and Molecular Mechanisms of Single and Collective Cell Migrations in *Drosophila* : Themes and Variations. *Annual Review of Genetics*, *48*(1), 295–318.

Porter, J. A., Ekker, S. C., Park, W. J., Von Kessler, D. P., Young, K. E., Chen, C. H., Ma, Y., Woods, A. S., Cotter, R. J., Koonin, E. V. & Beachy, P. A. (1996). Hedgehog patterning activity: Role of a lipophilic modification mediated by the carboxy-terminal autoprocessing domain. *Cell*, *86*(1), 21–34.

Pröls, F., Sagar, & Scaal, M. (2016). Signaling filopodia in vertebrate embryonic development. *Cellular and Molecular Life Sciences*, *73*(5), 961–974.

Ramírez-Weber, F. A., & Kornberg, T. B. (1999). Cytonemes: Cellular processes that project to the principal signaling center in Drosophila imaginal discs. *Cell*, *97*(5), 599–607.

Raposo, G., & Stoorvogel, W. (2013). Extracellular vesicles: Exosomes, microvesicles, and friends. *Journal of Cell Biology*, *200*(4), 373–383.

Ridley, A. J. (2011). Life at the leading edge. *Cell*, *145*(7), 1012–1022.

Riedl, J., Flynn, K. C., Raducanu, A., Gärtner, F., Beck, G., Bösl, M., Bradke, F., Massberg, S., Aszodi, A., Sixt, M. & Wedlich-Söldner, R. (2010). Lifeact mice for studying F-actin dynamics. *Nature Methods*, *7*(3), 168–169.

Rogers, K. W., & Schier, A. F. (2011). Morphogen Gradients: From Generation to Interpretation. *Annual Review of Cell and Developmental Biology*, *27*(1), 377–407.

Rojas-Ríos, P., Guerrero, I., & González-Reyes, A. (2012). Cytoneme-mediated delivery of Hedgehog regulates the expression of bone morphogenetic proteins to maintain germline stem cells in Drosophila. *PLoS Biology*, *10*(4).

Roy, S., Hsiung, F., & Kornberg, T. B. (2011). Specificity of Drosophila cytonemes for distinct signaling pathways. *Science (New York, N.Y.)*, *332*(6027), 354–8.

Roy, S., & Kornberg, T. B. (2015). Paracrine signaling mediated at cell-cell contacts. *BioEssays*, *37*(1), 25–33.

Sagar, Pröls, F., Wiegreffe, C., & Scaal, M. (2015). Communication between distant epithelial cells by filopodia-like protrusions during embryonic development. *Development (Cambridge, England)*, (January), 1–7.

Salas-Vidal, E., & Lomelí, H. (2004). Imaging filopodia dynamics in the mouse blastocyst. *Developmental Biology*, *265*(1), 75–89.

Sanchez-arrones, L., Cardozo, M., Nieto-lopez, F., & Bovolenta, P. (2012). The International Journal of Biochemistry Cdon and Boc : Two transmembrane proteins implicated in cell – cell communication. *International Journal of Biochemistry and Cell Biology*, *44*(5), 698–702.

Sánchez-Hernández, D. (2013). *Función de Ihog, Boi, Dally y DmWif en la formación del gradiente morfogenético de Hedgehog en el disco imaginal de ala de Drosophila*. Universidad Autónoma de Madrid. Thesis.

Sanchez-Hernandez, D., Sierra, J., Ortigao-Farias, J. R. & Guerrero, I. (2012). The WIF domain of the human and Drosophila Wif-1 secreted factors confers specificity for Wnt or Hedgehog. *Development (Cambridge, England)*, *139*(20), 3849–58.

Sanders, T. a, Llagostera, E., & Barna, M. (2013). Specialized filopodia direct long-range transport of SHH during vertebrate tissue patterning. *Nature*, *497*(7451), 628–32.

Sato, M., & Kornberg, T. B. (2002). FGF is an essential mitogen and chemoattractant for the air sacs of the Drosophila tracheal system. *Developmental Cell*, *3*(2), 195–207.

Seijo-Barandiarán, I., Guerrero, I., & Bischoff, M. (2015). In vivo imaging of hedgehog transport in Drosophila epithelia. *Methods in Molecular Biology*, *1322*, 9–18.

Simon, E., Aguirre-Tamaral, A., Aguilar, G., & Guerrero, I. (2016). Perspectives on Intra- and Intercellular Trafficking of Hedgehog for Tissue Patterning. *Journal of Developmental Biology*, *4*(4), 34.

Snyder, J. C., Rochelle, L. K., Marion, S., Lyerly, H. K., Barak, L. S., & Caron, M. G. (2015). Lgr4 and Lgr5 drive the formation of long actin-rich cytoneme-like membrane protrusions. *Journal of Cell Science*, *128*(6), 1230–40.

St Johnston, D. (2002). the Art and Design of Genetic Screens: Drosophila Melanogaster. *Nature Reviews Genetics*, *3*(3), 176–188.

Stanganello, E., Hagemann, A. I. H., Mattes, B., Sinner, C., Meyen, D., Weber, S., Schug, A., Raz, E. & Scholpp, S. (2015). Filopodia-based Wnt transport during vertebrate tissue patterning. *Nature Communications*, *6*, 5846.

Struhl, G., Barbash, D. A, & Lawrence, P. A. (1997). Hedgehog organises the pattern and polarity of epidermal cells in the Drosophila abdomen. *Development (Cambridge, England)*, *124*(11), 2143–54.

Tanimoto, H., Itoh, S., ten Dijke, P., & Tabata, T. (2000). Hedgehog Creates a Gradient of DPP Activity in Drosophila Wing Imaginal Discs. *Molecular Cell*, *5*(1), 59–71.

Taylor, F. R., Wen, D., Garber, E. A., Carmillo, A. N., Baker, D. P., Arduini, R. M., Williams, K. P., Weinreb, P. H., Rayhorn, P., Hronowski, X., Whitty, A., Day, E. S., Boriack-Sjodin, A., Shapiro, R. I., Galdes, A. & Pepinsky, R. B. (2001). Enhanced potency of human Sonic hedgehog by hydrophobic modification. *Biochemistry*, *40*(14), 4359–4371.

Tenzen, T., Allen, B. L., Cole, F., Kang, J. S., Krauss, R. S., & McMahon, A. P. (2006). The Cell Surface Membrane Proteins Cdo and Boc Are Components and Targets of the Hedgehog Signaling Pathway and Feedback Network in Mice. *Developmental Cell*, *10*(5), 647–656.

Tokusumi, Y., Tokusumi, T., Shoue, D. A., & Schulz, R. A. (2012). Gene regulatory networks controlling hematopoietic progenitor niche cell production and differentiation in the Drosophila lymph gland. *PLoS ONE*, *7*(7).

Trajkovic, K., Hsu, C., Chiantia, S., Rajendran, L., Wenzel, D., Wieland, F., Schwille, P., Brügger, B. & Simons, M. (2008). Ceramide Triggers Budding of Exosome Vesicles into Multivesicular Endosomes. *Science*, *319*(5867), 1244–1247.

Turing, A. M. (1990). The chemical basis of morphogenesis. *Bulletin of Mathematical Biology*, *52*(1–2), 153–197.

Varjosalo, M., & Taipale, J. (2008). Hedgehog: Functions and mechanisms. *Genes and Development*, *22*(18), 2454–2472.

Wehman, A. M., Poggioli, C., Schweinsberg, P., Grant, B. D., & Nance, J. (2011). The P4-ATPase TAT-5 inhibits the budding of extracellular vesicles in C. elegans embryos. *Current Biology*, *21*(23), 1951–1959.

Williams, E. H., Pappano, W. N., Saunders, A. M., Kim, M.-S., Leahy, D. J., & Beachy, P. a. (2010). Dally-like core protein and its mammalian homologues mediate stimulatory and inhibitory effects on Hedgehog signal response. *Proceedings of the National Academy of Sciences of the United States of America*, *107*, 5869–5874.

Wolpert, L. (1969). Positional information and the spatial pattern of cellular differentiation. *Journal of Theoretical Biology*, *25*(1), 1–47.

Wolpert, L., & Gustafson, T. (1961). Studies on the cellular basis of morphogenesis of the sea urchin embryo. *Experimental Cell Research*, *25*(2), 311–325.

Yan, D., Wu, Y., Yang, Y., Belenkaya, T. Y., Tang, X., & Lin, X. (2010). The cell-surface proteins Dally-like and Ihog differentially regulate Hedgehog signaling strength and range during development, *2044*, 2033–2044.

Yao, S., Lum, L., & Beachy, P. (2006). The Ihog Cell-Surface Proteins Bind Hedgehog and Mediate Pathway Activation. *Cell*, *125*(2), 343–357.

Zhang, W., Hong, M., Bae, G., Kang, J.-S., & Krauss, R. S. (2011). Boc modifies the holoprosencephaly spectrum of Cdo mutant mice. *Disease Models & Mechanisms*, *4*(3), 368–380.

Zhang, W., Kang, J. S., Cole, F., Yi, M. J., & Krauss, R. S. (2006). Cdo Functions at Multiple Points in the Sonic Hedgehog Pathway, and Cdo-Deficient Mice Accurately Model Human Holoprosencephaly. *Developmental Cell*, *10*(5), 657–665.

Zheng, X., Mann, R. K., Sever, N., Zheng, X., Mann, R. K., Sever, N., & Beachy, P. A. (2010). Genetic and biochemical definition of the Hedgehog receptor. *Genes and Development*, *24*(1), 57–71.

Resumen en castellano

El **desarrollo** de organismos multicelulares complejos a partir de una célula requiere de la coordinación de procesos como son: proliferación, muerte, determinación y diferenciación celular. Se designa como **morfogénesis** al conjunto de dichos procesos que dan lugar a los diferentes tejidos y órganos en los seres vivos. Las moléculas encargadas de transmitir la información en la comunicación celular durante el desarrollo reciben el nombre de **morfógenos,** y son secretados por las células productoras y actúan en las receptoras, dotando a las células del tejido un comportamiento coordinado que dirigirá los cambios en tamaño, patrón y forma. Los morfógenos forman gradientes de concentración que permiten la activación diferencial de genes diana dependiendo de la concentración de ligando que reciben, siendo también factores importantes en esta respuesta diferencial la duración de la exposición del morfógeno y el estado de las células diana. La precisa regulación de las vías de señalización de los distintos morfógenos es esencial para el correcto desarrollo de los organismos (Rogers & Schier, 2011; Turing, 1990; Wolpert, 1969).

La ruta de señalización de **Hedgehog (Hh)** está altamente conservada en la evolución y es esencial para el desarrollo de diversos organismos (Ingham et al. 2011; Briscoe & Therond 2013). Hh es un morfógeno que se dispersa desde las células productoras del compartimento posterior (P) hasta de células receptoras del compartimento anterior (A) formando un gradiente de actividad. Hh sufre modificaciones lipídicas que anclan la molécula fuertemente a las membranas celulares dificultando su transporte por difusión libre a través del medio extracelular (Guerrero & Chiang 2007; Gradilla & Guerrero 2013).

Existen diversos modelos propuestos para explicar cómo se transporta la proteína **Hh**: integrado en complejos lipoproteícos (Callejo et al., 2006; Panáková et al., 2005); formando multímeros solubles en un medio acuoso (Gallet et al., 2006); como fragmentos de la membrana plasmática o ectosomas (Matusek et al., 2014); o en vesículas que se transportan a lo largo de filopodios especializados ricos en actina, conocidos como citonemas (Callejo et al. 2011; Bilioni et al. 2013; Bischoff et al. 2013; Gradilla et al. 2014).

Este último modelo se ha visto reforzado gracias a estudios realizados en diferentes organismos donde se ha demostrado que, como los citonemas en la vía de señalización de Hh, otras vías también están reguladas por filopodios especializados ricos en actina que transportan los diferentes ligandos y receptores de dichas vías (Gradilla & Guerrero 2013a; Roy & Kornberg 2015; Pröls et al. 2016).

Recientemente, nuestro laboratorio ha demostrado que Hh se transporta en **citonemas,** producidos en la zona basal del epitelio, y que además llevan asociados distintos componentes de la vía de Hh (Bilioni et al., 2013; Bischoff, Gradilla, Seijo, Andrés, Rodríguez-navas, et al., 2013; Callejo et al., 2011). Entre ellos, se encuentran las proteínas del complejo receptor formado por los co-receptores Interference hedgehog (**Ihog**), Brother of Ihog (**Boi**) y el glipicano Dally-like (**Dlp**), involucrados en la recepción de Hh (Desbordes & Sanson, 2003; Lum et al., 2003; Williams et al., 2010) y el tráfico vesicular en las células secretoras de Hh (Callejo et al., 2011); otro glipicano Division abnormally delayed (**Dally**), necesario para la liberación de Hh (Eugster et al., 2007); Dispatched (**Disp**), también esencial para la liberación de Hh (Burke et al., 1999); y Shifted (**Shf**), fundamental para la estabilidad extracelular de Hh y su dispersión (Gorfinkiel et al., 2005). Los **citonemas** se observan con

mayor facilidad tras la expresión ectópica de **Ihog**, debido a que esta proteína altera su dinámica y **estabiliza** su estructura (Bischoff, Gradilla, Seijo, Andrés, Rodríguez-navas, et al., 2013).

Las proteínas **Ihog** y **Boi** de *Drosophila melanogaster* y sus homólogos en vertebrados **CDO** y **BOC** actúan como co-receptores de Hh y de Shh, respectivamente, teniendo una alta similitud en sus secuencias (Kang et al., 2002). Estas proteínas pertenecen a la superfamilia de las Inmunoglobulinas y están constituidas por una región extracelular comprendida por cuatro (Ihog, Boi y BOC) o cinco (CDO) **dominios Inmunoglobulina (Ig)**, y dos (Ihog y Boi: Fn1 y Fn2) o tres (CDO y BOC: Fn1, Fn2 y Fn3) **dominios Fibronectina tipo III (FNIII)**; además cuenta con un dominio transmembrana y un **dominio Carboxi-terminal (Ct)** intracelular cuya estructura y función son desconocidas (Kang et al. 2002; Yao et al. 2006). La **interacción de los dominios de Hh con los diferentes ligandos difiere entre ortólogos**: CDO interacciona con Shh por su dominio Fn3 (McLellan et al., 2008; Yao et al., 2006), mientras que Ihog interacciona con Hh a través de su dominio Fn1 (McLellan et al., 2006; Yao et al., 2006). Ihog también interacciona con Ptc por su dominio Fn2 (Zheng et al., 2010), lo cual no se ha visto en vertebrados. En discos imaginales de ala de *Drosophila melanogaster*, ambos **dominios FNIII** son esenciales para la **señalización de Hh** (Zheng et al., 2010).

Por otro lado se sabe que el co-receptor **Ihog interacciona con Dlp, Hh** y con el receptor canónico de la vía **Patched (Ptc)** en las células receptoras de Hh (Kim et al., 2011; Yan et al., 2010; Yao et al., 2006); es esencial para la localización de **Ptc en la membrana plasmática** (Zheng et al., 2010); y además se requiere para

mantener los **niveles extracelulares de Hh** (Bilioni et al., 2013; Callejo et al., 2011; Yan et al., 2010).

En este trabajo estudiamos los mecanismos del transporte y la señalización de Hh describiendo que dicho transporte tiene lugar a través de exovesículas que se mueven a lo largo de los citonemas. Para ello, hemos usado tejidos fijados de **discos imaginales de ala** de larvas de ***Drosophila melanogaster***, así como **histoblastos de abdomen de pupas** para los estudios de imagen 4D *in vivo*. Hemos hecho más énfasis en el estudio de la dinámica de los filopodios *in vivo* en condiciones silvestres o de sobrexpresión de la proteína Ihog normal o de mutantes que carecen de los diversos dominios funcionales de la misma.

El propósito de este trabajo es analizar la contribución de filopodios especializados en señalización (citonemas) en la vía de Hh y su papel en la formación del gradiente morfogenético. Para ello, hemos realizado un análisis *in vivo* de la dinámica de citonemas en histoblastos del abdomen de pupas de *Drosophila melanogaster*. Además, hemos estudiado las interacciones genéticas y moleculares entre componentes de la vía de señalización de Hh y los citonemas en los discos imaginales de ala de larvas en tercer estadio. A continuación se exponen los objetivos detallados de esta tesis:

1. Analizar la dinámica de los citonemas involucrados en la vía de señalización de Hh y su relación con la formación del gradiente morfogenético de Hh.
   1.1. Comparar la dinámica de los citonemas emitidos por las células productoras y receptoras de Hh.
   1.2. Estudiar si el ligando Hh y el receptor Ptc se distribuyen a lo largo de los citonemas.
   1.3 Analizar la respuesta a la activación de la señalización de Hh mediante la expresión de un reportero transcripcional de *ptc*.

2. Estudiar la función de Ihog durante el desarrollo de los discos imaginales de ala y de los histoblastos abdominales.
   2.1. Estudiar la dinámica de los citonemas en condiciones de falta de función o de ganancia de función de Ihog.
   2.2. Caracterizar los dominios funcionales de Ihog.
   2.3. Generar una línea transgénica de Ihog que no interaccione con el ligando Hh.

3. Estudiar las posibles interacciones de Ihog con proteínas involucradas en la vía de Hh y en la dinámica de actina.

La proteína Hh modificada por lípidos no puede difundir libremente por la matriz extracelular, por encontrarse fuertemente anclada a las membranas debido a sus modificaciones lipídicas. La manera en que Hh se transporta desde las células productoras a las receptoras es un campo de estudio muy debatido (Simon et al. 2016). Nuestro laboratorio ha propuesto un modelo de transporte mediante cuerpos multivesiculares para formar exosomas, moviéndose a lo largo de filopodios de actina o citonemas (Bilioni et al., 2013; Bischoff et al., 2013; Callejo et al., 2011; Gradilla et al., 2014). En este trabajo demostramos que la señalización de Hh está regulada por las maquinarias que regulan la polimerización de **actina** (Figure R-1; Figure R-2; Bischoff et al., 2013) y la formación de **exosomas** (Figure-R3; Gradilla et al. 2014). Además, hemos encontrado una fuerte **correlación** entre el alcance de los citonemas y la extensión del gradiente morfogenético de Hh (Figure R-2). Estos datos concuerdan con lo observado en la vía de señalización de Wnt/β-catenina en pez cebra (Stanganello et al., 2015).

Varios estudios recientes han demostrado que ligandos y receptores de diversas vías de señalización son transportados en vesículas a lo largo de filopodios especializados (Roy & Kornberg 2015; Pröls et al. 2016; Gradilla and Guerrero, 2013). Así mismo, en esta tesis hemos visto que el **ligando Hh** se localiza *in vivo* en **estructuras vesiculares** a lo largo de los **citonemas** de los histoblastos de abdomen de pupas (Figure R-7; Movie R-3; Movie R-4; Movie R-5). Además, Hh y Ihog **co-localizan con el marcador exosomal CD63** en estructuras vesiculares que se mueven a lo largo de los citonemas (Figure R-8; Gradilla et al. 2014). **Ihog promueve la acumulación de Hh** en la membrana plasmática y a lo largo de citonemas basales estabilizados, tanto de las células productoras como de las receptoras

de Hh (Figure R-7; Movie R-3; Movie R-4; Movie R-5). El **receptor Ptc** también **co-localiza con CD63** en estructuras vesiculares e incluso se puede apreciar a lo largo de lo que parecen **filopodios** marcados con CD63 (Figure R-8; Movie R-9; Movie R-10). Ptc **no se acumula en citonemas estabilizados por Ihog**, como lo hace Hh, estos resultados indican que el receptor Ptc es más difícil de localizar debido a que sufre un **rápido proceso de reciclaje** (González-Méndez et al., en preparación). Sin embargo, impidiendo su endocitosis, se consigue ver a Ptc asociado a estas estructuras filopodiales (González-Méndez et al 2017).

Al estudiar la dinámica de los citonemas de la vía de Hh en histoblastos de abdomen de pupas, hemos visto que éstos siguen **dos tipos de comportamientos**, que hemos denotado como: **dinámica de tipo triangular**, con velocidades de elongación y retracción constantes; y **dinámica de tipo trapezoidal**, con una fase estacionaria entre las fases de elongación y retracción (Figure R-5). Además, hemos demostrado que las **células productoras y las receptoras de Hh emiten citonemas dinámicos muy similares**. Se ha observado que con la **expresión ectópica de Ihog**, los citonemas adquieren una dinámica de **tipo trapezoidal** en la que la fase estacionaria se incrementa, volviéndose **más estables** y permitiendo una **mejor visualización en tejidos fijados** (Figure R-4; Figure R-6; Movie R-1; Movie R-2; Table R-1; Bischoff et al. 2013). Es importante resaltar que estos citonemas forman una **red dinámica que es independiente de la presencia de Hh o Ptc**, puesto que en ausencia de Hh o de Ptc la dinámica de los citonemas no se ve alterada (Figure R-9; Figure R-10; Movie R-13; Movie R-14). Estos datos concuerdan con un estudio anterior en el que citonemas marcados con la proteína de membrana CD8 no se veían alterados después de inducir Hh (Roy et al., 2011).

Los datos obtenidos en el **estudio *in vivo* de los citonemas** de Hh **concuerdan** con datos publicados sobre filopodios especializados de otras vías de señalización. Por ejemplo, alcanzan extensiones máximas de menos de 10 μm, como se había visto en diferentes estudios realizados en **ratones** (Salas-Vidal & Lomelí, 2004; Fierro-González, White, Silva, & Plachta, 2013; Koizumi et al., 2012), aunque otros estudios realizados en pollo, ratón, pez cebra o células humanas revelan extensiones de hasta 80 μm (Sato & Kornberg, 2002; Salas-Vidal & Lomelí, 2004; Koizumi et al., 2012; Sanders et al., 2013; Stanganello et al., 2015; Sagar, Pröls, Wiegreffe, & Scaal, 2015; Snyder et al., 2015). Los citonemas de Hh se **elongan** y se **retraen** a **velocidades similares** a las mostradas por embriones de **pollo** en la vía de **Wnt** (Sagar et al., 2015), aunque un estudio reciente en pollo en la vía de **Shh** muestra extensiones **más rápidas** de hasta 9 μm/min (Sanders et al., 2013). En **pez cebra** se ha visto que filopodios de la vía de **Wnt** tienen una **vida media de hasta 10 min** (Stanganello et al., 2015), lo que **concuerda con nuestros datos** de la vía de Hh obtenidos en los histoblastos (Table R-1).

Ihog y Boi parecen ser **redundantes** en su función como **co-receptores de Hh** (Zheng et al., 2010), pero **no en** su papel en la **regulación de la dinámica de citonemas**, puesto que la estabilización de los citonemas mediada por Ihog es independiente de Boi (Figure R-12; Movie R-19). Estos datos indican una **función específica de Ihog en la regulación de la dinámica de los citonemas**. Sin embargo, la falta de ambos no altera la formación de citonemas (Figure R-13; Movie R-20). Aún así, la co-expresión de Ihog y Boi hace que Boi también se vea acumulado en los citonemas estabilizados por Ihog en la superficie basolateral (Figure R-11; Movie R-15; Movie R-16; Movie R-18) aunque normalmente Boi se

encuentra en las superficies apical o lateral de discos imaginales de ala (Bilioni et al., 2013; Zheng et al., 2010) y su expresión ectópica produce citonemas dinámicos (Figure R-11; Movie R-17). Por otro lado, un estudio reciente en **pollo** muestra que **citonemas** que contienen **BOC** son significativamente **más estables que sin BOC** e indican que CDO también estabiliza dichos citonemas, aunque no se muestran los datos (Sanders et al., 2013), lo que recuerda nuestros resultados con Ihog (ortólogo de *Drosophila* de CDO), pero no con Boi (el ortólogo de *Drosophila* de BOC). Sería interesante investigar con más detalle el papel que ejerce la interacción de Ihog y Boi en la vía de señalización de Hh.

Hh se acumula en los citonemas cuando ***ihog*** **se sobreexpresa en las células productoras** de Hh y la **expresión de los genes diana de la vía** se ve **reducida** (Bilioni et al. 2013; Bischoff et al. 2013; Figure R-18), probablemente debido a que se impediría su liberación a las células receptoras. De manera opuesta, cuando *ihog* se sobreexpresa en las células **receptoras**, hay más Hh secuestrado por dichas células y el **gradiente de Hh se extiende** (González-Méndez et al., 2017).

Estudios anteriores habían descrito que **Shf** y **Dally** interaccionan con **Ihog**, y las tres se requieren para mantener los niveles normales de Hh (Bilioni et al., 2013; Gorfinkiel et al., 2005; Sánchez-Hernández et al., 2012). Los **dominios FNIII e Ig** de Ihog podrían estar **interaccionando** con **Shf y/o con el glipicano Dally** para regular la **retención de Hh** (Yan et al. 2010; Callejo et al. 2011; Bilioni et al. 2013; Figure R-7I-J; Movie R-3B'; Movie R-4B'), puesto que mutantes de delección de dichos dominios no acumulan Hh como lo hace Ihog sin estas delecciones (Figure R-17A; Movie R-24A-A'). Desafortunadamente, el mutante que carece de los dominios de Ig de

Ihog resultó tener además una mutación puntual en un aminoácido que pudiera interaccionar con Hh como se ha visto en un estudio cristalográfico (McLellan et al., 2006). Para saber con certeza si los dominios Ig están alterando la retención de Hh mediada por Ihog, es necesario un nuevo estudio con una proteína mutante de Ihog que carezca de los dominios Ig, pero no tenga la mutación puntual en el dominio Fn1 de posible interacción con Hh.

Los **dominios FNIII** de Ihog son esenciales para las **interacciones de Ihog con Hh y con Ptc** (McLellan et al., 2006; Zheng et al., 2010). De manera interesante, hemos visto que la **ausencia de ambos dominios o de uno de los dos altera los niveles de Hh** (Figure R-17; Movie R-25), lo que indica que ambos dominios FNIII podrían ser **necesarios para la acumulación de Hh en citonemas**, Fn1 de manera directa, puesto que se ha visto su interacción en un estudio cristalográfico de su estructura (McLellan et al., 2006; Yao et al., 2006) y Fn2 de manera indirecta, puesto que se desconoce su interacción con Hh basándonos en estos estudios.

Los dominios FNIII de Ihog regulan también **la dinámica de los citonemas**, puesto que su **ausencia** reduce la fase estacionaria de la dinámica trapezoidal de los citonemas, restaurando su **comportamiento dinámico** con velocidades de elongación y retracción similares a las condiciones normales sin sobreexpresión de Ihog (Figure R-15 comparada con Figure R-4; Movie R-21, Movie R-22 y Movie R-23 comparadas con Movie R-1 y Movie R-2).

En resumen, proponemos que los dominios FNIII **regulan la extensión del gradiente morfogenético de Hh** (Figure R-18), probablemente debido a su función tanto en la **regulación de la dinámica de los citonemas como en el secuestro de Hh**. Estas

funciones de los dominios FNIII son **independientes de la interacción de Ihog con Ptc**, puesto que al expresar el mutante que no interacciona con Ptc se observa que tanto la dinámica de los citonemas como el secuestro de Hh ocurren de forma similar a cuando se expresa Ihog silvestre (Figure R-16; Table R-4; Table R-5).

Finalmente, se ha observado que **Ihog regula los niveles de las integrinas en el borde de compartimento AP,** entre las células productoras y receptoras de Hh mediante sus **dominios FNIII** (Figure R-20), pudiendo tener esta interacción una función en el mantenimiento del borde de compartimento. Nuestros datos sugieren que la interacción entre Ihog y las integrinas y/u otras proteínas o componentes de la matriz extracelular podrían ser responsables de la **regulación de la dinámica de los citonemas**, la **retención de Hh** y en definitiva la **formación del gradiente de señalización**.

Proponemos un **modelo** en el que los **dominios FNIII de Ihog regulan la dinámica de los citonemas** probablemente mediante su **interacción** con componentes de la **matriz extracelular** (como Dally o Dlp) o con las **integrinas**, mientras que el dominio **C-terminal** podría estar interaccionando con **proteínas de unión a actina** regulando otras características de los filopodios intracelularmente (Figure D-1).

CONCLUSIONES

1. La señalización de Hedgehog (Hh) está regulada por las maquinarias de formación de exosomas y de formación de filopodios especializados ricos en actina (citonemas). Condiciones mutantes que afectan a la dinámica de actina y producción de exosomas también alteran el gradiente de Hh.

2. Hay una fuerte correlación entre el alcance de los citonemas y la extensión del gradiente morfogenético de Hh.

3. El ligando Hh y el receptor Patched (Ptc) se localizan tanto en muestras fijadas como *in vivo* en estructuras vesiculares que co-localizan con el marcador exosomal y de cuerpos multivesiculares CD63.

4. Hh se localiza in vivo a lo largo de citonemas dinámicos marcados con Lifeact y se acumula en citonemas estabilizados por Ihog en la parte basolateral del epitelio del abdomen de pupas. Ptc no se acumula en citonemas estabilizados por Ihog y es más difícil encontrar a Ptc en citonemas debido a su rápida endocitosis.

5. La existencia de una red de citonemas dinámicos es independiente de la presencia del ligando Hh y del receptor Ptc.

6. Los citonemas de histoblastos de abdomen de pupas tienen dos tipos de comportamiento: dinámica de tipo triángulo con velocidades de elongación y retracción constantes; y dinámica de tipo trapezoidal con una fase estacionaria entre las fases de elongación y retracción.

7. Las proteínas de adhesión y co-receptores de Hh (Ihog y Boi) se localizan en citonemas, pero sólo la expresión ectópica de Ihog los estabiliza.

8. Ihog regula la dinámica de los citonemas alterando la fase estacionaria de la dinámica de tipo trapezoidal. Los dominios fibronectina tipo III (FNIII) de Ihog son responsables de dicha regulación.

9. Los dominios FNIII de Ihog están implicados en la estabilidad extracelular de Hh. El segundo dominio FNIII (Fn2) podría estar indirectamente involucrado en la regulación de la retención de Hh mediada por Ihog.

10. Los dos dominios FNIII de Ihog tienen un papel específico en la regulación de la interacción entre Ihog y las integrinas a lo largo del borde de compartimento antero-posterior de compartimento entre las células productoras y receptoras de Hh.

Annex I

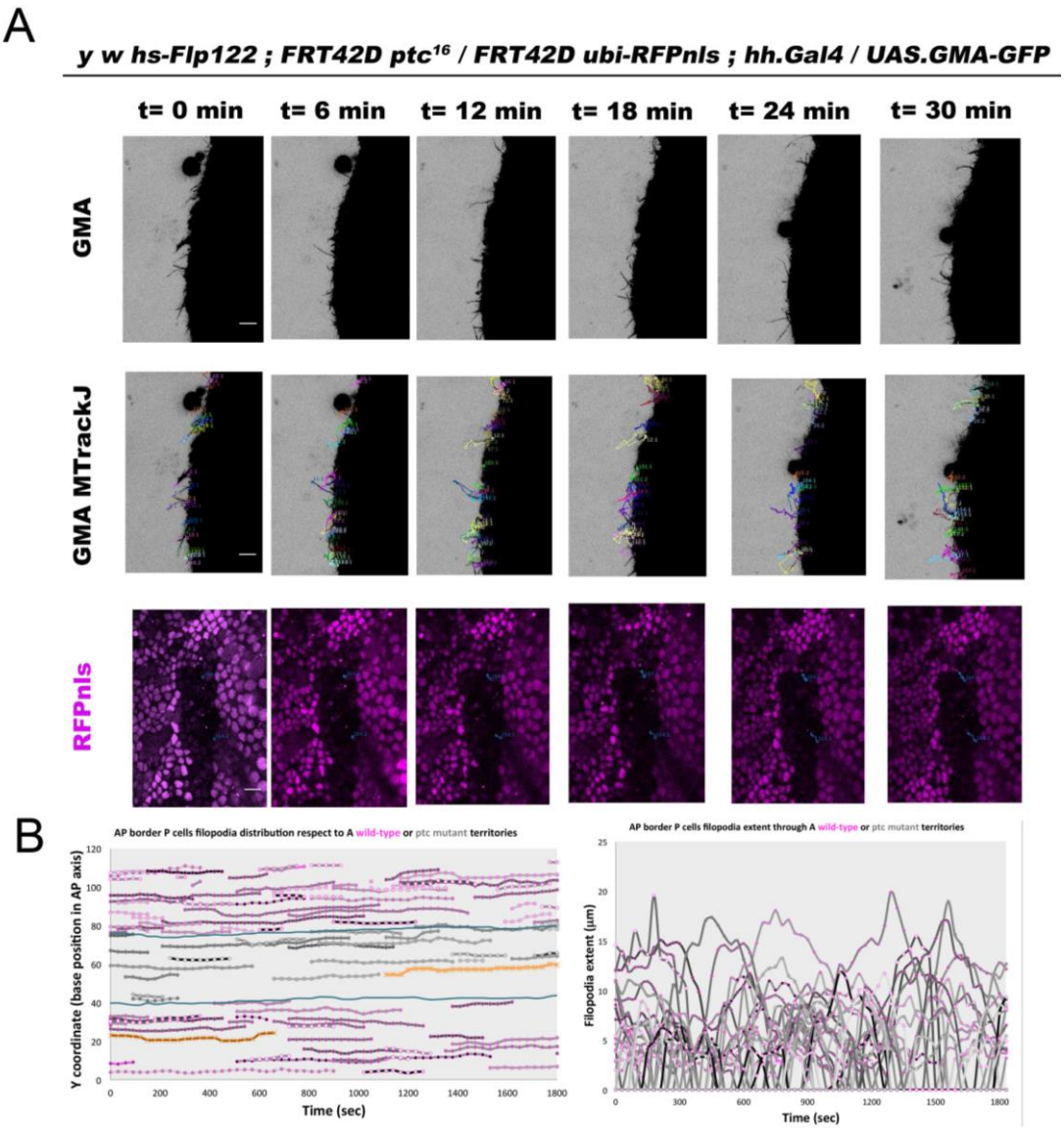

Figure S-1. Tracking of cytonemes crossing wild type and ptc mutant territories. This figure contains additional data from cytonemes analysis of Movie MM-1. **A**: Six time frames from Movie MM-1 displaying a Z-projection of GMA where basolateral Hh-producing cytonemes are visualized (top panels); the Z-projection of GMA-GFP and the tracking of filopodia using the MTrackJ plugin of Fiji (middle panels), where each filopodium has a color and the colored lines are the base and tip trajectories and two dying larval epithelial cells are tracked (orange tracks #165.1 and #165.2); and nuclear RFP (magenta) wild-type nuclei and *ptc* mutant clone (absence of magenta) tracked with MTrackJ (bottom panels) using the first and last region where there is no RFP-positive nuclei just anterior to the A/P boundary (blue tracks #164.1 and #164.2). Scale bars represent 10 μm. **B**: Graphs representing the distribution of GMA filopodia crossing wild-type territories (magenta) *ptc* mutant territories (grey), the references of the *ptc* mutant clone (blue) and the references of dying LECs (orange) on the left; and the GMA extent filopodia crossing willd type (magenta circles) or ptc mutant (grey circles) territories over time on the right.

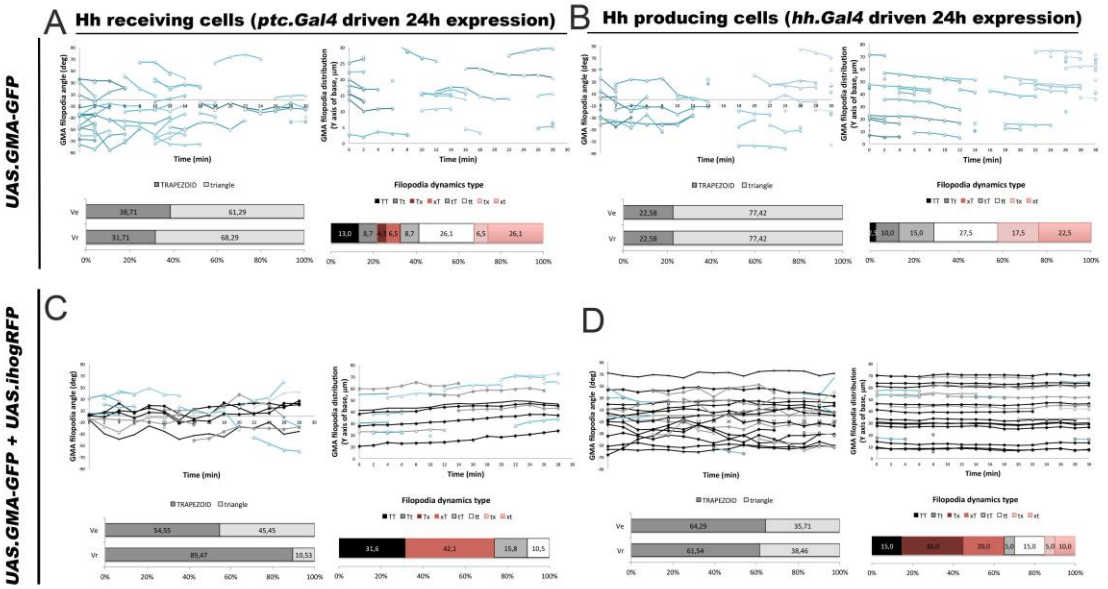

Figure S-2. Hh-producing and Hh-receiving cells emit similar dynamic cytonemes. This figure contains additional data from cytonemes analysis of Movie R-1 and Movie R-2. Graphs representing GMA cytoneme angle and distribution over time are shown in the upper-left and upper-right part of A-D. Percentage graphs of elongation (Ve) and retraction (Ve) velocities are shown in the lower-left side of A-D, while total dynamics type is represented in the lower-right side. For cytoneme dynamics type the first letter corresponds to elongation velocity and the second to retraction velocity. T:trapezoid-like, t:triangle-like, x:unknown. Notice that Hh-producing (B, D) and Hh-receiving (A, C) cytonemes have similar angle and distribution in the AP axis and also similar dynamics. Overexpression of Ihog (C, D) increases the percentage of trapezoid-like behavior.

Movie MM-1. Cytonemes in a *ptc* mutant region and their manual tracking using MTrackJ. **A-C:** Abdominal histoblasts of a *y w hs-Flipase122; FRT42D ptc*^{16} */ FRT42D ubiRFPnls; hh.Gal4 / UAS.GMA-GFP* pupae. GMA-GFP was induced during the whole development and *ptc*^{16} clones were induced by 1h heat-shock at 37ºC and analysed two days later. **A:** Z-projection of GMA-GFP using the inverted grey-scale lookup table of ImageJ. **B:** Z-projection of GMA-GFP and the tracking of filopodia using the MTrackJ plugin of Fiji, where the fist number refers to the number of filopodium tracked and the second name refers to the base (1) or the tip (2). Each filopodium has a colour and the coloured lines represent the base and tip trajectories. Notice that also two dying larval epithelial cells are tracked (orange tracks #165.1 and #165.2). **C:** Nuclear RFP (magenta) wild-type nuclei and *FRT42D ptc*^{16} mutant clone (absence of magenta) tracked using the first and last region where no RFP-positive nuclei are detected just anterior to the A/P boundary (blue tracks #164.1 and #164.2). Histoblasts move down towards the dorsal midline, and this is not shown because of the high magnification. Anterior is on the left. Pupa is around 30 hours APF (after puparium formation). Movie of 30 minutes imaging with a time interval between frames of 30 seconds. Scale bars represent 10 μm.

Movie R-1. *In vivo* dynamics of cytonemes from the P compartment abdominal histoblast cells expressing GMA alone or co-expressing Ihog. **A-B:** Z projection movies of abdominal histoblasts from pupae with the following genotypes: *w; tubGal80^{ts} /+; hh.Gal4 / UAS.GMA-GFP* (A) and *w; tubGal80^{ts} / UAS.ihog-RFP; hh.Gal4 / UAS.GMA-GFP* (B). **A:** The actin-binding domain of moesin fused to GFP (GMA-GFP) was expressed during 24h in the Hh-producing cells to visualize actin-based filopodia dynamics, easily detected using the inverted grey-scale lookup table tool of Fiji. Notice the highly dynamic filopodia emerging from P cells towards A cells. **B-B'':** co-expression of GMA-GFP (B) and Ihog-RFP (B') in Hh-producing cells. Observe in the merge panel (B'') that Ihog-containing filopodia are stabilized while few filopodia with low or no Ihog levels detected are more dynamic. Histoblasts move up (A) and down (B) towards the dorsal midline, and this is not shown because of the high magnification. Anterior is on the left. Pupae were around 30 hours APF (after puparium formation). Movies of 30 minutes imaging with time intervals between frames of 2 minutes. Scale bars represent 10 μm.

Movie R-2. *In vivo* dynamics of cytonemes from A compartment abdominal histoblast cells expressing GMA alone or co-expressing Ihog. **A-B:** Z projection movies of abdominal histoblasts from pupae with the following genotypes: *w; ptc.Gal4 / tubGal80^{ts}; UAS.GMA-GFP /+* (A) and *w; ptc.Gal4 / tubGal80^{ts}; UAS.GMA-GFP / UAS.ihog-RFP* (B). **A:** The actin-binding domain of moesin fused to GFP (GMA-GFP) was expressed during 24h in the Hh-receiving cells to visualize actin-based filopodia dynamics, easily detected using the inverted grey-scale lookup table tool of Fiji. Notice the highly dynamic filopodia emerging from A cells towards P compartment cells. **B-B'':** GMA-GFP (B) was co-expressed with Ihog-RFP (B') in Hh-receiving cells. Observe in the merge panel (B'') that Ihog-containing filopodia are stabilized while few filopodia with low or no Ihog levels detected are more dynamic. Histoblasts move up (A) and down (B) towards the dorsal midline, not shown because of the high magnification. Anterior is on the left. Pupae were around 30 hours APF (after puparium formation). Movies of 28 minutes imaging with time intervals between frames of 2 minutes. Scale bars represent 10 μm.

Movie R-3. Hh localization in Hh-producing histoblasts *in vivo*. **A-B:** Z projection movies of abdominal histoblasts from pupae with the following genotypes: *w; Bac.hh-GFP / + ; hh.Gal4,tubGal80^{ts} / UAS.Lifeact-RFP* (A) and *w; Bac.hh-GFP / + ; hh.Gal4,tubGal80^{ts} / UAS.ihog-RFP* (B). **A-A':** Histoblasts expressing the F-actin marker peptide Lifeact fused to RFP (Lifeact-RFP) during 24h in the Hh-producing cells emit highly dynamic filopodia shown in the merge channel (A), where Hh is more difficult to visualize along them (A') due to rapid movement. **B-B':** Histoblasts expressing Ihog-RFP during 24h in the Hh-producing cells emit more stable filopodia shown in the merge channel (B), where Hh is easily visualized due to its accumulation along them (B'). Histoblasts move up towards the dorsal midline, not shown because of the high magnification. Anterior is on the left. Pupae were around 30 hours APF (after puparium formation. Movies of 28 minutes imaging with time intervals between frames of 2 minutes. Scale bars represent 10 μm.

Movie R-4. Hh localization in Hh-producing histoblasts *in vivo*. **A-B:** Z-stack movies from apical to basal of abdominal histoblasts from pupae with the following genotypes: *w; Bac.hh-GFP / + ; hh.Gal4,tubGal80^{ts} / UAS.Lifeact-RFP* (A) and *w; Bac.hh-GFP / + ; hh.Gal4,tubGal80^{ts} / UAS.ihog-RFP* (B). **A-A':** Histoblasts expressing the F-actin marker peptide Lifeact fused to RFP (Lifeact-RFP) during 24h in Hh-producing cells emit basal filopodia shown in the merge channel (A). Hh is localized at membranes along the whole P compartment cells. **B-B':** Histoblasts expressing Ihog-RFP during 24h in the Hh-producing cells emit basal filopodia, shown in the merge channel (B). Hh is highly accumulated on membranes of the P compartment and along Ihog-labelled cytonemes (B'). Anterior is on the left. Pupae were around 30 hours APF (after puparium formation). Scale bars represent 10 μm.

Movie R-5. Hh localizes at the tip of cytonemes of Hh-producing histoblasts *in vivo*. 3D-view movie of abdominal histoblasts from a pupa with the genotype *w; Bac.hh-GFP / + ; hh.Gal4,tubGal80^{ts} / UAS.Lifeact-RFP.* Histoblasts expressing the F-actin marker peptide Lifeact fused to RFP (Lifeact-RFP) during 24h in Hh-producing cells emit basal filopodia (magenta) where Hh is shown at their tips (green). Zoom is used to easily visualize Hh at the tip of a filopodium.

Movie R-6. Hh localization in Hh-receiving histoblasts *in vivo*. **A-B:** Z-stack movies from apical to basal of abdominal histoblasts from pupae with the following genotypes: *w; Bac.hh-GFP, ptc.Gal4 / +; tubGal80^{ts} / UAS.Lifeact-RFP* (A) and *w; Bac.hh-GFP, ptc.Gal4 / +; tubGal80^{ts} / UAS.ihog-RFP* (B). **A-A':** Histoblasts expressing the F-actin marker peptide Lifeact fused to RFP (Lifeact-RFP) during 24h in the Hh-receiving cells emit basal filopodia that are more difficult to visualize due to their fast dynamic (A). Hh is localized along the whole P compartment cells. **B-B':** Histoblasts expressing Ihog-RFP during 24h in Hh-receiving cells emit basal filopodia easily visualized due to their stabilization (B). Hh is highly accumulated in basal cytonemes that come from A to P compartment cells but also from P to A compartment cells (B'). There are also more Hh accumulated on A compartment cells expressing Ihog (B) compared to those non-overexpressing Ihog (A). Anterior is on the left. Pupae were around 30 hours APF (after puparium formation). Scale bars represent 10 μm.

Movie R-7. Hh localization in Hh-receiving histoblasts *in vivo*. **A-B:** Z projection movies of abdominal histoblasts from pupae with the following genotypes *w; Bac.hh-GFP, ptc.Gal4 / +; tubGal80^{ts} / UAS.Lifeact-RFP* (A) and *w; Bac.hh-GFP, ptc.Gal4 / +; tubGal80^{ts} / UAS.ihog-RFP* (B). **A-A':** Histoblasts expressing the F-actin marker peptide Lifeact fused to RFP (Lifeact-RFP) during 24h in the Hh-receiving cells emit highly dynamic filopodia (A), where Hh is difficult to visualize (A'). **B-B':** Histoblasts expressing Ihog-RFP during 24h in Hh-receiving cells emit stabilized filopodia (B), where Hh is highly accumulated, but also accumulated in filopodia-like structures from P to A compartment cells (B'). Histoblasts move down towards the dorsal midline, not shown because of the high magnification. Anterior is on the left. Pupae were around 30 hours APF (after puparium formation). Movies of 30 minutes imaging with time intervals between frames of 2 minutes. Scale bars represent 10 μm.

Movie R-8. Ptc localization in Hh-receiving histoblasts *in vivo*. **A-D:** Z-stack movies from apical to basal of abdominal histoblasts from pupae with the following genotypes: *w; ptc.Gal4, tubGal80^{ts} / +; Bac.ptc-Cherry / UAS.Lifeact-GFP* (A); *w; ptc.Gal4, tubGal80^{ts} / +; Bac.ptc-Cherry / UAS.GMA-GFP* (B); *w; ptc.Gal4, tubGal80^{ts} / +; Bac.ptc-Cherry / UAS.CD4-GFP (C); and w; ptc.Gal4, tubGal80^{ts} / +; Bac.ptc-Cherry / UAS.ihog-YFP (D)*. Ptc localizes on punctae structures throughout the A compartment, but are not easily visualized along basal filopodia. Histoblasts expressing Lifeact (A), GMA (B), and CD4 (C) expressed in Hh-receiving cells produce basal filopodia more difficult to visualize because of their high dynamic behavior, while the expression of Ihog (D) produces basal filopodia that are easier to visualize due to their stability. Anterior is on the left. Pupae were around 30 hours APF (after puparium formation). Scale bars represent 10 μm.

Movie R-9. Ptc co-localizes *in vivo* with the exosomal and MVB marker CD63 along filopodia-like structure emanating from Hh-receiving histoblasts. Z-stack movie from apical to basal of abdominal histoblasts from a pupa with the genotype *w; ptc.Gal4, tubGal80^{ts} / +; Bac.ptc-Cherry / UAS.CD63-GFP*. Ptc (A') and CD63 (A'') co-localize in punctate structures throughout the A compartment (A) and in some punctae along a filopodia-like structure on the basal surface shown with CD63 (A, A''). Anterior is on the left. Pupae were around 30 hours APF (after puparium formation). Scale bars represent 10 μm.

Movie R-10. Ptc co-localizes *in vivo* with the exosomal and MVB marker CD63 along dynamic filopodia-like structures emanating from Hh-receiving histoblasts. Z projection (A-A'') and 3D-view (B) movies from a pupa with the genotype *w; ptc.Gal4, tubGal80^{ts} / +; Bac.ptc-Cherry / UAS.CD63-GFP*. Ptc (A') and CD63 (A'') co-localize in dynamic punctate structures throughout the A compartment (A) and in some punctae along highly dynamic filopodia-like structures with CD63 (A, A'') shown in basal surface (B). Histoblasts move down towards the dorsal midline, not shown because of the high magnification. Anterior is on the left. Pupae were around 30 hours APF (after puparium formation). Movies of 30 minutes imaging with time intervals between frames of 2 minutes. Scale bars represent 10 μm.

Movie R-11. The exosomal and MVB marker CD63 co-localizes with Ihog along stable cytonemes of Hh-receiving histoblasts *in vivo*. Z projection (A-A'') and 3D-view (B) movies from a pupa with the genotype *w; ptc.Gal4, tubGal80^{ts} / +; UAS.ihog-RFP / UAS.CD63-GFP*. Ihog (A') and CD63 (A'') co-localize in dynamic punctate structures throughout the A compartment and in dynamic punctae along stable cytonemes (A) shown on basal surface (B). Histoblasts move down towards the dorsal midline, not shown because of the high magnification. Anterior is on the left. Pupae were around 30 hours APF (after puparium formation). Movies of 28 minutes imaging with time intervals between frames of 2 minutes. Scale bars represent 10 μm.

Movie R-12. The exosomal and MVB marker CD63 co-localizes with Ihog along basal cytonemes of Hh-receiving histoblasts *in vivo*. Z-stack movie from apical to basal of abdominal histoblasts from a pupa with the genotype *w; ptc.Gal4, tubGal80^{ts} / +; UAS.ihog-RFP / UAS.CD63-GFP*. Ihog (A') and CD63 (A'') co-localize in punctate structures throughout the A compartment and along basal cytonemes (A). Anterior is on the left. Pupae were around 30 hours APF (after puparium formation). Scale bars represent 10 μm.

Movie R-13. *In vivo* dynamics of filopodia from P compartment abdominal histoblast cells expressing Ihog in wild type and *hh^{ts2}* mutant background. **A-B:** Z projection movies of abdominal histoblasts from pupae with the following genotypes: *w; en.Gal4, tubGal80^{ts} / UAS.ihog-RFP; + / +* (A) and *w; en.Gal4, tubGal80^{ts} / UAS.ihog-RFP; hh^{ts2}/ hh^{ts2}* (B). **A:** Histoblasts expressing Ihog-RFP in P compartment show stabilized cytonemes easily visualized with the inverted grey lookup table of ImageJ (A) and they are still stable under *hh^{ts2}* mutant background (B). Histoblasts move up towards the dorsal midline, and this is not shown because of the high magnification. Anterior is on the left. Pupae were around 30 hours APF (after puparium formation). Movies of 28 minutes imaging with time intervals between frames of 2 minutes. Scale bars represent 10 μm.

Movie R-14. Hh-producing abdominal histoblasts emit cytonemes that can cross a *ptc* mutant clone with similar dynamics to those crossing wild type territories. **A-C:** Abdominal histoblasts of a pupa with the genotype *y w hs-Flipase122; FRT42D ptc^{16} / FRT42D ubiRFPnls; hh.Gal4 / UAS.GMA-GFP*. GMA-GFP is expressed during the whole development at 18ºC and *FRT42D ptc^{16}* clones were induced by a heat-shock of 1h at 37ºC two days before imaging. **A:** Merge of nuclear RFP (magenta) and a z-projection of GMA-GFP (inverted grey-scale lookup table of ImageJ). Hh-producing cell cytonemes labelled with the actin marker GMA (inverted grey-scale lookup table of ImageJ) have the same dynamics and cross normally wild-type (nuclear RFP, magenta) and *FRT42D ptc^{16}* mutant clone (absence of magenta) territories. B: Merge of the z-projection of GMA (inverted grey-scale lookup table of ImageJ) and the lateral side (green) to show the morphology of the epithelium. C: Merge of nuclear RFP (magenta) and GMA in a lateral view (green). Here we visualize the *FRT42D ptc^{16}* mutant clone (absence of magenta) located just anterior to the A/P boundary. Histoblasts move down towards the dorsal midline, and this is not shown because of the high magnification. Anterior is on the left. Pupa is around 30 hours APF (after puparium formation). Movie of 30 minutes imaging with a time interval between frames of 30 seconds. Scale bars represent 10 μm.

Movie R-15. *In vivo* localization of Ihog and Boi in basal cytonemes when expressed in Hh-producing histoblasts. **A-B:** Z-stack movies from apical to basal of abdominal histoblasts from pupae with the following genotypes: *w; UAS.boi-YFP / + ; hh.Gal4,tubGal80^{ts} / +* (A) and *w; UAS.boi-YFP / UAS.ihog-RFP ; hh.Gal4,tubGal80^{ts} / +* (B). **A:** Histoblasts expressing Boi-YFP during 24h in Hh-producing cells emit basal cytonemes. **B-B'':** Histoblasts co-expression Boi-YFP and Ihog-RFP during 24h in Hh-producing cells emit basal cytonemes where Ihog and Boi co-localize. Anterior is on the left. Pupae were around 30 hours APF (after puparium formation). Scale bars represent 10 μm.

Movie R-16. Distinct roles of Ihog and Boi in cytoneme dynamics regulation. **A-B:** Z projection movies from pupae with the following genotypes: *w; UAS.boi-YFP / + ; hh.Gal4,tubGal80^{ts} / +* (A) and *w; UAS.boi-YFP / UAS.ihog-RFP ; hh.Gal4,tubGal80^{ts} / +* (B). **A:** Histoblasts expressing Boi-YFP during 24h in Hh-producing cells emit dynamic cytonemes. **B-B'':** Histoblasts co-expressing Boi-YFP and Ihog-RFP during 24h in Hh-producing cells emit stabilized cytonemes, leading Boi to be also localized along the Ihog-driven stabie cytonemes. Histoblasts move up towards the dorsal midline, and this is not shown because of the high magnification. Anterior is on the left. Pupae are around 30 hours APF (after puparium formation). Movies of 30 minutes imaging with a time interval between frames of 2 minutes. Scale bars represent 10 μm.

Movie R-17. Boi expression in Hh responding cells does not alter the normal dynamics of basal cytonemes. Z-stack from apical to basal (A) and Z-projection (B) movies from a pupa with the genotype *w; UAS.boi-YFP / ptc.Gal4 ; tubGal80^{ts} / +*. Histoblasts expressing Boi-YFP during 24h in Hh-receiving cells emit basal (A) highly dynamic (B) cytonemes. In B, histoblasts move down towards the dorsal midline, and this is not shown because of the high magnification. Anterior is on the left. Pupae are around 30 hours APF (after puparium formation). B: Movie of 30 minutes imaging with a time interval between frames of 2 minutes. Scale bars represent 10 μm.

Movie R-18. Ihog and Boi co-localize along basal cytonemes when co-expressed in Hh responding cells of fixed wing discs. Z-stack from apical to basal from a *w; UAS.boi-YFP / ptc.Gal4 ; tubGal80^{ts} / UAS.ihog-RFP* wing dics. Wing disc co-expressing Boi-YFP (A) and ihog-RFP (A') during 24h in Hh-receiving cells produces basal cytonemes where Ihog and Boi co-localize (A'') in both the peripodial membrane (PM) and wing pouch (WP). Anterior is on the left. Scale bars represent 10 μm.

Movie R-19. Ihog-driven cytoneme stabilization is independent of Boi. Z-stack from apical to basal (A) and Z-projection (B) movies obtained from a pupa with the genotype *w; UAS.boi-RNAi / + ; hh.Gal4 / UAS.ihog-RFP*. Histoblasts expressing Ihog-RFP in Hh-producing cells still produced basal (A) stable (B) Ihog-labelled cytonemes even with the RNA interference of boi (boi-RNAi) during the whole development. In B, histoblasts move down towards the dorsal midline, and this is not shown because of the high magnification. Anterior is on the left. Pupae are around 30 hours APF (after puparium formation). B: Movie of 30 minutes imaging with a time interval between frames of 2 minutes. Scale bars represent 10 μm.

Movie R-20. Hh-producing or Hh-receiving histoblasts with loss of function of both *ihog* and *boi* emit dynamic cytonemes. Z projection movies obtained from pupae with the following genotypes: *w; ptc.Gal4, tubGal80ts / + ; UAS.GMA-GFP /* + (A); *w; ptc.Gal4, tub.Gal80^{ts} / UAS.ihog-RNAi, UAS.boi-RNAi ; UAS.GMA-GFP /* + (B); *w; tub.Gal80^{ts} / UAS.ihog-RNAi, UAS.boi-RNAi ; UAS.GMA-GFP / hh.Gal4* (C); and *w; tub.Gal80^{ts} / + ; UAS.GMA-GFP / hh.Gal4* (D). Hh-producing cells (C, D) and Hh-receiving cells (A, B) produce highly dynamic filopodia expressing GMA for 48h alone (A, D) or co-expressing RNAi against both *ihog* and *boi* (B, C). Histoblasts move down (A, B, D) and up (C) towards the dorsal midline, and this is not shown because of the high magnification. Anterior is on the left. Pupae are around 30 hours APF (after puparium formation). Movies of 30 minutes imaging with a time interval between frames of 2 minutes. Scale bars represent 10 μm.

Movie R-21. Function of the Ihog domains in cytoneme dynamics regulation of Hh-producing histoblasts. Z projection movies from pupae with the following genotypes: *w; UAS.ihogΔIg-RFP / + ; hh.Gal4, tub.Gal80^{ts} / UAS.GMA-GFP* (A); *w; + / + ; hh.Gal4, tub.Gal80^{ts} / UAS.GMA-GFP, UAS.ihogΔFN-RFP* (B) and *w; + / + ; hh.Gal4, tub.Gal80^{ts} / UAS.GMA-GFP, UAS.ihogΔCt-RFP* (C). Hh-producing cells co-expressing GMA and Ihog without Ig domains (IhogΔIg) emit stabilized cytonemes (A-A''), with Ihog without FNIII domains (IhogΔFN) produces dynamic cytonemes (B-B'') and without the C-terminus (IhogΔCt) induces stabilized cytonemes (C-C''). Histoblasts move up (A) and down (B, C) towards the dorsal midline, and this is not shown because of the high magnification. Anterior is on the left. Pupae are around 30 hours APF (after puparium formation). Movies of 28 minutes imaging with a time interval between frames of 2 minutes. Scale bars represent 10 μm.

Movie R-22. Function of the Ihog domains in cytoneme dynamics regulation of Hh-receiving histoblasts. Z projection movies from pupae with the following genotypes: *w; ptc.Gal4, tub.Gal80^{ts} / UAS.ihogΔIg-RFP ; + / UAS.GMA-GFP* (A); *w; ptc.Gal4, tub.Gal80^{ts} / + ; + / UAS.GMA-GFP, UAS.ihogΔFN-RFP* (B) and *w; ptc.Gal4, tub.Gal80^{ts} / + ; + / UAS.GMA-GFP, UAS.ihogΔCt-RFP* (C). Hh-receiving cells co-expressing GMA with Ihog without Ig domains (IhogΔIg) produces stabilized cytonemes (A-A''), with Ihog without FNIII domains (IhogΔFN) produces dynamic cytonemes (B-B'') and without the C-terminus (IhogΔCt) produces stabilized cytonemes (C-C''). Histoblasts move up towards the dorsal midline, and this is not shown because of the high magnification. Anterior is on the left. Pupae are around 30 hours APF (after puparium formation). Movies of 30 minutes imaging with a time interval between frames of 2 minutes. Scale bars represent 10 μm.

Movie R-23. Ihog Fn2 domain role in Hh-receiving and Hh-producing cytoneme dynamics. Z projection movies obtained from pupae with the following genotypes: *w; ptc.Gal4, tub.Gal80^{ts} / UAS.ihogΔFn2-HA ; + / UAS.GMA-GFP* (A); *w; ptc.Gal4, tub.Gal80^{ts} / + ; + / UAS.GMA-GFP, UAS.ihogFn2** (B); *w; + / UAS.ihogΔFn2-HA ; hh.Gal4, tub.Gal80^{ts} / UAS.GMA-GFP* (C) and *w; + / + ; hh.Gal4, tub.Gal80^{ts} / UAS.GMA-GFP, UAS.ihogFn2** (D). Hh-receiving (A, B) and producing (C, D) histoblasts co-expressing GMA with IhogΔFn2 produce dynamic cytonemes (A, C), while the co-expression with Ihog with two point mutations in Fn2 that impair its binding to Ptc (IhogFn2*) induces stabilized cytonemes (B, D). Histoblasts move down towards the dorsal midline, and this is not shown because of the high magnification. Anterior is on the left. Pupae are around 30 hours APF (after puparium formation). Movies of 30 minutes imaging with a time interval between frames of 2 minutes. Scale bars represent 10 μm.

Movie R-24. Function of the Ihog domains in Hh retention *in vivo*. Z projection movies obtained from pupae with the following genotypes: *w; Bac.hh-GFP / UAS.ihogΔIg-RFP ; hh.Gal4, tub.Gal80^{ts} / +* (A); *w; Bac.hh-GFP / + ; hh.Gal4, tub.Gal80^{ts}; UAS.ihogΔFN-RFP* (B) and *w; Bac.hh-GFP / + ; hh.Gal4, tub.Gal80^{ts} / UAS.ihogΔCt-RFP* (C). In all movies the different Ihog constructs are expressed in the Hh-producing cells and in a Bac.hh-GFP background (a *hh-GFP* construct that mimics the endogenous *hh* expression). Note that the expression of a construct of Ihog without Ig domains (IhogΔIg) does not lead to Hh accumulation (A-A''); the expression of a construct of Ihog without FNIII domains (IhogΔFN) does not accumulate Hh either (B-B''); while the expression of a construct without the C-terminus (IhogΔCt) induces Hh accumulation along cytonemes (C-C''). Histoblasts move down towards the dorsal midline, and this is not shown because of the high magnification. Anterior is on the left. Pupae are around 30 hours APF (after puparium formation). Movies of 28 minutes imaging with a time interval between frames of 2 minutes. Scale bars represent 10 μm.

Movie R-25. Function of the Ihog Fn1 and Fn2 domains in Hh retention *in vivo*. Z projection movies obtained from pupae with the following genotypes: *w; Bac.hh-GFP / UAS.ihogΔFn1 ; hh.Gal4, tub.Gal80^{ts} / +* (A) and *w; Bac.hh-GFP / UAS.ihogΔFn2-HA ; hh.Gal4, tub.Gal80^{ts}; UAS.ihogΔFN-RFP* (B) and *w; Bac.hh-GFP / + ; hh.Gal4, tub.Gal80^{ts} / UAS.ihogFn2** (C). In all movies the different Ihog constructs are expressed in the Hh-producing cells and in a Bac.hh-GFP background (that expresses a *hh-GFP* construct that mimics the endogenous *hh* expression). The constructs of Ihog without either the first FNIII domain (IhogΔFn1) or the second FNIII domain (IhogΔFn2) do not induce the Hh accumulation (A and B, respectively), while the construct with the two point mutations in Fn2 that impair Ptc interaction (IhogFn2*) induces the accumulation of Hh in stabilized filopodia-like structures (C). Histoblasts move down towards the dorsal midline, and this is not shown because of the high magnification. Anterior is on the left. Pupae are around 30 hours APF (after puparium formation). Movies of 28 minutes imaging with a time interval between frames of 2 minutes. Scale bars represent 10 μm.

Annex II

The work done in this thesis has produced the following articles:

Bischoff, M., Gradilla, A.-C., Seijo I., Andrés, G., Rodríguez-Navas, C., González-Méndez, L. and Guerrero, I. (2013) Cytonemes are required for the establishment of a normal Hedgehog morphogen gradient in Drosophila epithelia. *Nat. Cell Biol*., 15(11):1269-81.

Gradilla, A. C., González, E., Seijo, I., Andrés, G., Bischoff, M., González-Mendez, L., Sánchez, V., Callejo, A., Ibáñez, C., Guerra, M., Ortigão-Farias, J.R., D. Sutherland, J., González, M., Barrio, R., Falcón-Pérez, J.M. and Guerrero I. (2014). Exosomes as Hedgehog carriers in cytoneme-mediated transport and secretion*. Nature communications*, 5: 5649.

Seijo-Barandiarán, I., Guerrero, I. and Bischoff, M. (2015). In vivo imaging of Hedgehog transport in Drosophila epithelia. *Hedgehog Signaling Protocols*, Chapter 2, 9-18.

González-Méndez, L., Seijo-Barandiarán, I. and Guerrero, I. (2017) Cytoneme-mediated cell-cell contacts for Hedgehog reception. *eLIFE*. In press.

Hedgehog (Hh) signaling is a well-conserved pathway essential for many developmental processes. Hh is a morphogen that spreads from posterior (P) compartment producing cells to anterior (A) compartment receiving cells in a graded manner, activating different target genes depending on the signal concentration. Hh is a dually lipid-modified molecule, being therefore hydrophobic and tightly attached to membranes.

To further research the mechanisms of Hh transport and signaling, we have used two paradigms in *Drosophila melanogaster*: fixed larval wing imaginal disc epithelium and *in vivo* pupal abdominal histoblasts epithelium.

In this work, we show that Hh signaling is regulated by both actin dynamics and intracellular vesicular traffick machinery. We describe that the Hh ligand and its receptor Patched (Ptc) are transported in vesicles along dynamic filopodia-like structures (cytonemes) at the basolateral surface of the epithelium. These cytonemes comprise a dynamic network that is independent of the presence of Hh or Ptc. They are easily visualized by overexpression of the Hh co-receptor Interference hedgehog (Ihog) due to its role in regulating cytoneme dynamics. We have seen that this stabilization is independent of its homologous protein Brother of Ihog (Boi). Besides we have identified the fibronectin type III domains of Ihog as responsible for the regulation of cytoneme dynamics. Ihog also plays a role in Hh retention and both of these two functions control the formation of the Hh morphogenetic gradient. Finally, we have seen that FNIII domains of Ihog also regulate integrins levels at the A/P compartment border between Hh-sending and Hh-receiving cells. We propose that Ihog interactions with integrins and components of the extracellular matrix could be responsible for Ihog functions as regulator of cytoneme dynamics, Hh retention and signaling gradient formation.